The Mechanics of the Contact Phase in Trampolining

by

David John Burke

A Doctoral Thesis

Submitted in partial fulfilment of the requirements for the award of
Doctor of Philosophy of Loughborough University

February 2015

ABSTRACT

The Mechanics of the Contact Phase in Trampolining

David John Burke, Loughborough University, 2015

During the takeoff for a trampoline skill the trampolinist should produce sufficient vertical velocity and angular momentum to permit the required skill to be completed in the aerial phase without excessive horizontal travel. The aim of this study was to investigate the optimum technique to produce forward somersault rotation. A seven-segment, subject-specific torque-driven computer simulation model of the takeoff in trampolining was developed in conjunction with a model of the reaction forces exerted on the trampolinist by the trampoline suspension system. The ankle, knee, hip, and shoulder joints were torque-driven, with the metatarsal-phalangeal and elbow joints angle-driven. Kinematic data of trampolining performances were obtained using a Vicon motion capture system. Segmental inertia parameters were calculated from anthropometric measurements. Viscoelastic parameters governing the trampoline were determined by matching an angle-driven model to the performance data. The torque-driven model was matched to the performance data by scaling joint torque parameters from the literature, and varying the activation parameters of the torque generators using a simulated annealing algorithm technique. The torque-driven model with the scaled isometric strength was evaluated by matching the performance data. The evaluation produced close agreement between the simulations and the performance, with an average difference of 4.4% across three forward rotating skills. The model was considered able to accurately represent the motion of a trampolinist in contact with a trampoline and was subsequently used to investigate optimal performance. Optimisations for maximum jump height for different somersaulting skills and maximum rotation potential produced increases in jump height of up to 14% and increases of rotation potential up to 15%. The optimised technique for rotation potential showed greater shoulder flexion during the recoil of the trampoline and for jump height showed greater plantar flexion and later and

quicker knee extension before takeoff. Future applications of the model can include investigations into the sensitivity of the model to changes in initial conditions, and activation, strength, and trampoline parameters.

ACKNOWLEDGMENTS

To Ola, and My Family

Contents

vii

List of Figures

List of Tables

Chapter 1: Introduction

Trampolining consists of alternating contact and flight phases, with somersaulting and twisting skills performed during the flight phases. In competitive trampolining, a sequence of ten different skills is performed in consecutive flight phases. The skills performed comprise different combinations of somersault rotation and twist rotation. A routine is scored based on a number of factors, including travel (the horizontal distance between consecutive landing positions) as well as the shape of the body during the skill.

During the flight phase it is possible for the trampolinist to control the speed of rotation through changes in body configuration which affect the moment of inertia of the body. Whilst airborne the trampolinist is unable to effect momentum changes affecting the movement of his centre of mass or his angular momentum. The skills performed in the flight phases are therefore limited by the orientation, configuration and angular and linear momenta of the trampolinist at the moment of takeoff and so it is during the contact phase that the correct motions must be made by the trampolinist to allow the trampolinist to perform the next skill.

In trampolining, the duration of the contact can be separated into two discrete phases: the depression and recoil phases, with the point of maximum bed depression forming the transition between the two. As the trampolinist depresses the trampoline bed there is a transfer of energy from the trampolinist to the trampoline, through which kinetic and gravitational potential energy is stored as elastic potential energy in the trampoline. During the recoil phase most of the elastic potential energy in the trampoline is released and transferred back to the trampolinist as the trampolinist is accelerated upwards.

During the recoil phase the trampolinist initiates rotation for the subsequent flight phase using hip flexion for forward somersaults and hyperextension of the back and hips for backward somersaults. However any flexion of the knees or hips during the recoil phase will absorb energy resulting in lower linear momentum for the subsequent flight phase. The compromise between height and rotation has also

been recognised and investigated in sports such as diving, but research on the takeoff phase of trampolining is limited.

1.1   Previous Trampolining Research

Early literature on the topic of trampolining or 'rebound tumbling', as it was also known, was based primarily on the observations and opinions of coaches with very little scientific basis or objective data in support. These texts are based predominantly around methods and progressions for teaching skills (Davis & McDonald, 1980; Horne, 1968; LaDue & Norman, 1954; Walker, 1983) but occasionally offer advice on the details of technique (Davis & McDonald, 1980; LaDue & Norman, 1954; Walker, 1983; Phelps & Phelps, 1990).

Early research of trampolining studied the effects of impulse on momentum in trampolining (Shvartz, 1967), the force-depression relationship of the trampoline bed (Lephart, 1971), the movements of the centre of mass during the contact phase (Lephart, 1972) and the kinetic properties of trampoline skills (Vaughan, 1980).

The majority of recent trampolining research has focused on the injury risks and prevalence of injuries sustained during recreational trampolining (Black & Amadeo, 2003; Furnival *et al.*, 1999; Larson & Davis, 1995; Murphy, 2000; Smith & Shields, 1998) and one research group has studied the effects of trampolining on sleep (Buchegger & Meier-Koll, 1988; Buchegger *et al.*, 1991), with some research having been dedicated to further understanding the mechanics of trampolining skills (Ollerenshaw, 2004), and some effort has been made to understand the physical properties of the trampoline (Jaques, 2008; Kraft, 2001).

Studies of the mechanics of trampolining are limited. Lephart (1972) explained how somersaults can be performed without travel by considering the motion of the centre of mass throughout the entire contact phase. He found that in forward somersaults the mass centre is travelling forwards at the time that the backwards force is applied; this force then decelerates the velocity centre of mass to zero at takeoff to produce rotation and eliminate the horizontal movement in flight. A

study by Ollerenshaw (2004) developed a method by which the contributions of horizontal and vertical reaction forces to the production of angular momentum in forward somersaults could be quantified. This study also developed a method for allocating force between foot contact locations for different levels of depression of the trampoline.

1.2   Statement of Purpose

The purpose of this study is to gain an understanding of the mechanics used to generate linear and angular momentum during the contact phase of trampolining and to investigate optimal technique for the production of somersault. This task will be made possible by the use of a computer simulation model of the trampolinist and the trampoline throughout the contact phase. The simulation model will then be evaluated before investigating the techniques used to create the required momenta for different skills and investigating optimal technique for the production of both forward and backward somersaults.

1.3   Research Questions

If air resistance is negligible, during the flight phase no external forces other than gravity act on the trampolinist and so at takeoff the trampolinist must have the required angular momentum with maximum vertical linear momentum and little or no horizontal linear momentum. The production of angular momentum requires energy from the trampoline that would otherwise be transferred into linear kinetic energy, reducing the vertical linear momentum (Miller & Munro, 1984). The interrelated nature of angular and linear momenta means that an optimal solution should produce the angular momentum required without compromising vertical takeoff velocity allowing the trampolinist to reach a maximal peak height.

Q1. For specific skills with a fixed rotational requirement what is the optimal takeoff technique to produce the required angular momentum with maximum peak height and minimum travel?

The interrelationship between angular and linear momenta produced during trampolining takeoff has been demonstrated (Miller & Munro, 1984; Sanders & Wilson, 1988). In order to maximise rotation potential (i.e. the product of angular momentum and flight time) the trampolinist must rotate quickly whilst staying airborne for a suitably long period of time. The greater the degree of flexion/hyperextension of the trampolinist during the contact phase and at takeoff, causes the reaction force to be more off-centre and more energy is used to create angular momentum rather than linear momentum resulting in less time in the air to complete rotation (Cheng & Hubbard, 2004, 2005; Sanders & Wilson, 1988, 1992). In order to complete the maximum amount of somersault rotation a technique that balances the production of linear and angular momenta must be found.

Q2. What is the optimal takeoff strategy to produce maximal somersault rotation potential in forward somersaults?

1.4   Chapter Organisation

Chapter 2 critically reviews the literature on the biomechanics of trampolining. The reviewed literature includes theoretical and experimental research studies, as well as coaching publications, identifying limitations of previous work and highlighting gaps in the research area.

Chapter 3 describes the methods used to collect kinematic performance data and anthropometric measurements from a trampolinist. The procedures employed to process and analyse the kinematic and anthropometric data are detailed, and graphic sequences of the trampoline movements are presented.

Chapter 4 describes the structure and function of the computer simulation model and the interactions with the trampoline suspension system. The kinetics of the trampolinist-suspension system interactions are discussed, and a method for determining the centre of pressure on the foot is outlined.

Chapter 5 details the application of the angle-driven computer simulation model of the trampolinist. The procedure for employed for the determination of the visco-elastic parameters is detailed and the angle-driven model is evaluated.

Chapter 6 details the structure and function of the torque-driven computer simulation model of the trampolinist. The torque-driven model is applied and the protocols used to scale the strength of the simulation model and to evaluate the model with fixed strength are detailed.

Chapter 7 describes the application of the torque-driven model to optimise technique and answer the research questions. The results of the optimisation of technique are reported and analysed.

Chapter 8 provides a summary of the thesis. The research questions are answered and the results obtained are summarised. The methods used in the study are discussed, and potential future applications of the simulation model are outlined.

Chapter 2: Review of Literature

2.1   Chapter Overview

In this chapter literature on the topics of trampolining and simulation modelling are reviewed. Literature concerning other areas specific to this study are also discussed and gaps in the literature are highlighted.

2.2   Overview of Trampolining Research

Early literature on the topic of trampolining was based primarily on the observations and opinions of coaches with very little scientific basis or objective data in support. Early texts are predominantly coaching literature focusing on methods and progressions for teaching skills (Davis & McDonald, 1980; Horne, 1968; LaDue & Norman, 1954; Walker, 1983) but occasionally offer advice on the details of technique (Davis & McDonald, 1980; LaDue & Norman, 1954; Walker, 1983; Phelps & Phelps, 1990).

Early research of trampolining examined the interactions between the trampolinist and trampoline; the effects of impulse on momentum in trampolining (Shvartz, 1967), and the force-depression relationship of the trampoline bed (Lephart, 1971). Research later progressed to studying the influence the trampolinist had on this interaction and how the trampolinist utilised the properties of the trampoline. Lephart (1972) examined the movements of the centre of mass during the contact phase and Vaughan (1980) investigated the kinetic properties of trampoline skills.

The majority of recent trampolining research has focused on the injury risks and prevalence of injuries sustained during recreational trampolining (Black & Amadeo, 2003; Furnival *et al.*, 1999; Larson & Davis, 1995; Murphy, 2000; Smith & Shields, 1998) and one research group has studied the effects of trampolining on sleep (Buchegger & Meier-Koll, 1988; Buchegger *et al.*, 1991), with some research having been dedicated to understanding the mechanics of trampolining skills (Ollerenshaw, 2004), and some effort has been made to

understand the physical properties of the trampoline further (Jaques, 2008; Kraft, 2001).

Investigations into the mechanics of trampolining are limited however. Studies such as those by Lephart (1972) and Ollerenshaw (2004) provide an insight into the mechanics of trampolining although there is still large scope for this to be expanded upon.

2.2.1 Takeoff

In trampolining the contact phase consists of five distinct elements: the moment of touchdown, the depression phase, the moment of maximal depression, the recoil phase and the moment of takeoff. Throughout the contact phase the trampolinist adjusts his motion so that at takeoff the trampolinist possesses sufficient linear and angular momentum to complete the next skill successfully. These two factors are required in order to provide the trampolinist sufficient flight time and angular momentum to complete the skill before touchdown for the subsequent contact phase, during which this process is repeated. It is necessary for a trampolinist to address his momenta prior to takeoff as during flight the only force acting on the trampolinist, gravity, is constant and so the motion of his centre of mass cannot be altered, but changes in his body configuration can be used to control the speed of rotation about the centre of mass. Therefore by the instant of takeoff the trampolinist must possess sufficient vertical velocity and sufficient angular momentum in order to complete the skill.

2.2.2 Height

In trampolining the peak height during flight does not currently affect directly the marks given to a routine although the maintenance of height from one skill to the next does receive consideration from the judges (FIG, 2013). Height is also important in trampolining because it provides time for skills to be executed and more than adequate height and time can give the illusion of ease that is associated with excellent performance (Miller & Munro, 1985; Sanders & Wilson, 1988).

Biomechanical studies of trampolining, diving and vertical jumping have identified some of the characteristics that can affect jump height. Both theoretical

(Cheng & Hubbard, 2004) and experimental (Shvartz, 1967) studies have associated maximal depression of an elastic surface with maximal jump height in both trampolining and diving.

Jump height is ultimately dependent on the vertical position and velocity of the mass centre at takeoff, although takeoff velocity has been found to be the primary factor in improving jump height (Feltner *et al.*, 1999; Sanders & Wilson, 1992). Many studies have associated an increase in takeoff velocity with an increase in touchdown velocity (Miller, 1984; Miller & Munro, 1984, 1985). Sanders & Wilson (1988) found that increased vertical velocity at touchdown in springboard diving allowed more energy to be stored in the springboard and then transferred back to the diver to increase takeoff velocity. In trampolining, however, the depression of the trampoline is limited by the height of the frame.

Studies investigating the movement strategies used to obtain maximal height have also been conducted in various contexts; these include squat jumps and countermovement jumps (Pandy & Zajac, 1991) and drop jumps from both rigid and compliant surfaces (Cheng & Hubbard, 2004, 2005; Miller & Munro, 1984, 1985; Sanders & Allen, 1993; Sanders & Wilson, 1988, 1992; Vaughan, 1980). Miller & Munro (1984) identified the two objectives of movement strategies in jumping from compliant surfaces as maximising the upward acceleration of the centre of mass relative to the surface during the depression phase and minimising the negative acceleration of the centre of mass relative to the surface during the last part of the recoil phase. These objectives are associated with an increased reaction force (Sanders & Wilson, 1992; Vaughan, 1980) and impulse (Shvartz, 1967) caused by maximal extension of the lower body during the depression phase (Cheng & Hubbard, 2004, 2005; Miller & Munro, 1984; Vaughan, 1980), used in conjunction with a well-timed arm swing (Miller & Munro, 1984), and maintenance of this extension throughout the recoil phase (Cheng & Hubbard, 2005).

Maximal extension of the lower body is performed from an optimally flexed position at touchdown to allow maximum range over which extension can take place (Sanders & Wilson, 1988), with hip extension beginning before touchdown (Sanders & Allen, 1993); however the amount of hip extension prior to

touchdown is limited by strength so that further flexion and energy absorption is not caused by the impact of landing. Then during the depression phase the body is not maximally extended in a proximal-to-distal sequence (Bobbert & Ingen Schenau, 1988) but with initial knee extension followed by hip and ankle (Cheng & Hubbard, 2005; Sanders & Allen, 1993; Selbie & Caldwell, 1996). The sequence does not follow the proximal-to-distal order because the body must re-orientate itself prior to propulsion (Selbie & Caldwell, 1996).

During the depression phase the trampolinist must also use the arms if the trampolinist is to apply maximal force to the bed during the contact phase (Cheng & Hubbard, 2008; Dapena, 1993; Hara *et al.*, 2006, 2008; Lees *et al.*, 2004; Payne *et al.*, 1968). Using an arm swing has also been found to increase the height of the centre of mass at takeoff in jumping (Lees *et al.*, 2004) and transfers momentum to the rest of the body when the trampolinist starts to decelerate (Harman *et al.*, 1990). In springboard diving, Miller and Munro (1984) suggested that the arm swing should commence before touchdown and should be beginning to positively accelerate at this moment, the arm swing should then continue through until takeoff or for as long as possible. However, the findings of Cheng & Hubbard (2008) suggest that another strategy allowing greater work to be done at the hips may be optimal.

During the recoil phase the trampolinist is accelerated upwards by the trampoline bed until takeoff. To maximise takeoff velocity and the height reached during a jump, the trampolinist must be able to utilise most of the energy stored in the trampoline and avoid leaving energy in the trampoline rather than transferring it into vertical velocity. An extended, straight posture, as well as increased stiffness of the knee and hip, has been associated with improved jump height (Cheng & Hubbard, 2004, 2005; Sanders & Wilson, 1988, 1992).

During the contact phase there is a continual transfer of energy between the trampolinist and trampoline suspension system. The trampolinist performs work on the trampoline during the depression phase, using a strong leg push and well-timed arm swing. The trampolinist then receives this work back from the trampoline during the recoil phase by continuing to extend in order to prevent any energy being absorbed or left behind.

2.2.3 Rotation

Rotation is caused by an external force whose line of action does not to pass through the body's centre of mass. The size of the torque and amount of angular momentum given to the body are dependent on the product of the magnitude of the force and the perpendicular distance between the line of action of the force and the axis of rotation (Stroup & Bushnell, 1969).

In trampolining the reaction force is controlled by moderating the force the trampolinist applies to the trampoline and the distance is controlled by altering the position of the centre of mass through changes in body configuration and orientation during the depression phase. The generation of angular momentum has been found to primarily take place during the recoil phase of contact (Mathiyakom & McNitt-Gray, 2007; Miller & Munro, 1985) and it is controlled by movements of the centre of mass (Ollerenshaw, 2004). Angular momentum can be transferred, during the recoil phase, from remote body segments to adjacent, more proximal body segments (Hamill *et al.*, 1986; Cheng & Hubbard, 2008).

Body configuration can be changed to create a torque by bending at the hips moving the centre of mass away from the line of action of the force (Aaron, 1970; Blajer & Czaplicki, 2001; Mathiyakom & McNitt-Gray, 2007). Leaning to change body orientation, by relaxing the plantar flexors for forward rotations, can produce a torque, moving the centre of mass from above the base of support away from the line of action of the reaction force (Page, 1974).

Early coaching literature on the production of angular momentum (specifically of forward somersaults) was of the consensus that at takeoff the arms should be thrown forward from their initial overhead position and the hips thrust backwards by piking at the hips (Musker *et al.*, 1968; Loken & Willoughby, 1967; Keeney, 1961). These motions cause the feet to push forward on the trampoline creating a horizontal reaction force backwards at the feet, producing a torque about the mass centre. These principles can also be used to explain the production of a forward reaction force in backward somersaults where the body is hyper-extended and the arms rotated backwards overhead (Cheng & Hubbard, 2008). One problem that arose from early explanations of the production of angular momentum in trampolining was the explanation of lack of gain. Whilst some authors, who were

advocates of leaning to produce angular momentum (Bunn, 1955), were confused about the position and movements of the centre of mass, others did not consider the linear effects of a non-vertical force (Griswold, 1948; Dyson, 1964).

Lephart (1972) explained how somersaults can be performed without travel by considering the motion of the centre of mass throughout the entire contact phase. He found that in forward somersaults the mass centre is travelling forwards at the time that the backwards force is applied. The horizontal reaction force then decelerates the velocity centre of mass to zero at takeoff to produce rotation and eliminate the horizontal movement in flight. The study also concluded that throughout the contact phase the centre of mass was always above the base of support, this is in agreement with Frohlich (1979) and limits the contributions of lean to the production of angular momentum.

More recent studies have shown that more complex skills require larger angular momentum at takeoff (Hamill *et al.*, 1986; Miller & Sprigings, 2001; Ollerenshaw, 2004; Sanders & Wilson, 1987). Ollerenshaw (2004) investigated the contributions of vertical and horizontal forces to the production of angular momentum in trampoline takeoffs using an experimental approach. Ollerenshaw (2004) concluded that the horizontal force, in agreement with the findings of Lephart (1972), controlled travel and also developed torque through movements of the centre of mass relative to the vertical force.

2.2.4 Inter-relationship of Height and Rotation

It has been widely recognised that both vertical velocity and angular momentum at takeoff are critical factors for the performance of somersaults (Brüggemann, 1983, 1987; Hwang *et al.*, 1990; King & Yeadon, 2004). In order for a trampolinist to rotate maximally, the trampolinist must possess a large amount of angular momentum and a large vertical velocity at takeoff, so that the trampolinist rotates quickly and has a long flight time in which to rotate (King & Yeadon, 2004). Both the generation of angular momentum and the production of jump height are dependent on the vertical force experienced by a trampolinist (Ollerenshaw, 2004; Vaughan, 1980). To reach maximal height a trampolinist must maintain a straight body position (Cheng & Hubbard, 2004) and to create

rotation a trampolinist must assume a piked position (Lephart, 1972). Thus in order to perform an optimal takeoff the trampolinist must compromise between these two factors. It is important, for the execution of somersaults, that the technique used does not produce flight time at the expense of angular momentum, and vice versa; hence optimal technique will achieve a balance between the two.

Both experimental studies of diving (Miller & Munro, 1984; Sanders & Wilson, 1988) and theoretical calculations (Stroup & Bushnell, 1969) have observed this inter-relationship. These studies found that as the somersault requirement increased there was a reduction in jump height.

The production of angular momentum requires changes in body shape but such movements detract from jump height, and therefore to produce optimal performance it is sensible that the movements must be performed with the correct sequencing, timing and magnitude (Kong, 2005). It has been suggested that for the similar motion of diving takeoffs, the optimal technique may vary depending on the individual qualities and preferences of a diver (Xu & Zhang, 1996; Xu, 2000). Kong (2005) modelled diving takeoffs with the aim of finding an optimal technique. Little is known however about optimal technique, in terms of height and rotation, for trampolining takeoffs.

2.2.5   Summary

It has long been established that the production of angular and linear momenta during the takeoff phase is of primary importance for any airborne activity. As the rotation requirement of the activity increases, the trampolinist must alter his movement patterns accordingly, although the extent to which these patterns need to be altered is unknown. The compromise between angular and linear momenta is well established, but no investigation as to the optimal balance of these factors in trampolining has been made.

2.3   The Trampoline

Competitive trampolines consist of a bed of webbed nylon suspended within a steel frame by approximately 120 steel springs. The frame of a trampoline stands

approximately 5 m x 3 m x 1 m with the bed measuring approximately 4 m x 2 m. Trampoline beds can have various sizes of webbing, ranging between 25 mm and 4 mm wide, with the width and spacing of the webbing affecting the stiffness of the bed. The springs have a natural length of approximately 35 cm, and suspend the bed in tension by hooking on to the frame and bed along both the length and breadth of the trampoline.

2.3.1   Modelling the Trampoline

Few attempts have previously been made to model the trampoline (Blajer & Czaplicki, 2001; Jaques, 2008; Kraft, 2001; Lephart, 1971); more effort has been made to model other compliant surfaces, such as springboards (Kong, 2005; Kooi & Kuipers, 1994; Sprigings *et al.*, 1989) and crash mats (Mills, 2005).

Lephart (1971) made an early attempt to understand the force-displacement relationship of the trampoline by taking static measurements of the upward pull of the trampoline bed when depressed using scales. By measuring the force at one inch intervals up to a depression of twenty inches, a non-linear vertical force-displacement relationship was identified. In other early analyses of trampolining, Riehle (1979) and Vaughan (1980) modelled the vertical motion of a trampolinist as simple harmonic motion, and Vaughan (1980) included damping to account for discrepancies in the accelerations. However, Kraft (2001), in agreement with Lephart (1971), believed that the trampoline could not be accurately represented by an ideal Hookian spring due to the construction of the trampoline, even if the trampoline springs were themselves linear springs, due to the changing angle of the springs throughout the contact phase.

Kraft (2001) developed a theoretical equation for the vertical force, F_v, exerted by a trampoline at a given depression based on the physical geometry of the trampoline as a cross-section across the trampolines width. The relationship he derived is shown in Equation 2.2.1.

$$Fv = \frac{-D.s.[l_0 + \sqrt{(s^2 + b^2)} - b]}{\sqrt{(s^2 + b^2)}}$$

(2.2.1)

Where: s = vertical depression of the bed

D = stiffness of the springs

l_0 = stretch of the springs at equilibrium

b = distance from the frame to the nearest point of action

This model combined the 20 springs on either side of the trampoline to represent them as a single spring. The model was then used to investigate vertical trajectory and contact time in trampolining.

Blajer and Czaplicki (2001) investigated the vertical, horizontal and rotational force-displacement relationship of a trampoline in order to understand the motion of a gymnast. The study found the vertical force to be non-linear with respect to displacement and a linear horizontal force-displacement relationship.

Kennett *et al.* (2001) used finite element modelling to simulate a recreational trampoline as a system of 7948 isolinear 4-noded membrane elements suspended by 88 springs. In experimentation with various types of spring model it was discovered that the pretension of the trampoline is a vital element of the response of the trampoline bed. However the model was unsuccessful as the software used was unable to add the required level of damping, resulting in high frequency vibration of the trampoline bed, much like a drum skin.

All the previous studies have neglected the inertial characteristics of the trampoline itself, and their effect on the force-displacement relationship. Jaques (2008) modelled the trampoline as a system of linear springs and point masses based on experimental measurements and found that the vertical and horizontal force-displacement relationships were non-linear and linear respectively with the horizontal force also dependent upon the vertical displacement. The trampoline model was a system of thirty-eight undamped linear springs and 15 point masses in order to represent the stiffness and inertial properties of the bed and springs of the trampoline. Such complexity allowed this model to simulate off centre impacts, although with limited resolution. The springs that represented the elastic properties of the bed and springs were given different stiffnesses to characterise

their different properties, and multiple trampoline springs were represented in this simplified model with a single spring of increased stiffness. This model was evaluated using forces measured by force transducers during dynamic tests, and was found to closely represent the vertical motion of the bed. It was less accurate however in modelling horizontal forces.

Other compliant surfaces have been modelled by masses and springs in multiple arrangements. Sprigings *et al.* (1989) modelled a springboard as a single mass and undamped linear spring in order to represent its vertical motion, whilst Kooi and Kuipers (1994) developed a model that consisted of a series of torsional springs connected by solid bars; this modelled the motion of the springboard in two dimensions. Kong (2005) modelled the springboard as a rod with vertical, horizontal and rotational degrees of freedom. Mills (2005) modelled gymnastic landing mats as three damped linear spring and masses in series representing the different component layers.

2.3.2   Measuring Trampoline Parameters

The equation derived in Kraft (2001) required three parameters to be determined: the stiffness of the springs, the stretch of the springs with the bed at equilibrium and the shortest distance from the frame to the point of force application. These parameters were determined experimentally with the use of simple static length and displacement measurements. The stiffness, k, of the springs can be determined by the application of Hooke's Law:

$$F = k.y \qquad (2.2.2)$$

Where: F = applied load

y = resulting extension

The lengths of eight randomly selected springs were measured when in situ with the trampoline at rest before being removed from the trampoline and measured with loads of 0, 5, 10, 15 and 20 kg. From these measurements the mean stiffness of each spring was determined to be 703 Nm^{-1}, this relationship was extrapolated, correcting for weight, to find that the natural length of the springs and their extension when the trampoline is at rest. The trampoline was also tested as a

whole by loading centrally positioned trays of 20 cm x 20 cm with 15 loads up to 362 kg and 40 cm x 50 cm with five loads between 153 kg and 533 kg. The vertical stiffness of the trampoline for different contact areas was then determined by minimising the sum of error squares for the measurements from the two trays; this spring constant is the stiffness of the trampoline bed and is different to the spring constant, k.

Simple laboratory tests were used by Kennett *et al.* (2001) to determine the parameters of their model. They conducted drop tests over the area of the trampoline bed and took measurements using a string potentiometer to measure time-displacement properties. Although the method used by Blajer and Czaplicki (2001) to determine input parameters is unclear, it seems that known loads were applied and the resulting displacements were measured as well as damping coefficients being observed from vibrations of the trampoline bed. The authors acknowledged that better measurements of bed deflection during performance were required to improve the accuracy of the model.

The input parameters for the model of Jaques (2008) were determined through static measurement of the stiffness of the springs and length and mass measurements of the bed and springs in situ and in their natural state. The dimensions of the bed and springs were measured whilst under tension before being removed from the trampoline to be weighed and to measure the dimensions of the bed and length of the springs under no tension. The springs were then loaded with known masses up to 35 kg, to give a range of extension representative of those experienced by the springs during trampolining. The extension of the springs under each load was measured and the stiffness of the springs was calculated using Hooke's Law. In the construction of the model the mass of the bed and springs was distributed between the point masses depending on the mass of the components represented by the elements connected to that specific mass. The stiffnesses of the springs representing the bed were calculated with extensions taken from the difference between the length measurements taken under tension and in the natural state, assuming they were in equal tension with the springs connected at either end.

2.3.3   Limitations of Previous Trampoline Models

Previous models of trampolines have either given estimates of forces relative to displacements (Lephart, 1971), only modelled the vertical component of force (Kraft, 2001; Lephart, 1971), not been properly evaluated (Blajer & Czaplicki, 2001; Kennett *et al.*, 2001; Kraft, 2001; Lephart, 1971), or have neglected the effect that the mass of the trampoline suspension system, and the force required to accelerate this mass, affects the reaction force experienced by the trampolinist.

2.4   Computer Simulation Models

2.4.1   Overview

Computer simulation of human movement involves the description of motion through the development and application of mathematical equations and can help us to understand the mechanics of a sporting movement. The processes required to develop a computer simulation model include the definition of the problem, the derivation of the governing mathematical equations, the writing of the computer program, the determination of input values, validation of the model, and the completion of simulation experiments (Vaughan, 1984). The use of simulation models is very useful in experiments where variables can be changed and controlled in a way that would be impossible in experimental studies, allowing new techniques to be investigated without the risk of injuring an elite athlete.

However useful computer simulation models may be to investigate physical phenomena, they require expertise in both the field of mathematics and computer programming to develop and implement (Vaughan, 1984) and the result is still only a group of mathematical equations that may or may not be representative of the problem at hand or have sufficient accuracy to answer the problem posed (Panjabi, 1979; Sargent, 2005). Specialised computer programs for the construction and development of simulation models are commercially available to help derive the mathematical equations (e.g. AUTOLEV, DADS, MADYMO), and have broadened the scope of simulation modelling. However, knowledge of the movement, modelling and an understanding of the processes is essential to apply the software correctly and interpret its output. If mathematical theory and

the modelling process are applied correctly the resulting model should be representative of the problem but this cannot and must not be assumed. All simulation models should be verified and validated before any findings from the model are trusted (Sargent, 2005). Yeadon *et al.* (1990) performed such an evaluation through the comparison of the performance outcome from their simulation model to experimental data obtained from a performance of the trampoline skill upon which the simulation was matched.

2.4.2 Trampolining Simulation Models

Simulation models have been used in trampolining in order to learn about numerous aspects of the sport, including the determination of joint torques (Blajer & Czaplicki, 2001, 2003) and internal forces during contact (Blajer & Czaplicki, 2003, 2005), to understand the controlling movements in somersaults (Flynn & Simms, 2003), as well as more technical usage in the development of trampolining robots (Takashima *et al.*, 1998) and image recognition systems (Kikuchi & Nakazawa, 2004). However progress has been slowed by the complexity of modelling the trampoline itself and the only study to utilise a specialised trampoline model is that of Flynn and Simms (2003). Simulation work of similar sports, such as gymnastics and diving, that do not require such a complex prerequisite as well as aerial movement in general, are much more advanced (Cheng & Hubbard, 2008; King & Yeadon, 2004; Yeadon, 1990a, b, c; Yeadon *et al.*, 1990).

Previous studies on trampolining by Yeadon (1990) have been in two dimensions with the exception Kikuchi & Nakazawa (2004) who used a three-dimensional simulation model consisting of sixteen segments with thirty-one degrees of freedom (DOF). This model was only used to track the motion of a trampolinist during the flight phase and so did not require feet, however the spine was modelled as two segments along with a separate segment for the pelvis.

Takashima *et al.* (1998) developed a planar three-segment, 5 DOF model actuated by torque generators to be used in conjunction with a robot in order to try and replicate the repeated bouncing of a trampolinist. The segments represented the lower leg, thigh and trunk of a trampolinist, and the torque generators were simple

to represent the motors of the robot rather than the complex torque development profile of human muscle. The aim of the simulation was to perform jumps without rotating so that it did not fall down, jump off the trampoline or lose height. This simple model was able to achieve this for over 100 consecutive jumps. The robot however could only perform ten jumps, showing that there were differences between the model and the robot.

Blajer and Czaplicki (2001, 2003, 2005) used a planar, seven-segment rigid link system driven by six torque generators in order to investigate the joint torques and internal joint forces that act during the contact phase. The model assumed that bilateral limb movements were synchronous and used a single segment to represent the foot. In this study the joint torques were calculated by inverse dynamics, or similar method, for use in the forward dynamics simulation. This model, although being simple, performed well and demonstrated that joint torques determined by inverse dynamics can be used as input for a forward dynamics model, although this has limitations in the modelling of hypothetical movements.

A simulation model was constructed by Flynn and Simms (2003) in order to study the rotation of back somersaults and was used in conjunction with a Kraft (2001) trampoline model. The model was angle-driven and consisted of eight segments, including single segment feet but no arms, the mass of the arms being included in the torso. The model was driven by joint angle time histories from digitised video of performances of ¾ and 1¼ back somersaults having been given the same initial conditions to investigate the effects of changes in the body configurations.

Previous simulation models of trampolining have been relatively simple and have not attempted any kind of optimisation of performance, possibly due to the lack of an accurate model representing the important characteristics of the trampoline. The aims of trampolining are quite clear, to produce linear and angular momentum whilst controlling the horizontal motion of the centre of mass. The construction of a satisfactory model of the forces exerted by a trampoline on a trampolinist could be combined with a trampolinist in order to answer more complex questions concerning the movements required during the contact phase in order to produce optimal performance.

2.4.3   Non-trampolining Takeoff Simulation Models

A large volume of research has been conducted using computer simulation of takeoffs in various sporting contexts, ranging from standing vertical jumps [e.g. basketball] (Anderson & Pandy, 1999; Dapena, 1999; Feltner *et al.*, 1999; Haguenauer *et al.*, 2006; Jacobs *et al.*, 1996; Pandy *et al.*, 1990; Selbie & Caldwell, 1996; Spägele *et al.*, 1999; van Soest *et al.*, 1993; Virmavirta, *et al.*, 2007), to running vertical and horizontal jumps [e.g. high jump and long jump] (Alexander, 1990; Dapena & Chung, 1988; Hatze, 1981a; Mesnard *et al.*, 2007), jumping from compliant surfaces [e.g. springboard diving] (Boda, 1992; Cheng & Hubbard, 2004, 2005, 2008; Kong, 2005; Liu & Wu, 1989; Sprigings *et al.*, 1986; Sprigings & Miller, 2002; Sprigings & Watson, 1985) and somersaulting jumps [e.g. gymnastics] (Hamill *et al.*, 1986; King & Yeadon, 2004; Yeadon & King, 2002). Whilst being applied in very different ways many of these models are similar in their construction often with slight changes to apply a certain goal of performance. These models of similar tasks can provide an important insight into modelling trampolining takeoffs.

Some studies have used extremely complicated simulation models in an attempt to reproduce the kinetic, kinematic and muscular patterns of vertical jumps (Anderson & Pandy, 1999; Hatze, 1981a; Spägele *et al.*, 1999). Hatze (1981a) used a 17-segment muscle-driven model that had 42 DOF and 46 muscle groups to simulate long jump takeoffs. This is still one of the most comprehensive models used to date although the amount of input data required to run the model led it to be a time consuming process. Anderson and Pandy (1999) developed a three-dimensional, 10-segment model of vertical jumping with 23 DOF powered by 54 muscle groups that was able to accurately reproduce all elements of a vertical jump (Pandy & Anderson, 2000).

Yeadon and King (2002) developed a subject-specific, five-segment, torque-driven model of tumbling which was personalised through the determination of subject-specific strength parameters (King & Yeadon, 2002). The same model was later used in other studies to investigate the robustness of the model to perturbations in layout somersaults (King & Yeadon, 2003) and to optimise somersault performance in tumbling (King & Yeadon, 2004).

An eight-segment model with eight DOF, with wobbling masses and actuated by torque generators was used by Kong (2005) to optimise the performance of a diver. The model had a two-segment foot and the foot/springboard interface was modelled using three pairs of perpendicular damped linear springs. The model was personalised to the diver through inertia, torque and visco-elastic parameters, and was used in conjunction with a springboard model in an optimisation process which first matched simulations to performances and then found a strategy to produce an optimal amount of rotation during flight. Values for the input parameters describing the elastic properties of the foot contact for the torque-driven model were extremely difficult to determine experimentally and so these were obtained through a matching procedure using an angle-driven model. This model was able to increase angular momentum by 28% and increase maximum height by two centimetres.

2.4.4 Wobbling Mass Models

The majority of biomechanical models of the human body are composed of rigid segments; however the human body is not rigid and is composed of soft flesh surrounding a rigid bone structure. The soft flesh comprises muscle and organs held in place by connective tissues with elastic properties, whilst the muscles themselves alter the elastic properties when activated. Cavagna (1970) conducted an early study to investigate the elastic properties of the body during a landing on the balls of the feet with the calf contracting, following a small vertical jump. The stiffness of the elastic structures of the body was measured by observing the oscillatory motion of the body and was found to increase with the load on the body in a similar relationship to that of the series elastic component of muscle.

Nigg and Liu (1999) used a wobbling mass model to simulate impacts during running and to investigate peak GRF. The model used two pairs of rigid and wobbling masses to represent the supporting leg and the rest of the body linked by a combination of springs and spring-damper units to represent the series elastic components and contractile elements, respectively, of muscle tendon units. The model was able to closely match experimental force measurements, and was used to conclude that the elastic properties of the connections between the soft and rigid elements of the model had a strong influence on the peak impact forces.

Similarly, Gruber *et al.* (1998) conducted a comparative investigation of rigid segment and wobbling masses, looking at the ground reaction force (GRF) and joint torques produced by the two models. The models consisted of three segments with identical inertia parameters, however the wobbling mass model separated the mass of each segment into fixed and wobbling parts that were coupled with quasi-elastic and strongly damped connections. The study showed that rigid body models are inadequate to represent the GRF and internal torques during impact and that the use of a forward dynamics rigid body model could lead to systematic over-estimations of GRF and joint torques.

The use of wobbling mass models has continued in modelling impacts of the lower leg, investigating the effects of a heel pad, the elastic properties of the rigid mass-wobbling mass connection and the segmental bone-soft tissue ratios on GRF, energy dissipation, joint torques and joint reaction forces. Pain and Challis (2001) used a model combining wobbling masses with a heel pad and a deformable knee to investigate the effect of all soft tissue in lower leg impacts. The knee and heel pad were modelled by spring dampers in series with the lower leg represented by a wobbling mass coupled to the rigid body by non-linear translational spring damper actuators. This model was then impacted by a pendulum to study the energy dissipated during impacts. It was concluded that both the heel pad and the wobbling mass play vital roles in the dissipation of energy during impacts.

The same research group used a three-segment model with wobbling masses and a heel pad to investigate the sensitivity of the simulated GRF and thigh angle to changes in the model's parameters (Pain & Challis, 2004). The parameters were changed by ±20% and whilst the segmental bone-soft tissue mass ratios and joint stiffnesses were found to have large effects, changes in the stiffness of the connection between the bone and soft tissue had little effect. Subsequently the same model was used with subject-specific input parameters to investigate GRF, joint torques and joint reaction forces during impacts (Pain & Challis, 2006). Subject-specific inertia parameters were determined, the mass ratios of the rigid and wobbling masses were based on cadaver data of Clarys & Marfell-Jones (1986), a heel pad model was included and the spring-damper connection

parameters and initial kinematics were experimentally determined. This model was able to simulate the GRF to within 5% over the first 40 ms and within 12% over the first 100 ms, as well as matching joint angles to within 3° after the first 40 ms.

The majority of research using wobbling mass models has been in simulating impacts with rigid surfaces, however recently some investigation into impacts with compliant surfaces have taken place. Yeadon *et al.* (2006b) determined a single set of subject-specific input parameters for an eight-segment, wobbling mass model of springboard diving to be used for multiple performances by combining the visco-elastic parameters determined for individual performances in order to generalise them for multiple performances. The results of the model were tested for sensitivity to changes in the wobbling mass parameters, and a change of less than 1.5% was found for increases of 500 times in all the wobbling mass parameters. This result suggests that simulating jumping from compliant surfaces does not require the inclusion of wobbling masses. Wilson *et al.* (2006) also used a combined matching approach for the determination of visco-elastic parameters for use in a wobbling mass simulation of running jumps. Mills *et al.* (2008) has also used a simulation model including wobbling masses to study the influence of model complexity on estimates of internal loading in gymnastics landings onto a compliant mat.

2.4.5 Summary

Simulation modelling is an extremely useful tool when answering speculative questions, and has become increasingly popular in sports biomechanics as advancements in technology have been made. The level of complexity that is required in the simulation model is dependent on the level of accuracy required to answer the questions of the researcher. Assumptions made in the creation of the model can be validated when the model is evaluated by attempting to match an actual performance. After validation the model can be applied to situations for which it has been validated to investigate and optimise techniques.

2.5   Simulation Model Input

Simulation models require parameters as an input to provide information concerning the initial conditions of a simulation, the characteristics of the model's components, the capabilities of the model and how the different components of the model interact. Model parameters, such as strength and inertia parameters can be determined experimentally, through the application of another model or through optimisation when the information required cannot be measured directly.

2.5.1   Strength Parameters

In a torque-driven or muscle-driven simulation model the strength parameters of the model greatly affect the resulting simulations of human movement; therefore it is important that the strength parameters are representative of the subject and the capabilities of the muscles about the joints. In order to achieve this, muscle models have been developed and are personalised to subjects using methods described in this section.

2.5.1.1 Muscle Modelling

Human muscle is a complex structure, comprising many elements which have their own complexities, and is activated through electrical signals in the nervous system. Muscle reacts to the same activation differently under different conditions involving length, velocity of shortening and previous activation history. For over 70 years researchers have been endeavouring to understand the properties and relationships associated with muscular contractions and studies have investigated the behaviour of muscle at microscopic and whole-muscle levels.

An initial attempt made to investigate the behaviour of muscle was made by Hill (1938), through investigations of the thermodynamics of muscle action under controlled experimental conditions. A frog muscle was tetanically activated under isolated conditions and observations of a relationship between the force produced by the muscle and the velocity at which it was shortening during the contraction were made. The results of these experiments were used as the basis for a model with a structure that represented the muscle along with the connective tissues as a contractile element (CE), a series elastic element (SE) and a parallel elastic

element (PE). The CE represents the muscle fibres, the SE represents the tendons and other elastic connective tissues that are connected in series with the muscle fibres, and the PE represents the passive elastic properties of the muscle fibres along with the elastic connective tissues that encase the muscle fibres.

The experimental results of Hill (1938) were used to derive a hyperbolic function describing the force-velocity relationship of the muscle during concentric contraction, which took the form:

$$(F + a)(v + b) = (F_{max} + a) b \qquad (2.4.1)$$

Where: F = tensile force produced by the muscle

v = shortening velocity of the muscle

F_{max} = maximum tensile force produced by the muscle

a, b = constants

Hill (1938) was able to express a complex function of human muscle successfully using a simple equation. This has enabled the widespread use of Hill-type muscle models and allows many muscle models to be used in one simulation, leading to the development of complicated muscle driven simulation models (Hatze, 1981a).

The classical models have been tailored for use in many simulation models with a number of different modifications and structures being used (Bobbert *et al.*, 1986; Hatze, 1981a) and also with the addition of activation profiles that have attempted to simulate EMG profiles (Pandy *et al.*, 1990; Rácz *et al.*, 2002). Hawkins and Smeulders (1998, 1999) modified a Hill-type model to translate the force-velocity relationship of muscle into a torque-velocity relationship for multiple muscles acting about a joint whilst also incorporating an activation profile. Recent investigations into the accuracy of a Hill-type model to different types of muscle have found that modifications have to be made to the model in order to account for the proportions of fast and slow twitch muscle fibres within the muscle (Raikova & Alodjov, 2005; Stojanovic *et al.*, 2007). Scovil and Ronsky (2006) studied the sensitivity of a Hill-based model to perturbations in the model parameters, the authors discovered that whilst the muscle model is very sensitive

to changes in a large number of parameters, simulations of running and walking were not as sensitive and were affected by changes in fewer parameters.

Further investigation into the contraction characteristics of muscle has led to the determination of the force-velocity relationship in eccentric contractions as well as the discovery of a force-length relationship. Throughout a complete range of velocities the force-velocity relationship of muscle has been found to be double-hyperbolic in nature (Edman, 1988) with greater forces generated in maximal eccentric than isometric contractions. Huxley (1957) conducted a study of muscle at a microscopic scale and developed a theory concerning the structure and action of muscle at the molecular level, and developed the cross-bridge muscle model. Gordon *et al.* (1964, 1966a, b) continued this work and described this force-length relationship.

It has been shown that the Hill model of muscle action does not accurately represent all the characteristics of muscular contraction. Despite the limitations of the model it has still become widely accepted and has been used in many successful simulation models. The primary strengths of Hill-type models is in their simplicity and their ability to represent the function of a whole muscle in vivo; because so little computation is required, multiple Hill-type models can be used within the same simulation. Anderson and Pandy (1999) employed a 10-segment model driven by 54 different Hill-type models to simulate vertical jumping in three dimensions.

Sporting simulations, such as Anderson and Pandy (1999), have used whole body models driven by many muscle models. However this adds an unnecessary level of complexity unless the sequencing of individual muscle activity is the question at hand. Recent studies have moved toward the use of a single torque generator about a joint in order to represent the rotational effects of all the muscles acting about the joint (Yeadon & King, 2002).

2.5.1.2 Strength Measurement

In order to personalise a simulation model to an individual, muscle parameters must be based on the capabilities of that person; this requires knowledge of the strength of the individual in performing particular actions. It has been shown previously in experimental studies that measured EMG activity can be used as a measure of the torque produced about a joint (Cramer, 2002; Tate & Damiano, 2002) and a relationship between EMG and muscle force has long been suggested (Bayer & Flechtenmacher, 1950). However the exact nature of the relationship and the mechanism that acts between EMG and muscle force is still disputed and so the ultimate goal of determining muscle forces from EMG data has been attempted using quantitative data (Hof & van den Berg, 1981a, b, c, d) but cannot yet be performed reliably; Alkner *et al.* (2000) found three differing relationships for three different quadriceps muscles in a single subject. It seems that the relationship between EMG and muscle force remains uncertain and does not provide an accurate means to drive a simulation model.

A single torque generator can be used to represent the net torque produced by all the muscles that act about a joint removing the complexities of individual muscle actions, and the torque production capabilities of an individual can be measured directly using an isovelocity dynamometer. Electronic isovelocity dynamometers (e.g. Contrex, Biodex, Kin-Com) measure the torque applied by a muscle group about a joint during isotonic concentric and eccentric motions, as well as during isometric contractions. Data can be collected for all the required muscle groups for a large range of velocities and can be processed to provide a complete strength profile for a subject to be used in conjunction with a simulation model (King & Yeadon, 2002; Yeadon *et al*, 2006a).

An isovelocity dynamometer measures the net torque applied to a mechanical lever arm rotating about an axis therefore the axes of the joint and the dynamometer must be aligned properly and fixed securely in place or a conversion must take place so the torque data corresponds to the actual joint angle rather than the crank angle of the dynamometer. The net torque output of the dynamometer must also be corrected for the torque due to gravity (Herzog, 1988) as this has been shown to introduce up to 510% error in knee flexion (Winter *et*

al., 1981). Herzog (1988) also noted that the inertial effects of the machine and the non-rigidity of the crank arm-human system must be taken into account in order to accurately derive joint torque data from the dynamometer output.

As discussed earlier, human muscle is complex and accurate representation of its properties requires consideration of the velocity and length of the muscle. In order to create an accurate representation of an individual's ability to create a torque about a joint the isovelocity dynamometer must be used to collect data over a range of velocities and joint angles that encompasses the joint motions that the simulation model will be applied to. Kawakami *et al.* (2002) studied the shift of the angle at which peak torque occurred with velocity and concluded that the evaluation of force-velocity relationship of muscle through isovelocity dynamometry should be conducted by means of peak torque rather than angle-specific torque. On the other hand Rácz *et al.* (2002) concluded that the use of mean torque reflected the working capacity of the muscle and allowed a superior fit to a Hill-type model. However, in order to represent all the properties of muscle a three-dimensional surface function must be adopted to show the maximum torque capabilities at a particular angle and velocity (e.g. Khalaf *et al.*, 2000; King & Yeadon, 2002).

Such torque profiles model maximal torques and assume that the torque production about a joint is only dependent on the position and velocity of the joint but this is not the case, the torque produced about a joint is also dependent on the activation level of the muscles that act about the joint (Westing *et al.*, 1990) and, in the case of biarticular muscles, can also depend on the position and velocity of adjacent joints.

Yeadon *et al.* (2006a) combined a model of a tetanic torque-angular velocity relationship with an activation-angular velocity relationship and the resulting product was able to closely fit experimental data, the study concluded that an activation profile must be included in a model simulating actions with both maximal concentric and eccentric phases. Starting knee angle has also been shown to affect the angle of peak torque (Pavol & Grabiner, 2000); this is possibly associated with activation levels. However this highlights the importance of the range over which torque is measured and movement history; torques measured

28

over a range of angles should not be applied to movements over angles outside the measured range without caution and previous movements should be taken into consideration.

Pavol and Grabiner (2000) also found that both the knee and hip angles had large effects on knee extensor torques as well as there being a large variation in the effects between subjects. Attempts have been made to understand the contributions of biarticular muscles to various motions in investigations utilising simulation models (e.g. Jacobs *et al.*, 1996) and it would be advantageous to include the effects of adjacent joint positions and velocities within the model of a torque generator that represents the action of biarticular muscles. Lewis *et al.* (2012) modelled the leg and found that whilst torque-driven models that account for the angle and angular velocity of adjacent joints can more accurately represent the torque output of biarticular muscles, it is only necessary when the knee was flexed by an angle of 40° or greater.

Previous muscle-driven simulation models have obtained their muscle parameters from values published in various literature sources, however such models are not specific to any particular subject and therefore the validity of their application is limited. Attempts have also been made to construct a generic torque-driven model from data collected from a small population, although it was found that inter-subject variation in torque-velocity responses greatly limited the value of such a model (Hawkins & Smeulders, 1999).

King and Yeadon (2002) developed a method of determining a set of subject-specific strength parameters to be used in conjunction with a simulation model of dynamic jumping by simulating the muscle function of contractile and series elastic components. An eighteen parameter surface function was produced to express the torque-angle-angular velocity relationship of a joint in which the torque-angular velocity relationship was modelled by a six parameter exponential function. Each of the positive parameters was expressed as a quadratic function of joint angle to incorporate the torque-angle relationship. The model parameters were determined by fitting the relationship to data obtained from experimental protocol using an isovelocity dynamometer. Wilson (2003) developed a nine parameter function using a similar method.

Yeadon *et al.* (2006) combined a seven parameter function that matched torque-angular velocity profiles measured using an isovelocity dynamometer in conjunction with a three parameter activation profile. The inclusion of the activation profile improved the specificity of the muscle-tendon complex to the function of human muscle. The activation profile incorporated the ramping characteristics of human muscle activation. Such activation profiles can be used to control the number of times that a torque generator can ramp up and down.

Recent methods have used indirect measurements of joint torques; King et al. (2009) developed a novel method to determine joint torque parameters without direct measurement. Joint torques profiles were obtained from computer simulations of multiple actual diving takeoff performances, with the maximum values taken from the selection of performances. This meant that the final joint torque profiles could achieve the maximum torques produced during the recorded performances. This approach has the advantage of not requiring dynamometer measurements to implement, which also requires both access to the subject and time to measure and process the data.

2.5.1.3 Summary

In order for a simulation model to represent human performance accurately it must be limited in its abilities by parameters that are the equivalent of the limiting factors in humans. One of the primary limiting factors in sporting performance is strength, which can be measured using isovelocity dynamometers over a range of velocities and angles at a number of joints. The resulting strength profiles can then be used in conjunction with muscle models to power whole-body simulation models using a single torque generator at each joint, or contractile elements representing individual muscles, or simply using the strength profile to limit the torques produced by an angle-driven model.

2.5.2   Body Segmental Inertia Parameters

In order to simulate the motion of a body it is essential to know the inertial characteristics of the body and all its constituent parts. These inertial characteristics are the mass, position of the centre of mass and the moment of

inertia, and when simulating a movement using a model consisting of multiple segments it is necessary to have knowledge of these three parameters for each segment of the simulation model. Previous studies have obtained this data for human beings from dissecting cadavers and directly measuring each quantity experimentally (Chandler *et al.*, 1975; Dempster, 1955) and the resulting segmental inertia parameter data has been used in many different simulation models (e.g. Yeadon, 1990c).

Cadaver data can also be scaled by use of regression equations (Hinrichs, 1985; Yeadon & Morlock, 1989; Zatsiorsky & Seluyanov, 1985) and other methods (Forwood *et al.*, 1985). Forwood *et al.* (1985) found scaling to height to be better than scaling to segment lengths although this was still inaccurate and the method was not applicable about the longitudinal axes of segments. Hinrichs (1985) was successful in scaling inertia parameters using linear regression equations but only for a limited range of statures. In the process of reducing the data for analysis each segment was simplified to be symmetrical about the longitudinal axis. Zatsiorsky and Seluyanov (1985) developed predictive regression equations based on cadaver data and data obtained from CT scans (Zatsiorsky & Seluyanov, 1983), the reference points for which were then adjusted by de Leva (1996) to enable them to be used more easily. Yeadon and Morlock (1989) investigated the use of different linear and non-linear regression equations to estimate inertia parameters based on the data of Chandler *et al.* (1975), and discovered that non-linear regressions were able to predict moments of inertia with less than twenty percent error whereas other regression equation could give negative moments of inertia in extreme body types (Hinrichs, 1985). However, although Chandler's data can be scaled to individuals, the cadavers from which the data were taken were not representative of an athletic population and so the scaled data may not even be close to the actual inertial characteristics of an athlete, and a set of subject-specific segmental inertia parameters would be a large improvement.

Subject-specific segmental inertia parameters can be obtained from geometrical models such as those developed by Hanavan (1964), Jensen (1976), Hatze (1980) and Yeadon (1990). Geometrical models represent the body as a number of different geometric shapes in place of the body segments, the dimensions of the

shapes are scaled to fit anthropometric measurements taken from the subject and are given densities based on cadaver data. From the known shapes and densities the segmental inertia parameters can then be calculated for use in a simulation model. Such geometric models differ from each other in the different segments used in the model, the shapes that are used to represent the segments and the methods for obtaining the anthropometric measurements.

Sarfaty and Ladin (1993) developed a method of estimating segmental inertia parameters based on video footage and density data from Dempster (1955). The method modelled segments as cylinders and assumed that mass was evenly distributed throughout the body segments.

Done and Quesada (2006) used an innovative method of deriving body segment parameters for the lower leg from kinematic data and evaluating work and energy of the body segment. Durkin and Dowling (2006) experimented with using dual energy X-ray absorptiometry (DEXA) scans and anthropometric measurements to develop and validated a three-segment model of the lower leg; however this method would be expensive to determine a complete set of inertia parameters for multiple subjects.

The various methods of estimating body segment parameters have been compared within experimental simulations of complex airborne movements by Kwon (1996; 2000; 2001). Kwon (2001) found that methods provided very similar results for rotations about the lateral axis although body segment parameters determined through personalised methods provided more accurate rotations about the longitudinal and frontal axes. Hatze (2005) also compared different methods of estimating segmental inertias and concluded that the use of anthropometric measurements was the most accurate method.

2.5.3   Kinematic Data

2.5.3.1 Image Analysis

Alongside the measurement of forces and other kinetic methods, the analysis of images to obtain kinematic data is a primary branch of biomechanics. Two-dimensional image analysis has been widely carried out through various methods

of digitisation where the positions of landmarks of the image are logged as coordinates. However more recently analysis of three-dimensional motion has become increasingly important and so three-dimensional analysis of images is required. Three-dimensional image analysis requires movements to be filmed within a calibrated environment by two or more cameras for digitisation by manual or automatic systems. The images must be synchronised so that the timing offsets between all images are known. This can be achieved through the use of timing lights, genlocking the cameras, observation of critical events in explosive movements, through mathematical methods (Pourcelot *et al.*, 2000; Yeadon & King, 1999) or by using the audio band (Leite de Barros *et al.*, 2006). The synchronised and digitised image coordinates can then be reconstructed in three-dimensional space using the direct linear transformation (DLT) (Abdel-Aziz & Karara, 1971). DLT requires 11 parameters, concerning the position and orientation of the camera, and scale and shear factors of the images, to be calculated from points in the calibration images before the movement coordinates can be reconstructed in three dimensions. These points used to calculate the parameters should be spread evenly throughout the calibration volume to achieve accuracy through the space (Yeadon & Challis, 1994). DLT methods have also been developed to accommodate panning (Yu *et al.*, 1993) and tilting has been accomplished in a non-DLT method (Yeadon, 1989) of cameras for use over larger areas or where space is limited.

2.5.3.2 Data Processing

Raw kinematic data obtained from digitisation, whether it be manual or automatic, will contain random noise created by errors in the digitisation process that contaminate the signal. Random noise can be amplified by any numerical differentiations that may be performed on the data. Ideally there would be no noise and to try and remove the noise, and increase the signal-to-noise ratio of the data, smoothing procedures, in the form of mathematical functions, can be applied. Butterworth filters (Pezzack *et al.*, 1977), Fourier series (Hatze, 1981b), quintic splines (Wood & Jennings, 1979) and quintic splines with cross-validation (Craven & Wahba, 1979; Woltring, 1985) are some of the methods of data smoothing. However the amount of smoothing required and other effects of

smoothing procedures must be considered in order to select an appropriate method (Yeadon & Challis, 1994). All the methods mentioned above are proven to fit displacement data accurately although a digital filter such as a Butterworth filter comprises two frequency cut off points outside of which data is removed, this results in an output that is not suitable for further computations such as differentiation. Other functions, such as Fourier series and cross-validated polynomial fits require equidistant data and so can only be applied to data with consistent sampling rates (Wood, 1982; Woltring, 1985). Wood (1982) concluded that spline functions were ideal to interpolate time history data, whilst quintic splines have been shown to provide the most accurate second derivative data (Challis & Kerwin, 1988) and not to suffer from boundary effects in the endpoint regions (Vint & Hinrichs, 1996; Woltring, 1985).

2.6 Optimisation

Optimisation algorithms are frequently used alongside simulation models to search for an optimal solution to a problem, to find an optimal technique (e.g. Hiley & Yeadon, 2007) or to match a simulation to a performance to attain the best set of parameter values (e.g. Ait-Haddou *et al.*, 2004). The optimisation of computer simulations is necessary when there are parameters that govern the performance that cannot be measured, either directly or indirectly. Search algorithms are able to converge on the optimal set of parameters through the systematic search of a specified area to minimise or maximise a cost function.

The optimisation of sports techniques has been accomplished using various different optimisation algorithms including the simulated annealing algorithm (Corana *et al.*, 1987), Powell's algorithm (Press *et al.*, 1992) and the downhill simplex method (Press, 1997) and genetic algorithms (Davis, 1991). Goffe *et al.* (1994) found the simulated annealing method (Corana *et al.*, 1987) to be superior to other optimisation procedures for it is able to find a global optimum rather than local optima as well as being robust to exceptionally difficult problems. Whilst van Soest and Casius (2003) found that both simulated annealing and genetic

algorithms were able to find a global optimum solution when solving tough optimisation problems.

Simulated annealing is a heuristic search algorithm which learns about its search space with each solution and takes a probabilistic approach to determining its next starting point. It is based on the cooling of a material to form crystals by lowering the total energy within the system, taking the form of the cost function. The speed of the convergence is governed to allow the search to find the global optimal solution and not get stuck in local optima (Corana *et al.*, 1987).

Genetic algorithms solve a problem by modelling the problem as a population undergoing evolution via natural selection. Chromosomes representing the parameters from the population are selectively mated with one another depending on their fitness for purpose, evolving the population through generations until a solution is found (Davis, 1991). However the genetic algorithm will take a long time to find the best solution to a problem if the population size is too large (Harik *et al*., 1999).

In the past computational limitations has caused inferior optimisation methods to be used for the sake of saving time, however as computational power has improved the time taken to run optimisations has been dramatically reduced and more complex problems have been optimised (e.g. Anderson & Pandy, 1999). Optimisation algorithms can also perform very differently when asked to solve different kind of problems, simple functions without local optima can be solved quickly and reliably using a simple downhill method, however more complex functions, like those describing human movements, require a more robust approach.

2.7   Chapter Summary

Torque-driven simulation models can be personalised to a subject by using a set of subject-specific strength parameters determined experimentally on an isovelocity dynamometer measuring the net torque produced about specific joints. Body segmental inertia parameters can be accurately calculated from anthropometric

measurements used as input for a geometric model. Kinematic data describing the motions performed to be simulated by the model can be obtained by smoothing raw data collected through the digitisation and reconstruction of synchronised video images into three-dimensional coordinates. The next chapter describes the collection and processing of kinematic and anthropometric data.

Chapter 3: Data Collection

3.1   Chapter Overview

In this chapter the experimental protocol to collect kinematic and anthropometric data from a trampolinist is described. The methods used to process the kinematic data are detailed. Segmental inertia parameters for the trampolinist are reported.

3.2   Kinematic Data Collection

3.2.1   Camera Set-up

A VICON motion capture system, comprising 16 MX cameras, was used to record trampolining performances on a sunken trampoline. The motion capture system was set-up to capture a volume extending to five metres above and one metre below the level of the trampoline bed but with particular focus on capturing the right-hand side of the subject. The positions of the cameras are shown in Figures 3.2.1 and 3.2.2. The volume was calibrated so that each camera was accurate to within 0.35 mm and gave a dynamic wand test accuracy of 0.004%. The system was calibrated at 480 Hz with kinematic data subsequently recorded at 300 Hz.

Figure 3.2.1 A view of the experimental set up.
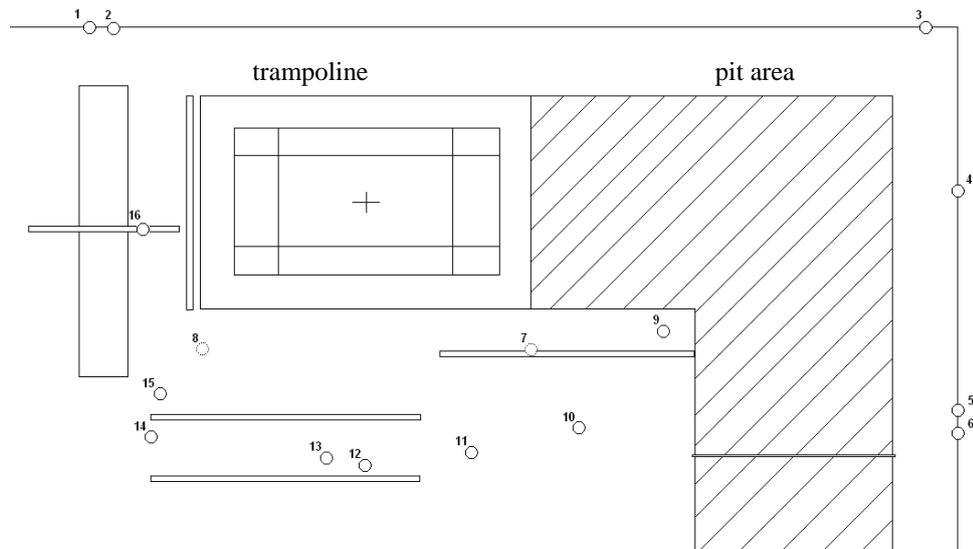
Figure 3.2.2 Illustration of the 16 camera positions for data collection.

3.2.2 Data Collection

An elite male trampolinist competing at junior international level (mass = 60.1 kg, height = 1.69 m) participated in the study. The subject was briefed on the data collection procedure before written informed consent was obtained (Appendix 1). Opto-reflective markers were placed on landmarks of the right-hand side of the

body as well as the left hip and head. The full marker set comprised markers on the front and back of the head, the sternum, both hips, the posterior aspect of the right shoulder, elbow, wrist, the lateral aspect of the right knee and ankle, and on the superior aspect of the metatarsal-phalangeal joint and toes of the right foot as illustrated in Figure 3.2.3. The markers were placed over the joint centres and landmarks, so in order to relate the marker positions to the joint centre locations and to help reflect the position coordinates of the right-side of the body to represent the left-side, a number of marker offsets were measured. The offset measurements included the position of the foot markers in relation to the floor, metatarsal-phalangeal joint centre and midline of the toe, and the lateral distance between the markers on the limbs and the midline; a full list of offsets can be found in Table 3.2.1. The values of the measured offsets can be found in Appendix 2b.

Figure 3.2.3 Photograph showing the marker set employed to collect position data.

Table 3.2.1 List of marker offsets measured.

Marker	Offset axes
Sternum	frontal
Shoulder	lateral
Elbow	lateral
Wrist	lateral
Hip	lateral
Ankle	lateral, frontal
Ball	frontal
Toe	frontal

Following the completion of the measurements the subject was given a period of familiarisation with the trampoline before performing a specified sequence of forward and backward rotating skills with various amounts of somersault as well as straight jumps of different heights. Each skill was performed until a satisfactory trial with no noticeable travel or cast was obtained. The trampolinist performed 21 skills in total in order to obtain satisfactory trials for 12 different skills (see Table 3.2.2).

Table 3.2.2 List of recorded performances.

Skill	Shape	Satisfactory?
Front S/S	Straight	Y
1¾ Front S/S	Pike	Y
1¾ Front S/S	Open Pike	N
1¾ Front S/S	Open Pike	Y
2¾ Front S/S	Tuck	Y
Triffus	Pike	N
Triffus	Pike	Y
High Jumping		Y
Back S/S	Pike	N
Back S/S	Pike	N
Back S/S	Pike	Y
Back S/S	Straight	N
Back S/S	Straight	Y
1¼ Back S/S	Straight	N
1¼ Back S/S	Straight	Y
Double Back S/S	Tuck	N
Double Back S/S	Tuck	Y
Double Back S/S	Pike	N
Double Back S/S	Pike	N
Double Back S/S	Pike	Y
Medium Jumping		Y

3.2.3   Body Segmental Inertia Parameters

Body segmental inertia parameters of the trampolinist were calculated using 97 anthropometric measurements in conjunction with the mathematical inertia model of Yeadon (1990b) (Appendix 2). Table 3.2.3 shows the mass, moment of inertia

and length of each segment as well as the distance of the centre of mass of the segment from the proximal joint. For the limbs the mass and moment of inertia included are those of the combined left and right limbs with the average length and distance of the centre of mass from the proximal joint given.

Table 3.2.3 Body segmental inertia parameters calculated using the inertia model of Yeadon (1990b).

Segment	Mass (kg)	Length (m)	Moment of Inertia $(kg.m^2)$	CM distance from proximal joint (m)
forearm and hand	3.13	0.426	0.041	0.162
upper arm	3.28	0.245	0.009	0.112
trunk, head and neck	29.13	0.865	1.554	0.383
thigh	14.91	0.372	0.178	0.165
lower leg	7.76	0.407	0.100	0.171
foot	1.59	0.145	0.003	0.061
toes	0.28	0.065	0.0002	0.028

The foot was modelled as two segments: a triangle representing the foot between the ankle and metatarsal-phalangeal joints, and a rod representing the toes, shown in Figure 3.2.4. The extra segments required additional segmental inertia parameters describing the position of the centre of mass within each segment, the mass and moment of inertia of each individual segment.
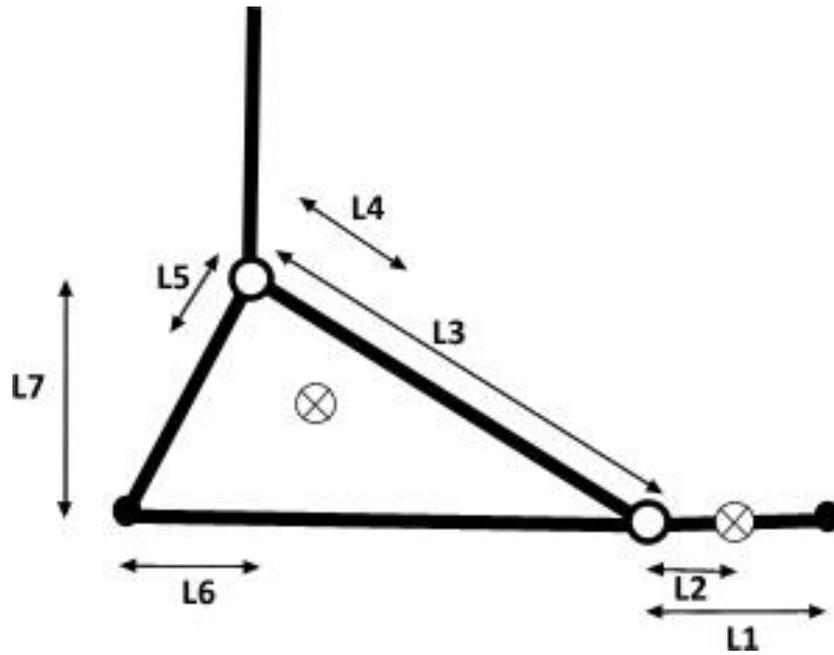
Figure 3.2.4 The foot modelled by a triangle and rod segment.

Lengths L1-L4 were calculated by the inertia model of Yeadon (1990b), L6 and L7 were measured directly from the subject during the data collection, whilst L5 was estimated using a subject-specific scaling method. Table 3.2.4 summarises the dimensions of the two-segment foot.

Table 3.2.4 Dimensions of the two-segment foot.

Parameter	Length (mm)
L1	65
L2	28
L3	145
L4	61
L5	17
L6	48
L7	78

3.3   Kinematic Data Processing

3.3.1   Joint Centre Positions

The position data recorded by the motion capture system and the offset measurements were combined, under the assumption of symmetrical body movement to create a whole-body pseudo-set of three-dimensional joint centre position data. This involved the relocation of data points towards the joint centres using the offset measurements and the calculation of a central head position.

Transposing data points along the frontal axis was potentially a problematic activity as these offsets were within the primary plane of motion. However the sternal landmark data did not need to be transposed since it was not to be employed as input to the simulation model and a method used to relocate the position of the metatarsal-phalangeal joint and the toe centres was devised to minimise the associated errors.

The method used to transpose the foot landmarks along the frontal axis was to subtract the offset of the height of the marker centre from the base of the marker from the offset measurement leaving the depth of the foot at these locations. The offsets at the metatarsal-phalangeal joint and toe were calculated by adding the height of the marker centre to half the calculated depth of the foot at these points. These offsets were applied in the direction perpendicular to the line passing through the ankle marker and the original marker position, shown in Figure 3.3.1.
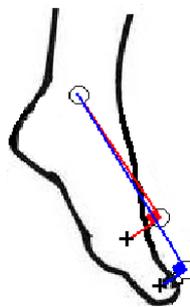
Figure 3.3.1 The transposition of foot markers.

The offset measurements taken in the direction of the lateral axis were used to transpose the data positions to the joint centres before the joint centre positions were reflected in the plane of the body that bisected the two hip markers vertically, in order to create a full body data set. The position of the centre of the head was taken to be the mean position of the markers on the front and back of the head.

The segment lengths calculated from the joint centre position data, shown in Table 3.3.1, are consistent between separate trials as shown by the small standard deviations, the largest standard deviations being found in the lengths of the head and trunk segments. Within the trials the standard deviations of the segment lengths were larger, and once again the segments with the largest variability in length were the head and trunk.

Table 3.3.1 Mean segment lengths calculated from joint centre position data.

	Upper Arm	Forearm and Hand	Thigh	Lower Leg	Foot	Trunk	Head
	(m)	(m)	(m)	(m)	(m)	(m)	(m)
mean	0.256	0.232	0.447	0.397	0.216	0.436	0.273
standard deviation between trials	0.009	0.003	0.016	0.008	0.003	0.023	0.019
mean standard deviation within trials	0.018	0.007	0.010	0.005	0.017	0.049	0.053

The increased variability in length within trials could possibly be attributed to marker movement due to movement of the underlying soft tissue or clothing. The trunk segment was defined by the shoulder and hip markers. It is possible that the movements of the shoulder joint could affect the position of the marker even though the marker position was chosen to minimise this possible effect, the hip marker may also have been subject to movement as it was placed on top of

clothing. The head segment also used the shoulder marker as a reference point so may have also been influenced by shoulder joint movements.

Table 3.3.2 Differences in segment lengths between the inertia model and static trials.

Segment		Difference
Upper Arm	(m)	0.016
Forearm and Hand	(m)	-0.014
Thigh	(m)	0.068
Lower Leg	(m)	0.008
Foot	(m)	0.007
Trunk	(m)	-0.059
Head	(m)	-0.1

By examining the difference between the segment lengths given by the inertia model output and the static trials it was observed that there was a difference in length of 59 mm in the trunk segment and -68 mm in the thigh segment. On examination of photographs of the subject it seemed that clothing may have been rearranged following the taking of anthropometric measurements and before the three dimensional position data was collected, altering the location of the hip marker. It was estimated that the hip markers were 64 mm higher than the hip centres, the mean of the differences in trunk and thigh length.

The hip centres calculated from the hip marker positions were adjusted as follows:

$$H \rightarrow H + \frac{64}{565} \overrightarrow{SH} = H + \frac{64}{565}(H - S) \qquad (3.3.1)$$

Where: H = hip centre location

S = shoulder centre location

3.3.2 Joint Angle Time Histories

The joint centre position data was used to calculate whole body orientation and joint configuration angles and angular velocities of the gymnast throughout each of the recorded performances (Yeadon, 1990a). When combined with segmental inertia parameters, the joint angle time histories allow the calculation of centre of mass position and velocity, as well as the angular momentum of the whole body about the centre of mass (Yeadon, 1990c). The joint configuration angles calculated were those of the metatarsal-phalangeal, ankle, knee, hip, shoulder and elbow joints; to be used in conjunction with the seven-segment simulation model. All the joint angles calculated were the interior angles formed between the adjacent segments in the sagittal plane. The whole body orientation angle was defined as the angle formed by the shoulder, hip and the forward horizontal. The time histories of the whole body orientation and joint configuration angles were fitted using quintic splines (Wood & Jennings, 1979).
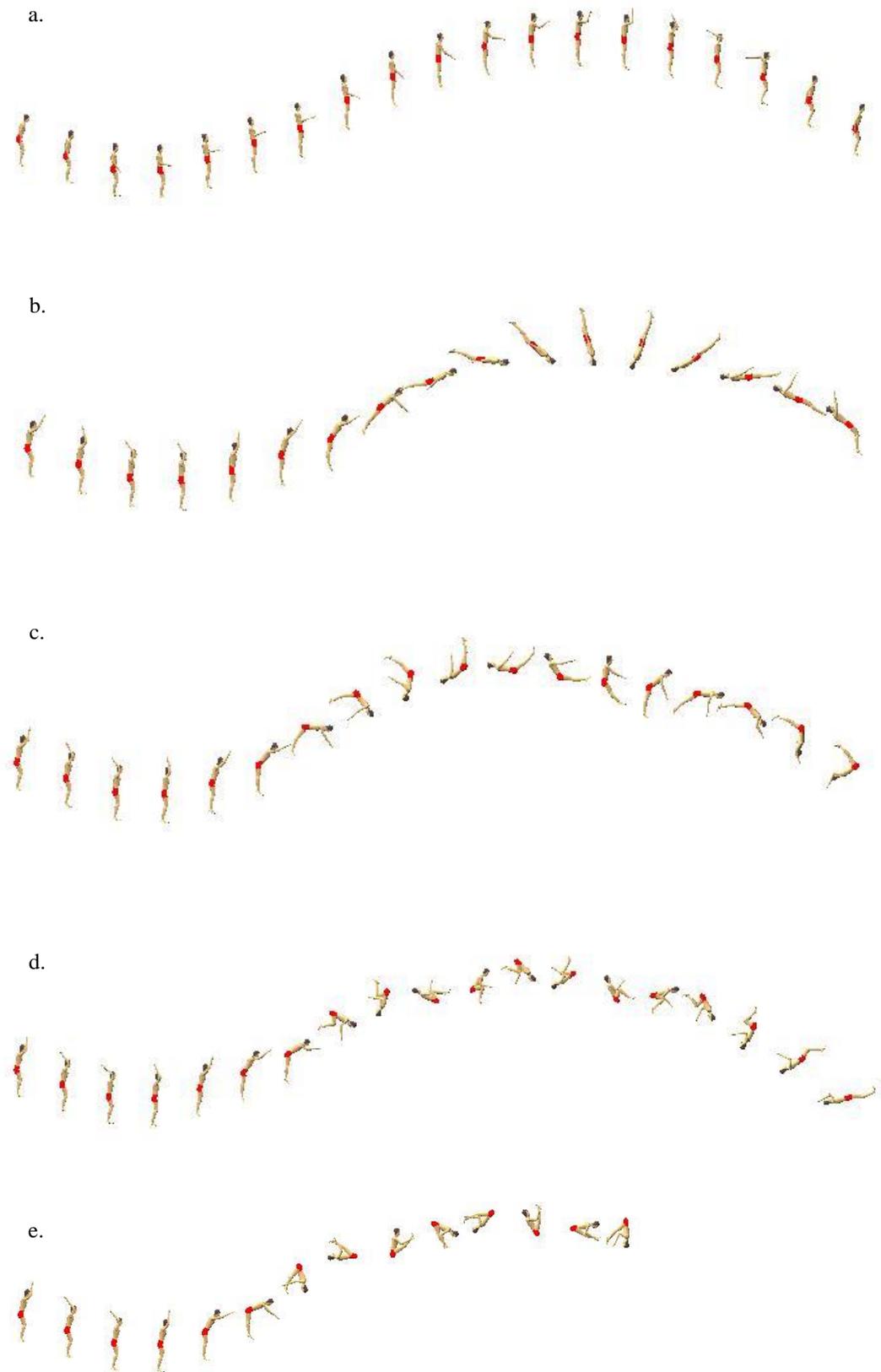
Figure 3.3.2 Representation of the captured motion of the trampolinist during (a) straight bouncing, (b) straight front somersault, (c) 1¾ (open) piked front somersault, (d) 2¾ tucked front somersault, (e) triffus piked (before initiating twist).

48
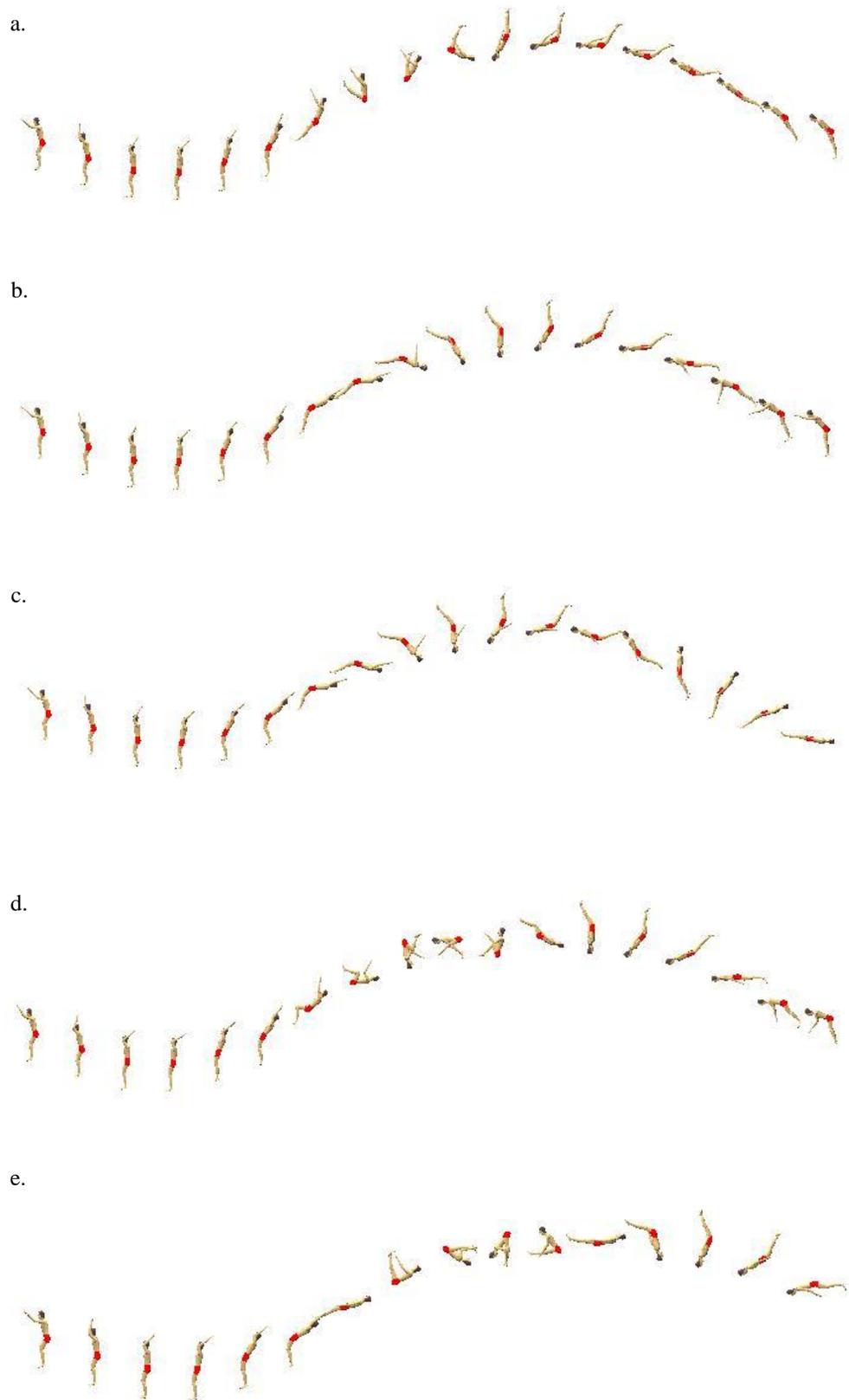
Figure 3.3.3 Representation of the captured motion of the trampolinist during (a) piked back somersault, (b) straight back somersault, (c) 1¼ straight back somersault, (d) tucked double back somersault, (e) piked double back somersault.

49

(a) Single front somersault   (b) Triple front somersault

(c) Single back somersault   (c) Double back somersault
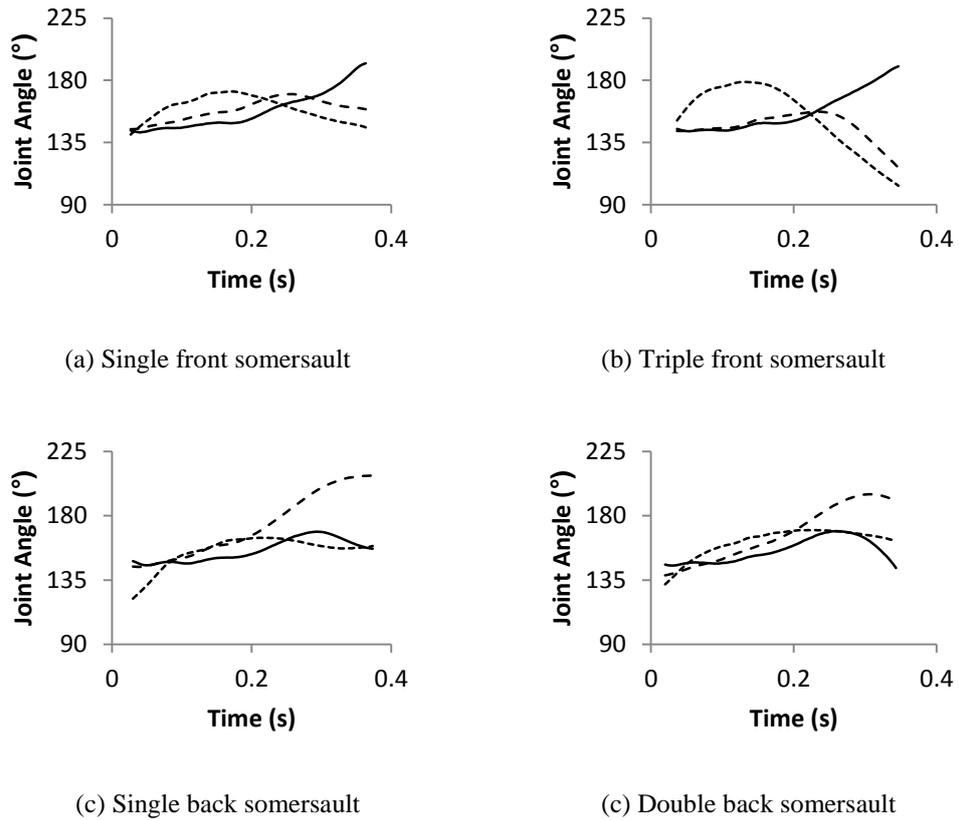
Figure 3.3.4 Joint angle time histories of the knee (solid), hip (dashed), and shoulder (dotted) during the contact phase directly preceding different somersaults.

The joint angle data was used to inform the design of the simulation model. The data showed that throughout all the trials there was significant movement of the elbow joint with a mean range of movement of $46.9\pm8.1°$ (forward: $44.8\pm6.0°$, backward: $45.1\pm5.6°$). The movement of the head and neck was found to be $22.9\pm10.7°$ on average, however a larger difference was found between forward ($13.0\pm3.2°$) and backward ($31.8\pm6.9°$) somersaults.

The motion of the simulation model was also restricted to joint movements that the trampolinist was actually able to perform. The data was analysed to find the limits of the range of motion for each joint movement that the trampolinist achieved during the data collection procedure. The shoulder showed a full, 360° range of motion in the recorded performances due to the projection of the movements on to a two dimensional plane. The minimum and maximum ranges of motion for the ball, ankle, knee, hip and elbow joints are displayed in Table 3.3.3.

Table 3.3.3 Minimum and maximum joint angles achieved in the recorded performances.

Joint	Limit of Motion (°)	
	Minimum	Maximum
Ball	109.3	151.2
Ankle	95.4	150.3
Knee	135.3	193.7
Hip	108.5	211.1
Elbow	85.3	170.9

Although the hip achieved a large degree of hyperextension, 211.1°, this was assumed to include some arching of the back and was limited to immediately prior to takeoff in backward rotating skills. Conversely the knee hyperextension was limited to immediately prior to takeoff in forward rotating skills.

3.3.3   Trampoline Bed Movement

The movement of the trampoline bed throughout the contact phase of each trial was also analysed. Each contact was normalised for the maximum depression of the trampoline bed and the duration of the contact phase for analysis. A quintic spline was then fit to the data.

$$z = 1.3057t^5 - 11.058t^4 + 17.963t^3 - 6.1303t^2 - 2.074t - 0.021$$
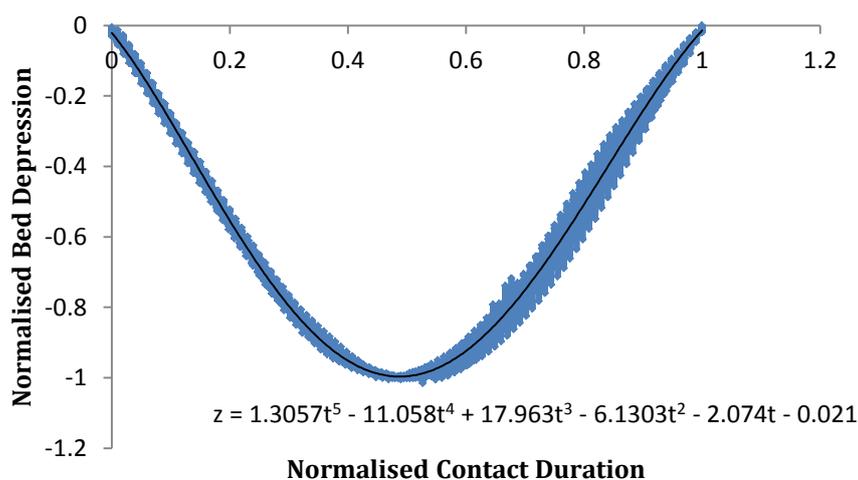
Figure 3.3.5 Plot of normalised bed depression against normalised contact time for 15 trials.

The point of maximum depression was found to be at 48.7% of the contact duration with the minimum vertical velocity of the bed occurring 13.6% of the way through the contact and maximum vertical velocity at 84.2% of the contact time. Maximum vertical acceleration of the bed occurred just prior to maximum depression, 47.2% of the way through the contact.

3.4   Chapter Summary

In this chapter the collection of kinematic performance data of trampolining is described. The techniques for the determination of subject-specific inertia parameters are described. Details of the data processing techniques were reported. The following chapter describes the development of a computer simulation model of a trampolinist and trampoline suspension system.

Chapter 4: Model Development

4.1 Chapter Overview

A simulation model representing a trampolinist and the reaction forces of the trampoline suspension system was required to study the mechanics of the takeoff from trampoline. This chapter describes the features of the simulation model of the trampolinist and trampoline suspension system.

4.2 The Trampolinist Model

The trampolinist was represented by a planar seven-segment model consisting of the torso, head and neck as one segment, the upper arms, lower arms and hands, thighs, lower legs and a two-segment foot. Each segment was modelled as a single rigid body as it has been shown that the inclusion of wobbling masses representing soft tissue movement is not necessary when modelling impacts with compliant surfaces (Yeadon *et al*., 2006b). The arm was modelled as two segments as the data showed significant changes in elbow angles during the contact phase preceding both forward and backward somersaults. Despite the range of neck motion preceding backward somersaults being found to be over 30°, the torso, head, and neck were modelled as a single rigid segment as this movement was thought to have little mechanical effect. The foot was modelled as a triangle with a rod, representing the toes, connected at the metatarsal-phalangeal joint. The orientation and configuration of the trampolinist was described by seven angles, the angle of the trunk to the vertical θ_t and the six internal angles at the shoulder θ_s, elbow θ_e, hip θ_h, knee θ_k, ankle θ_a, and metatarsal-phalangeal θ_m joints.
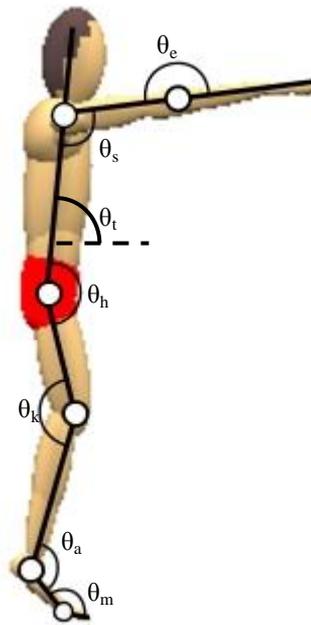
Figure 4.2.1 A seven-segment angle-driven model of a trampolinist.

4.3 Foot/Suspension-System Interface

During the takeoff from the trampoline, the surface of the trampoline suspension system is depressed then recoils as the trampolinist lands from the previous flight phase and jumps into the subsequent flight phase. Previous studies have found the force-displacement relationships of the trampoline suspension system to be non-linear vertically and linear horizontally (Blajer & Czaplicki, 2001; Jaques, 2008; Kraft, 2001; Lephart, 1971), however the exact relationship is individual to each trampoline.

In the present study, the modelling of the foot-suspension system interface is simplified to include all the relevant forces within a single expression to represent the reaction forces acting on the trampolinist. The total reaction force is then allocated between three points on the foot at the heel, ball and toes. The ratio of the allocation of reaction force between the three points is based on the depression of the trampoline suspension system at the heel, ball and toe.

54

4.3.1 Kinetics of the Foot/Suspension-System Interactions

When a trampolinist lands on the bed of the trampoline suspension system the reaction force accelerates the mass of the bed and springs downwards, while the opposite reaction force accelerates the trampolinist upwards. Subsequently, any elastic force created by the extension of the springs, accelerates the masses of both the suspension system and the trampolinist upwards.
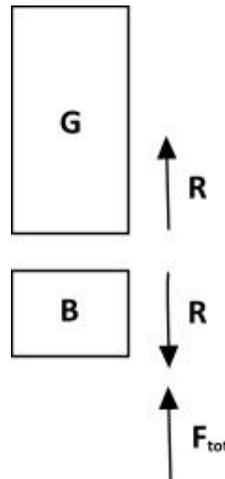
Figure 4.33.1 Free body diagram showing the vertical forces acting on the trampolinist, G, and trampoline, B.

$$R - m_G g \ = \ m_G \ddot{z}_G \qquad (4.3.1)$$

$$F_{tot} - R = m_B \ddot{z}_B \quad \therefore \quad R = F_{tot} - m_B \ddot{z}_B \qquad (4.3.2)$$

Where: m_G = mass of the gymnast

m_B = mass of the trampoline bed

$\ddot{z}_G$ = vertical acceleration of the gymnast's mass centre

$\ddot{z}_B$ = vertical acceleration of the trampoline bed's mass centre

F_{tot} = total vertical force exerted by the trampoline suspension system

R = vertical reaction force acting between the gymnast and trampoline bed

The weight of the bed of the suspension system has been neglected here as F_{tot} will be calibrated to be zero when the bed is in its stationary position.

For example, if the initial impact of the trampolinist landing on the bed of the suspension system were to be considered instantaneous, with the stationary bed with an equivalent mass, $m_B = \frac{1}{6}50 \approx 8kg$ (Jaques, 2008), conservation of linear momentum would give:

$$m_G v_G = m_G v_G' + m_B v_G' \qquad (4.3.3)$$

$$v_G' = \frac{m_G}{m_G + m_B} v_G$$

Where: v_G = impact velocity of the gymnast

v_G' = velocity of the gymnast after impact

If the mass of the trampolinist, $m_G = 60kg$.

$$v_G' = \frac{60}{60 + 8} v_G = 0.88 v_G$$

Taking an impact velocity, $v_G = -9ms^{-1}$, during the impact the trampolinist would slow to $-7.94ms^{-1}$ and the bed of the suspension system would accelerate to $-7.94ms^{-1}$.

The impulse, J, of this instantaneous impact is:

$$J = \frac{m_B m_G}{m_G + m_B} \cdot v_G \qquad (4.3.4)$$

For example the impulse on the suspension system may be expressed as:

$$m_B v_G' = 8(-7.94) = -63.5 Ns$$

Or the impulse on the gymnast as:

$$m_G (v_G' - v_G) = 60(1.06) = 63.5 Ns$$

Since the impact is not instantaneous, this impulse is spread over a finite time. Initially, upon impact, the area of the bed beneath the point of impact will be accelerated to match the velocity of the feet. This acceleration will occur over a duration of around 30 ms, the rest of the bed will then be accelerated over a period

of around 100 ms. These estimates were made from inspection of the vertical locations of the foot and trampoline bed during a landing. The impulse can be represented by an inverted cosine function as:

$$F_{imp} = \frac{J}{T}\left[1 - \cos\frac{2\pi t}{T}\right]$$ (4.3.5)

Where F_{imp} is the force arising from the impact with the stationary bed of the suspension system and the impulse J is calculated using Equation 4.3.4.
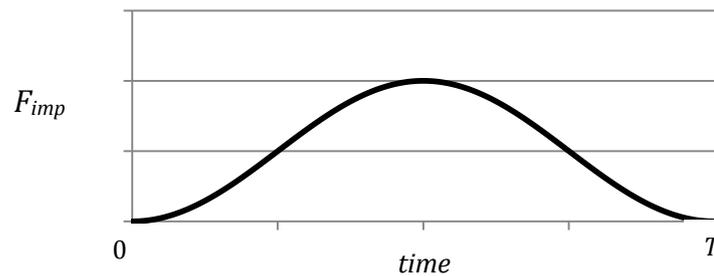
Figure 4.3.2 Graph showing the development of impact force as a function of T.

In order to determine T using optimisation the bounds for T should be set between 0.06 and 0.18 s as the total time taken for the bed to reach maximum depression is approximately 180 ms. F_{imp} provides the impulse required to accelerate the mass of the trampoline suspension system to match the speed of the feet of the trampolinist and so should vary with the mass centre vertical velocity of the trampolinist at the time of contact.

The vertical reaction force R acting on the feet of the trampolinist may be calculated as:

$$R = F_{tot} + F_{imp} - m_B\ddot{z}_B$$ (4.3.6)

The acceleration of the bed of the suspension system will not be measured but in a simulation $\ddot{z}_B$ will be calculated as the foot acceleration, $\ddot{z}_F$. Typically there is no net change in foot velocity in the first $60ms$ of contact; this means that only the spring force and the impact force are involved in the early portion of the contact phase via Equation 4.2.6. Foot acceleration can be calculated as an average of the

accelerations of the 3 points on the foot with weightings proportional to the vertical components of F_{tot} or $F_{tot} + F_{imp}$.

For momentum calculations, the movement of the suspension system can be represented by a mass m_B moving at $\frac{1}{6}v_B$ or a mass $\frac{1}{6}m_B$ moving at v_B, however when it comes to calculating the energy left in the bed after takeoff it does make a difference, as $\frac{1}{2}m_B(\frac{1}{6}v_B)^2 \neq \frac{1}{2}(\frac{1}{6}m_B)v_B^2$. If at takeoff the velocity of the bed of the trampoline suspension system is $4.5ms^{-1}$ the energy remaining in the bed is either

$$E = \frac{1}{2}m_B(\frac{1}{6}v_B)^2 = \frac{1}{2}50(0.75)^2 = 14\,Joules$$

or

$$E = \frac{1}{2}(\frac{1}{6}m_B)v_B^2 = \frac{1}{2}8(4.5)^2 = 84\,Joules$$

If the trampolinist takes off at $9ms^{-1}$ then this equates to 0.5% or 3.5% of the energy being lost in the suspension system. In reality the amount of energy lost is likely to lie between these two extreme values, possibly around 2%.

Energy will also be lost due to the viscosity of the suspension system. To incorporate this energy loss into the modelling of the foot-suspension system interactions, a damping force, proportional to the square of the bed velocity:

$$F_d = kv_B^2 \tag{4.3.7}$$

will act between the foot and the suspension system.

The total force acting on the foot of the simulation model of the trampolinist will take the form:

$$R = F_{tot} + F_{imp} - m_B\ddot{z}_B - kv_B|v_B| \tag{4.3.8}$$

The vertical and horizontal force-displacement relationships of the trampoline suspension system will be represented by non-linear and linear relationships respectively (Jaques, 2008):

58

$$FZ_{tot} = k_1 z^2 + k_2 z \qquad (4.3.9)$$

Where: FZ_{tot} = vertical reaction force

$\quad\quad k_1$ = non-linear vertical spring stiffness

$\quad\quad k_2$ = linear vertical spring stiffness

$\quad\quad z$ = vertical displacement

$$FY_{tot} = ky \qquad (4.3.10)$$

Where: FY_{tot} = horizontal reaction force

$\quad\quad k$ = horizontal spring stiffness

$\quad\quad y$ = horizontal displacement

The spring stiffness and damping parameters were determined, along with parameters describing the effective mass of the trampoline and impact force period, through a matching procedure in the evaluation of the simulation model.

4.3.2 Locating the Centre of Pressure during Foot Contact

The reaction force described is allocated between three points on the foot in ratios governed by the relative depressions of the three points in order to accurately represent the position of the centre of pressure beneath the foot on the compliant surface. The surface of the trampoline suspension system acts in such a way that when depressed the surface of the suspension system forms new contours and the suspensions system will only exert reaction forces around a localised depression if an adjacent point is depressed beyond the new contours of the suspension system.

In the following description it is assumed that the total vertical force F, is a non-linear function of the maximal vertical depression of the trampoline surface, corresponding to the lowest part of the foot. Within the simulation model the total vertical reaction force acting on the foot F, is represented by three reaction forces exerted at the heel H, ball B, and toe T.
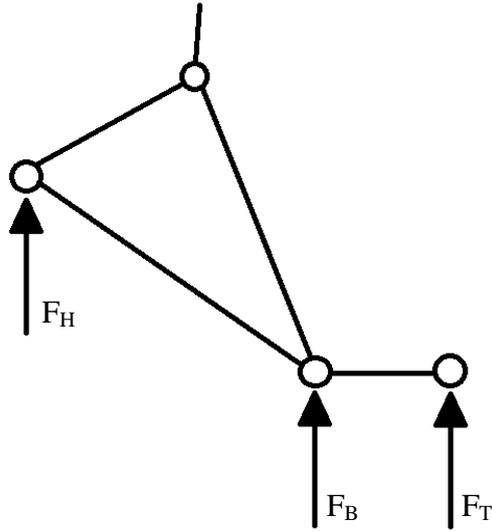
Figure 4.3.3 Showing the three separate reaction forces acting on the foot.

Suppose that the ratio of the distances d, between the three points is known:

$$d(HB) = 0.7\, d(HT) \quad \text{and} \quad d(BT) = 0.3\, d(HT)$$

If we assume that the natural 'slope' ($sin\Phi$) of the bed is kz, where z is the maximum depression of the surface and k is a constant. The angle of the foot (HB) and toe (BT) segments as proportions of the natural slope can be expressed as μ and λ respectively.

$$\mu = \frac{(z_H - z_B)}{d(HB)kz} \quad \text{where } -1 \le \mu \le 1 \qquad (4.3.11)$$

If $\mu < -1$ then the ball is unloaded ($F_B = 0$), so let $\mu = -1$. If $\mu > 1$ then the heel is unloaded ($F_H = 0$), so let $\mu = 1$.

Similarly,

$$\lambda = \frac{(z_T - z_B)}{d(BT)kz} \quad \text{where } -1 \le \lambda \le 1 \qquad (4.3.12)$$

If $\lambda < -1$ then the toe is unloaded ($F_T = 0$), so let $\lambda = -1$. If $\lambda > 1$ then the ball is unloaded ($F_B = 0$), so let $\lambda = 1$.

If H, B and T are at the same level then $\mu = \lambda = 0$ and the pressure distribution is even along the length of the foot. This may be represented by:

$$F_H = 0.35\,F \tag{4.3.13}$$

$$F_B = 0.35\,F + 0.15\,F = 0.50\,F \tag{4.3.14}$$

$$F_T = 0.15\,F \tag{4.3.15}$$

which has a centre of pressure at the midpoint between H and T, where F is the total force.

If H, B and T are at different levels then we may define the vertical forces as follows.

$$F_H = [0.35\,\mu' - (0.15\,\lambda \times 0.5\,\mu')]\,F \tag{4.3.16}$$

$$F_B = [0.5 + (0.35\mu \times 0.5\,\lambda') - (0.15\,\lambda \times 0.5\,\mu')]\,F \tag{4.3.17}$$

$$F_T = [0.15\,\lambda' - (0.35\,\mu \times 0.5\,\lambda')]\,F \tag{4.3.18}$$

Where $\mu' = 1 - \mu$ and $\lambda' = 1 - \lambda$.

So that the sum of F_H, F_B, and F_T is F, and when $\mu = \lambda = 0$ Equations 4.3.16-18 give the relationships described by (4.3.13-15).

This process allocates the proportion of the total vertical force over the three points based on the values of μ and λ, representing the slope of the bed around the point of maximal depression whilst maintaining a vertical force at a minimum of one point.

If $\lambda = \pm 1$ and $\mu = \pm 1$, then all the vertical force is exerted at the lowest point.

If $\mu = 1$, then the centre of pressure lies between B and T and moves towards the lowest as $\lambda \to \pm 1$.

4.3.3 Determining the Natural Slope of the Surface of the Suspension System during Depression

In order to allocate accurately the reaction force from the trampoline between multiple points on the foot, we must be able to say how much further a second, adjacent point is depressing the trampoline given another point of greater depression.

The natural slope, kz, of the trampoline from a depressed point was measured from video of a single contact phase. The position of the toe was digitised in each frame, along with a point on the surface of the suspension system consistent with the initial slope of the bed moving away from the toe.
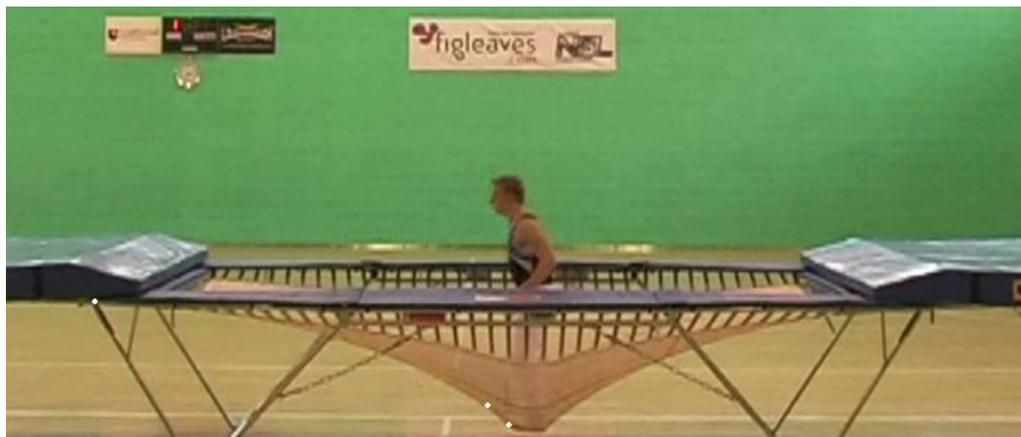
Figure 4.3.4 The points used to determine the natural slope of the suspension system.

The natural slope, defined as $\Delta z/\Delta y$, of the trampoline bed was then calculated from the digitised points in each frame and the relationship between the natural slope and the depression of the trampoline bed was determined. A linear function was fitted to the data and a relationship between the natural slope of the surface of the suspension system and the point of maximal depression was found.

natural slope = 1.226*depression
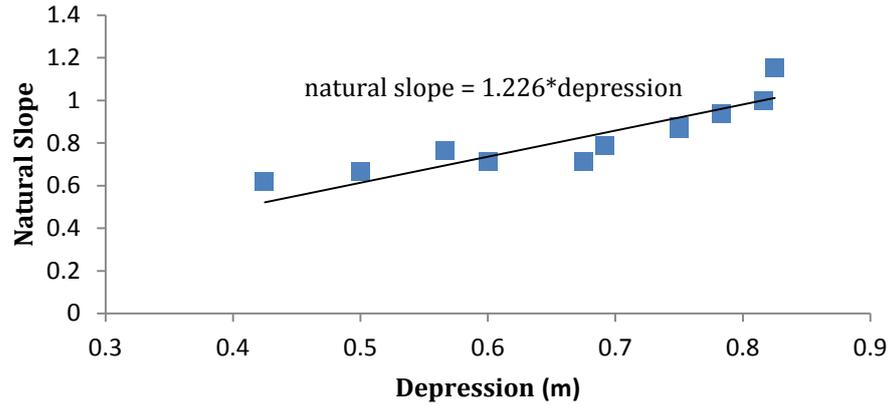
Figure 4.3.5 Graph showing the relationship between natural slope and the depression of the surface of the suspension system.

The relationship determined between the natural slope of the surface of the suspension system and the depression of the trampoline was used as the initial value but was allowed to vary in the optimisation of the model parameters.

4.3.4 Equations of Motion

The equations of motion were formulated for both the angle-driven and torque-driven models using Autolev^{TM} Professional Version 4.1. The software package facilitates the creation of multibody simulation models and uses Kane's method (Kane and Levinson, 1996) to derive the equations of motion. Kane's method uses generalised coordinates for each segment to define the position and orientation relative to the global coordinate system or other, previously defined segments. Generalised speeds are calculated as the time derivatives of the generalised coordinates (Kane and Levinson, 1985). Inertia parameters, torques, and internal and external forces are defined so that expressions for the generalised inertia and generalised active forces can be calculated. The Autolev^{TM} command files (Appendix 3), when run produced an output code in FORTRAN programming language, containing the equations of motion derived using Kane's method and code to advance the simulation over a period of time using a Kutta − Merson numerical integration algorithm with a variable step size Runge-Kutta integration method. The FORTRAN programs were customised to create the foot-suspension system interface described in this chapter and to incorporate the torque generators as described in Section 6.3.

4.4   Chapter Summary

In this chapter the details of the construction of the computer simulation model have been described. The force-displacement relationships governing the interactions between the models of the trampolinist and the trampoline suspension system were developed and the methods used to determine the distribution of the reaction force on the feet of the simulation model was described. The following chapter will detail the application of the angle-driven simulation model of trampolining.

Chapter 5: The Angle-Driven Model

5.1   Chapter Overview

The present chapter describes the method for the determination of the visco-elastic properties of the trampoline suspension system using an angle-driven simulation model. The results from the determination of the visco-elastic parameters are detailed. The method for the evaluation of the angle-driven model is then detailed and the results are reported.

5.2   Visco-Elastic Parameter Determination

The simulation model requires the input of numerous parameters in order for the resulting simulations to accurately mimic the movements and interactions of a trampolinist and trampoline suspension system. Some of these parameters can be measured directly, whilst others, for example the elastic properties of the trampoline during impact, are very difficult to measure directly through experimental methods. In order to determine values for the uncertain parameters, a subject-specific, angle-driven model was developed.

The angle-driven model was used to ascertain values for the eight parameters that govern the modelled force interactions of the foot and the trampoline suspension. These parameters are three spring stiffness and two damping parameters describing the vertical and horizontal force-displacement relationships, along with parameters describing the effective mass of the trampoline, impact force period and natural slope of the trampoline.

By using known initial conditions and driving the model with joint angle time histories from recorded performances, an optimisation procedure could be used to determine the uncertain parameters by letting them vary whilst minimising the difference between the simulation and performance. A simulated annealing algorithm (Corana *et al.*, 1987) varied the model parameters governing the foot-suspension system interactions to minimise a cost function designed to match

simulations to recorded performances. In order to obtain results from the matching procedure that can be used to simulate a varied range of different skills a number of different performances were used (Wilson *et al.*, 2006). Seven trials were selected to be used in the matching procedure. These trials covered a broad range of rotational requirements over both forward and backward somersaults; the skills were: straight jumping S, a straight single forward somersault F_1, a piked 1¾ forward somersault F_2, a piked triffus F_3, a piked single backward somersault B_1, a straight single backward somersault B_2 and a piked double backward somersault B_3.

5.2.1   Model Inputs

The inputs of the angle-driven model were the initial conditions of the trampolinist immediately prior to first contact with the trampoline and body segmental inertias. The initial conditions prior to contact were the horizontal and vertical position and velocities of the toe, orientation angle and angular velocity of the trunk. Throughout a simulation the movements of the simulation model were driven by joint angle time histories. Both the initial conditions and joint angle time histories were determined from the two dimensional pseudo-data sets generated from the kinematic data. The output of the model included the horizontal and vertical mass centre velocities, trunk angle and whole–body angular momentum.

Table 5.2.1 Initial conditions of seven selected skills.

Initial condition		S	F_1	F_2	F_3	B_1	B_2	B_3
					Skill			
Hor. toe position	(m)	-0.405	-0.226	-0.364	0.106	-0.197	0.046	-0.031
Vert. toe position	(m)	0.119	0.090	0.101	0.076	0.087	0.096	0.081
Hor. toe velocity	(ms^{-1})	0.858	0.155	0.912	0.375	0.146	-0.183	-0.236
Vert. toe velocity	(ms^{-1})	-7.83	-7.51	-7.24	-7.43	-7.79	-7.52	-7.32
Orientation	(°)	72.9	77.2	77.3	76.5	77.5	77.9	77.0
Trunk ang. velocity	(°s^{-1})	40.0	-13.3	-32.9	-15.4	-30.4	-34.4	-11.1

During the matching procedure the initial horizontal and vertical velocities of the toe, and angular velocity were allowed to vary slightly for each individual trial so that the simulated initial centre of mass velocities could be adjusted to match to the recorded centre of mass velocity. The horizontal and vertical velocities of the toe were allowed to vary by up to 1 ms^{-1} and the angular velocity was allowed to vary by up to 0.5 rad. s^{-1}.

5.2.2 Cost Function

A cost function was developed in order to assess objectively the extent to which each simulation matched the recorded performances. The cost function was designed so that the objective score it outputted, when minimised, would match the movement characteristics of the simulation to the recorded performance both throughout the contact phase and at takeoff.

The cost function comprised terms comparing the initial horizontal centre of mass position, initial horizontal and vertical centre of mass velocities, toe position in both the horizontal and vertical dimensions throughout the simulation, horizontal and vertical takeoff velocities, orientation angle and angular velocity of the trunk.

The toe position difference was calculated as a root mean squared difference between the simulation and performance throughout the contact period, the linear velocity terms were calculated as a percentage of actual resultant takeoff velocity, the trunk orientation was simply the difference in orientation in degrees at takeoff and the angular velocity difference was calculated as the percentage difference at takeoff. The cost function was a root mean square of these nine component scores, as shown by Equation 5.2.1.

$$COST = \sqrt{\frac{\Delta y_i^2 + \Delta \dot{y}_i^2 + \Delta \dot{z}_i^2 + \Delta y^2 + \Delta z^2 + \Delta \dot{y}^2 + \Delta \dot{z}^2 + \Delta \theta^2 + \Delta \dot{\theta}^2}{9}}$$

(5.2.1)

Where: Δy_i = difference in initial horizontal COM position [cm]

$\Delta \dot{y}_i$ = difference in initial horizontal COM velocity [ms^{-1}]

$\Delta \dot{z}_i$ = difference in initial vertical COM velocity [ms^{-1}]

Δy = root mean squared difference in horizontal toe position [cm]

Δz = root mean squared difference in vertical toe position [cm]

$\Delta \dot{y}$ = horizontal takeoff velocity difference [%]

$\Delta \dot{z}$ = vertical takeoff velocity difference [%]

$\Delta \theta$ = takeoff orientation difference [°]

$\Delta \dot{\theta}$ = takeoff angular velocity difference [%]

When the seven trials were matched using a common set of parameter values, the overall score was calculated as the mean of the cost function values across the seven trials.

5.2.3 Results

When the seven trials were matched the simulated annealing algorithm was able to optimise the parameter values so that the average score across the seven trials was 3.3% difference. The individual simulations matched the recorded performances with scores of 2.2% (*S*), 4.1% (*F₁*), 4.2% (*F₂*), 3.6% (*F₃*), 2.9% (*B₁*), 2.5% (*B₂*) and 3.5% (*B₃*). Table 5.2.2 shows the common set of parameters determined by the combined matching procedure. Table 5.2.3 shows the

adjustments made to the initial horizontal, vertical, and angular velocities for the individual simulations.

Table 5.2.2 Common parameter values determined by the combined matching procedure.

Parameter		
M_T	(kg)	18.615
T_{imp}	(s)	0.165
K_{z1}	$(N.m^{-2})$	7531.30
K_{z2}	$(N.m^{-1})$	-374.138
K_y	$(N.m^{-1})$	58418.45
D_z	$(N.s.m^{-1})$	0.485
D_y	$(N.s.m^{-1})$	7773.38
∇		-1.060

M_T – effective mass of trampoline, T_{imp} – impact duration, K_{z1}, K_{z2} – vertical stiffnesses, K_y – horizontal stiffness, D_z – vertical damping, D_y – horizontal damping, ∇ - natural slope.

Table 5.2.3 Adjustments made to the initial horizontal, vertical, and angular velocities for the individual simulations.

	Adjustments to Initial conditions		
	$\dot{y}$ (ms^{-1})	$\dot{z}$ (ms^{-1})	$\dot{\theta}$ $(°.s^{-1})$
S_1	0.357	0.272	-0.019
F_1	0.577	0.200	0.008
F_2	0.775	0.621	-0.022
F_3	0.679	0.816	-0.031
B_1	0.598	0.476	0.051
B_2	0.406	0.459	0.049
B_3	0.697	0.475	0.020

$\dot{y}$ = horizontal velocity, $\dot{z}$ = vertical velocity, $\dot{\theta}$ = angular velocity

The mean score of 3.3% across the seven selected trials shows that the simulation model was capable of replicating the motion of a trampolinist both throughout the contact phase and at takeoff. Table 5.2.5 shows the component scores achieved by the combined matching procedure for each of the seven skills and the mean value of each component score.

Table 5.2.4 Cost function component scores of angle-driven simulations.

| | Component Score | | | | | | | | | Score |
	Δy_i (cm)	$\Delta \dot{y}_i$ (m/s)	$\Delta \dot{z}_i$ (m/s)	Δy (cm)	Δz (cm)	$\Delta \dot{y}$ (%)	$\Delta \dot{z}$ (%)	$\Delta \theta$ (°)	$\Delta \dot{\theta}$ (%)	(%)
S_1	2.71	1.51	2.84	2.18	2.20	1.81	1.29	3.55	0.05	2.2
F_1	0.78	2.01	1.80	2.19	4.37	5.83	4.66	5.20	6.19	4.1
F_2	1.75	1.84	2.50	2.93	2.40	8.11	1.44	2.55	7.60	4.2
F_3	1.93	2.28	5.16	1.13	2.25	4.53	6.51	1.32	3.28	3.6
B_1	1.44	1.48	0.31	1.57	5.75	5.39	1.12	0.71	1.99	2.9
B_2	1.49	1.52	0.03	1.58	4.68	4.52	0.85	0.24	2.45	2.5
B_3	1.94	1.56	2.62	1.85	4.77	6.63	3.13	1.14	4.22	3.5
Mean	1.72	1.74	2.18	1.92	3.77	5.26	2.71	2.10	3.68	3.3

Δy_i – difference in initial horizontal COM position, $\Delta \dot{y}_i$ – difference in initial horizontal COM velocity, $\Delta \dot{z}_i$ – difference in initial vertical COM velocity, Δy – RMS difference in horizontal toe position, Δz – RMS difference in vertical toe position, $\Delta \dot{y}$ – horizontal takeoff velocity difference, $\Delta \dot{z}$ – horizontal takeoff velocity difference, $\Delta \theta$ – takeoff orientation difference , $\Delta \dot{\theta}$ – takeoff angular velocity difference.

The initial motion characteristics of the centre of mass were matched closely across all of the skills, because the optimisation procedure allowed the initial horizontal, vertical and angular velocities to vary. The largest component score was found in the difference in horizontal velocity at takeoff (5.26%).

5.3   Evaluation of the Angle-Driven Model

In order to ensure that the set of parameter values obtained through the combined matching procedure could be applied generally to all trampoline impacts and were not just specific to the seven selected skills, the angle-driven model was evaluated. The evaluation was conducted by selecting two new skills, a 2¾ tucked front somersault (F_4) and a tucked double back somersault (B_4), and simulating these skills using the parameter values determined by the combined matching procedure. The initial conditions of the two skills selected for the evaluation can be found in Table 5.3.1.

Table 5.3.1 Initial conditions of two skills used in the evaluation procedure.

		Skill	
Initial condition		F_4	B_4
Horizontal toe position	(m)	0.143	0.492
Vertical toe position	(m)	0.087	0.104
Horizontal toe velocity	(ms^{-1})	0.465	0.393
Vertical toe velocity	(ms^{-1})	-7.28	-7.74
Orientation angle	(°)	75.9	74.9
Angular velocity	(°s^{-1})	6.95	-14.8

The scores for the two skills used for evaluating the angle-driven model were calculated using Equation 5.2.1. The simulations were found to match very closely with the recorded performances as the simulations returned scores of 3.6% and 2.3% for F_4 and B_4 respectively.

Figures 5.3.1 and 5.3.2 show visual representations for comparison of the trampoline contact phase of the recorded and simulated performances of F_4 and B_4.
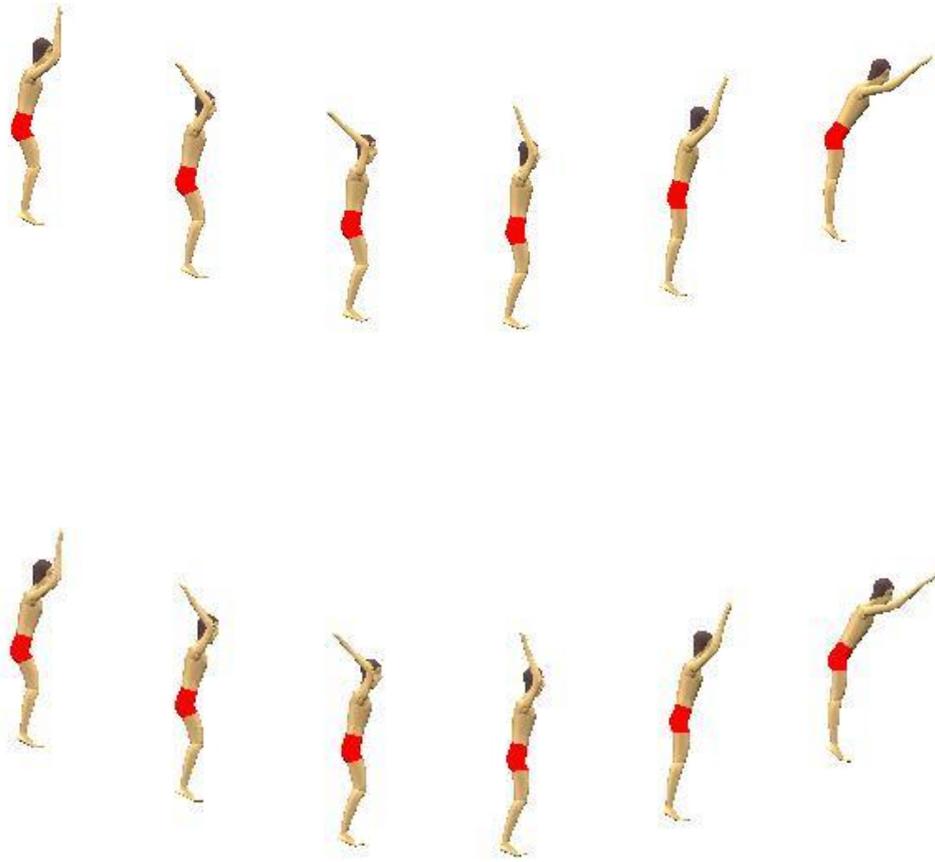
Figure 5.3.1 Comparison of F_4 trampoline contact phase between recorded performance (above) and simulated performance (below).
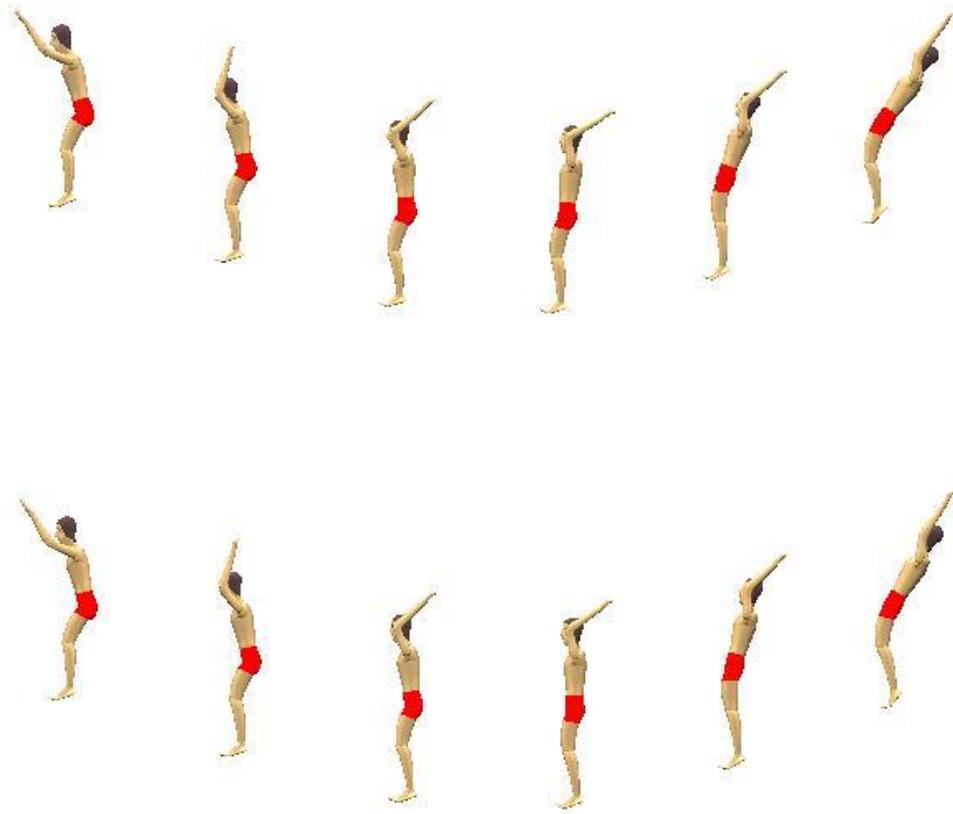
Figure 5.3.2 Comparison of B_4 trampoline contact phase between recorded performance (above) and simulated performance (below).

5.4   Chapter Summary

The angle-driven simulation model was employed to determine the visco-elastic properties of the trampoline suspension system. The combined matching procedure produced a common set of parameters for the group of seven skills. The common set of parameters was then applied to simulations of two other skills which also matched closely to the recorded performances. The next chapter details the application of a torque-driven simulation model of trampolining.

Chapter 6: The Torque-Driven Model

6.1   Chapter Overview

In this chapter the details of the torque-driven simulation model are described. The methods used to scale the strength of torque generators and to evaluate the model in the fixed strength protocol are described. The results from the strength scaling and fixed strength protocols are detailed and discussed.

6.2   Structure of the Torque-Driven Model

The torque-driven simulation model is of identical construction to the angle-driven model, with seven segments representing the body of the trampolinist in two dimensions. The movements of the ankle, knee, hip and shoulder joints are driven by four pairs of torque generators, whilst the metatarsal-phalangeal and elbow joints are angle-driven. The reaction force exerted by the trampoline on the feet acts in the same manner as on the angle-driven model. At the four torque-driven joints a pair of torque generators act, one to exert an extensor torque and one to exert a flexor torque, as shown by Figure 6.2.1.
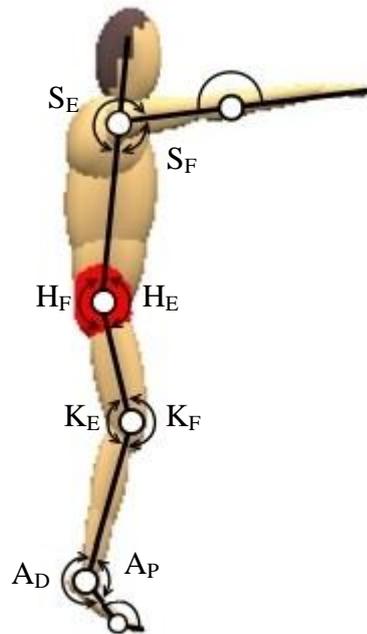
Figure 6.2.1 A seven-segment torque-driven model of a trampolinist.

The inputs for the torque-driven model are the initial conditions determined from kinematic data, the parameters governing the foot-suspension system interactions that were determined using the angle-driven simulation model (as described in Chapter 4), body segmental inertia parameters, strength parameters, and the activation profiles for each of the individual torque generators that was used to drive the simulation. The initial conditions, determined just prior contact, were the horizontal and vertical position and velocities of the toe, initial joint angles and angular velocities, as well as the orientation angle and angular velocity of the trunk.

Throughout a simulation the movements of the torque-driven joints of the simulation model were driven by the joint torques, which were governed by activation profiles of each torque generator. The movements of the angle-driven joints were governed by joint angle time histories at the elbow, whilst the metatarsal-phalangeal joint was governed by a function of the depression of the

75

trampoline suspension system. The output of the model included the joint angle and orientation angle time histories, time histories of the horizontal and vertical mass centre velocities, and whole–body angular momentum at takeoff.

6.3   Torque Generators

Extensor and flexor torque generators at the ankle, knee, hip, and shoulder joints were used to drive the simulations. The eight torque generator actions were ankle plantar flexion (A_P), ankle dorsi flexion (A_D), knee extension (K_E), knee flexion (K_F), hip extension (H_E), hip flexion (H_F), shoulder extension (S_E), and shoulder flexion (S_F). Each of the ankle, knee, and hip torque generators was modelled as a muscle-tendon complex consisting of a contractile component (CON) and series elastic component (SEC), whilst the shoulder torque generators were modelled with only a contractile component.

Figure 6.3.1 depicts the muscle tendon complex at a joint, where the joint angle (θ) is comprised of two angles representing the contractile component (θ_{con}) and series elastic component (θ_{sec}).
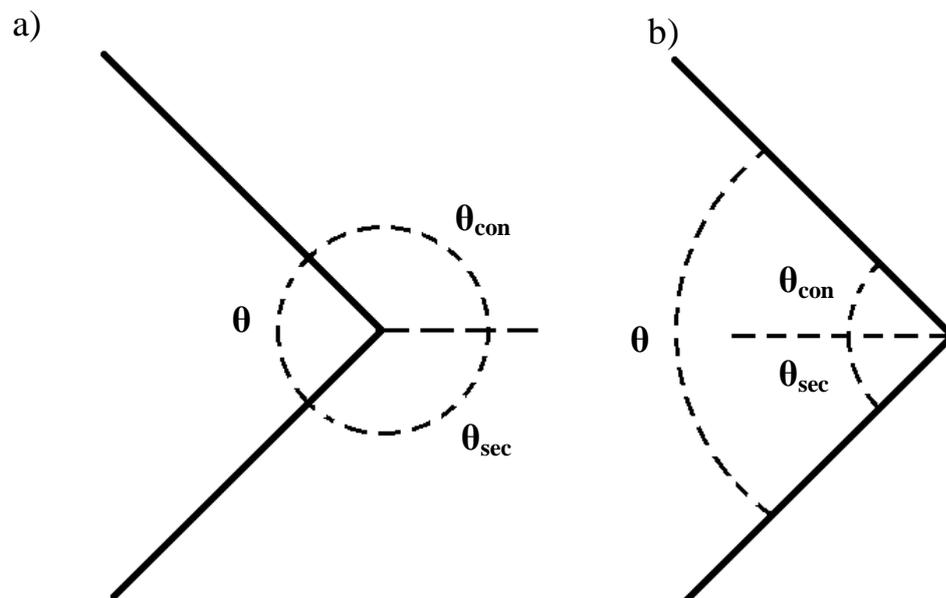
Figure 6.3.1 The muscle tendon complex consisting of a contractile component and series elastic component for both (a) a joint extensor and (b) a joint flexor.

The geometric relationship between the joint angle (θ), contractile component angle (θ_{con}) and series elastic component angle (θ_{sec}) are defined by the relationships:

Flexors:

$$\theta = \theta_{con} + \theta_{sec}$$

(6.3.1)

Extensors:

$$\theta = 2\pi - (\theta_{con} + \theta_{sec})$$

(6.3.2)

The muscle-tendon complex consists of an elastic component in series with a contractile component, therefore the torque across the series elastic component, $T_{sec,}$ must be equal to the torque across the contractile component, T_{con}. The torque produced by the contractile component is dependent on the contractile component angle and angular velocity, and the strength of the muscle across the joint; this relationship is detailed in Section 6.3.1. The torque produced by the series elastic component, T_{sec}, is dependent on the stiffness, k_{sec}, and θ_{sec}, such that:

$$T_{sec} = k_{sec} \cdot \theta_{sec}$$

(6.3.3)

6.3.1 Torque – Angle – Angular Velocity Relationship

The maximum voluntary torque that is capable of being produced about a joint has been found to be dependent on the angle and angular velocity of that joint Yeadon *et al*. (2006). All torque generators were modelled as to represent monoarticular muscles and were not affected by movements at adjacent joints as biarticular torque generators have been shown to only be necessary when the knee is flexed by 40° or more (Lewis *et al.*, 2012). As the limit of the range of motion observed during the recorded performances was 45° and the majority of the movements were outside this range, the advantages of biarticular torques over monoarticular torques were assumed to be negligible.

<u>6.3.1.1 Torque – Velocity Relationship</u>

The torque – velocity relationship is described by a four-parameter function governing the maximum voluntary torque produced over the range of contractile

component velocities, and a three-parameter function defining the differential activation of muscles during concentric and eccentric actions.

The four parameters that describe the maximum voluntary torque produced over the range of contractile component velocities are: the maximum torque T_{max} in the eccentric phase, the isometric torque T_0, the angular velocity ω_{max} at which the curve reaches zero torque, and ω_c defined by the vertical asymptote $\omega = -\omega_c$ of the Hill hyperbola (Hill, 1938).

During concentric muscle action the torque – velocity curve was given by a rotational equivalent of the classic Hill hyperbola:

$$T = \frac{C}{(\omega_c + \omega)} - T_c \qquad \text{(if } \omega \leq 0),\qquad\qquad (6.3.4)$$

Where $T_c = \frac{T_0 \omega_c}{\omega_{max}}$, $C = T_c(\omega_{max} + \omega_c)$.

During eccentric muscle action the relationship between T and ω was represented by the rectangular hyperbola:

$$T = \frac{E}{(\omega_E + \omega)} - T_{max} \quad \text{(if } \omega \geq 0),\qquad\qquad (6.3.5)$$

Where $\omega_E = \frac{(T_{max} - T_0)}{kT_0} \frac{\omega_{max}\omega_c}{(\omega_{max} + \omega_c)}$, $E = -(T_{max} - T_0)\omega_e$, and k is the ratio of the slopes of the eccentric and concentric functions at $\omega = 0$, the value of which Huxley (1957) predicted, 4.3, was used.

The torque – velocity curve describing both concentric and eccentric phases is shown by Figure 6.3.2.
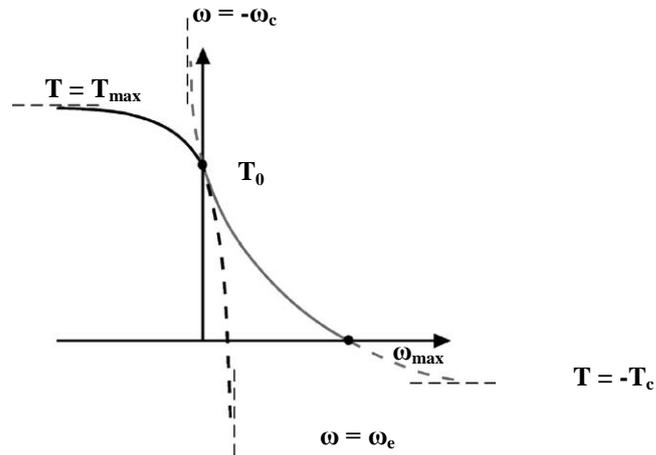
Figure 6.3.2 The four-parameter maximum torque function comprising branches of two rectangular hyperbolas with asymptotes T = -T$_c$ and ω = -ω$_c$; and T = Tmax and ω = ω$_e$ (Yeadon et al., 2006).

6.3.1.2 Differential Activation

During eccentric voluntary contractions, neural inhibition prevents the muscle from achieving full activation (Westing *et al*., 1991). Forrester *et al*. (2011) defined the differential activation of muscles during concentric and eccentric actions using a sigmoid function. Three parameters governed the relationship: the lowest level of activation in the eccentric phase a_{min}, the angular velocity ω_1 at the point of inflection of the function, and a parameter ω_r that described the rate at which the activation increases from a_{min} to a_{max} ($\approx 10\ \omega_r$). The differential activation was defined by Equation 6.3.6.

$$a = a_{min} + \frac{(a_{max} - a_{min})}{\left[1 + \exp\left(\frac{-(\omega - \omega_1)}{\omega_r}\right)\right]}$$ (6.3.6)

Where the maximum activation level a_{max} was assumed to be equal to 1.0.

79
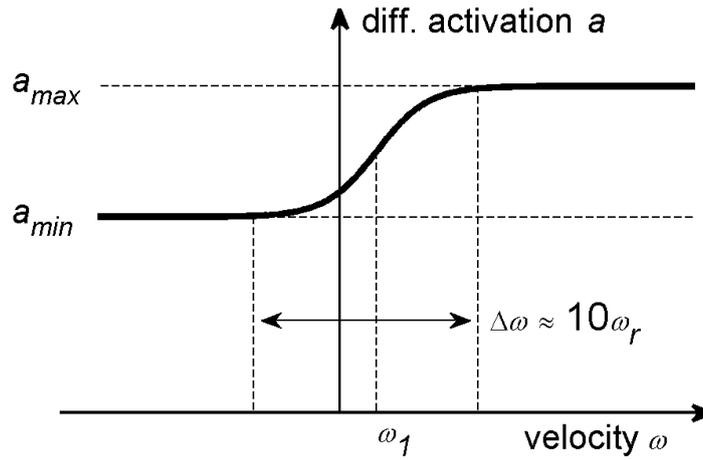
Figure 6.3.3 The three parameter differential activation function in which the activation a rises from a_{min} to a_{max} with a point of inflection at $\omega = \omega_1$ (Forrester et al., 2011).

The four-parameter function (Equations 6.3.4 and 6.3.5) and three-parameter functions (Equation 6.3.6) were multiplied together to give a seven-parameter function defining the maximum voluntary torque as a function of contractile component angular velocity.

6.3.1.3 Torque – Angle Relationship

In addition to varying with the angular velocity of the contractile component, the maximum voluntary torque produced by a joint also varies with the length of the contractile component, in the situation of a torque generator described by the angle θ_{con}. The torque – angle relationship was represented by a bell curve (Edman & Regianni, 1987).

$$t_a = e^{-(\theta - \theta_{opt})^2 / (2k_2{}^2)} \tag{6.3.7}$$

Where θ_{opt} = angle at which maximum torque can be produced

k_2 = width of the curve

The two-parameter function defining the torque – angle relationship was multiplied by the seven-parameter function defining the torque – angular velocity relationship, giving a nine-parameter function representing the torque – angle – angular velocity relationship.

80

6.3.2 Strength Parameters

Each torque generator requires nine parameters to govern the torque – angle – angular velocity relationship of the contractile component and an additional parameter defining the stiffness of the series elastic component. These parameter values were obtained from previous studies before being scaled within a matching procedure employed to evaluate the torque driven model.

Allen (2009) and Jackson (2010) collected joint torque data, from a triple jumper and gymnast respectively, using an isovelocity dynamometer. The data was subsequently fitted with a surface representing the nine-parameter torque – angle – angular velocity relationship to determine the parameter values. Series elastic component stiffness parameters were estimated based on the properties of the major muscle groups contributing to the motion (Allen, 2009; Jackson, 2010). The torque parameters for the hip, knee, and ankle joints were taken from the values measured from the gymnast by Jackson (2010) and the parameters for the ankle were taken from Allen's measurements of the triple jumper (2009). The joint torque parameters are given in Table 6.3.1.

Table 6.3.1 Torque generator strength parameter values.

	T_{max} (Nm)	T_0 (Nm)	ω_{max} (s^{-1})	ω_c (s^{-1})	a_{min}	ω_1 (s^{-1})	ω_r (s^{-1})	k_2 (rad)	θ_{opt} (rad)	k_{sec} (Nm.rad^{-1})
A_P	351	206	30.80	15.38	0.88	1.38	0.40	0.37	4.22	641
A_D	107	64	26.00	3.90	0.99	-1.57	0.44	0.44	2.13	195
K_E	421	301	38.44	2.88	0.81	-0.10	0.10	0.51	4.08	805
K_F	147	105	33.26	5.43	0.80	-0.13	0.15	1.11	2.11	173
H_E	315	225	18.06	2.20	0.78	0.74	0.14	1.06	4.21	1004
H_F	235	168	18.36	4.59	0.80	-0.10	0.13	1.22	2.40	306
S_F	130	93	38.14	9.52	0.88	-0.13	0.08	1.29	3.35	1574
S_E	202	144	32.50	8.13	0.75	-0.06	0.38	1.83	3.96	1988

The effects of using joint torque parameters that were not specific to the subject used within the kinematic data collection procedure were minimised by scaling the isometric torque values to those required during the matching procedure. The process used to accomplish this is detailed in Section 6.3.4

As the contractile and elastic components are in series, the torque expressed by the contractile component T_{con} is equal to the series elastic component torque T_{sec}. The initial value (t = 0) of T_{con} is calculated assuming the contractile component angular velocity ($\dot{\theta}_{con}$) is equal to the joint angular velocity ($\dot{\theta}$). Using Equations 6.3.1-3, an iteration calculated the value of θ_{con} for which T_{con} and T_{sec} were equal. After this initial time step, θ_{con} was updated by integration, assuming constant velocity:

$$\theta_{con} = \theta_{con} + \dot{\theta}_{con} dt \qquad (6.3.8)$$

The series elastic component angle θ_{sec} was then determined using Equations 6.3.1 and 6.3.2, before T_{sec} was calculated using Equation 6.3.3, and T_{con} was equated to T_{sec} in order to determine $\dot{\theta}_{con}$.

6.3.3   Muscle Activation Profiles

The nine–parameter, torque – angle – angular velocity function calculates the maximum voluntary torque that can be produced about a joint at a given contractile component angle and angular velocity. In order to calculate the torque applied at the joint $T(t)$ it is necessary to multiply the maximum voluntary torque T_{vol} by a muscle activation level $A(t)$:

$$T(t) = A(t) \cdot T_{vol} , \quad \text{where } 0 \leq A(t) \leq 1 \qquad (6.3.9)$$

A quintic function with zero velocity and acceleration at the end points was used to ramp up and down the muscle activation levels (Yeadon and Hiley, 2000):

$$A(t) = a_i + (a_f - a_i)\left(\frac{t-t_i}{t_f-t_i}\right)^3 \left(6\left(\frac{t-t_i}{t_f-t_i}\right)^2 - 15\left(\frac{t-t_i}{t_f-t_i}\right) + 10\right)$$

(6.3.10)

where $A(t)$ is the activation level at time t, a_i is the initial activation level at time t_i and a_f is the final activation level at time t_f.

The muscle activation profiles allowed two separate rampings and were defined by seven parameters; three activation levels a_0, a_1 and a_2, the start time of the two ramps t_{s1} and t_{s2}, and two ramping durations t_{r1} and t_{r2}.
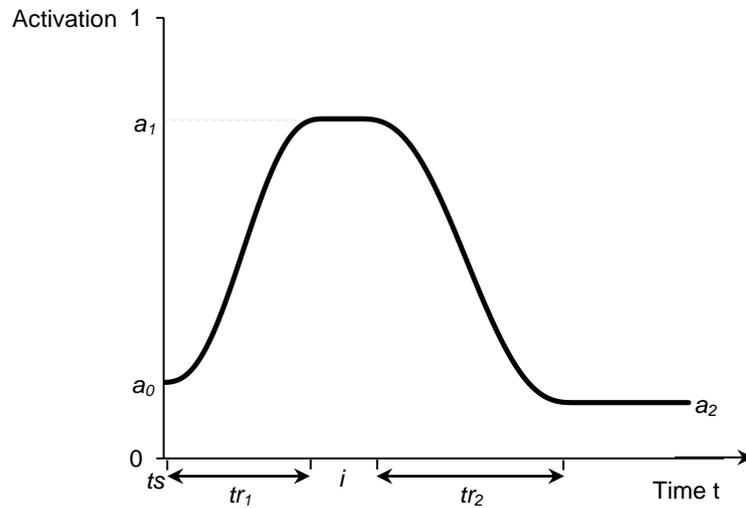
Figure 6.3.4 Example of a muscle activation profile.

Table 6.3.2 Seven parameters defining muscle activation profiles.

Parameter	Definition
a_0	Pre-impact, initial activation level
a_1	Maximal/minimal activation level
a_2	Final activation level
t_s	Start time of the first ramp
t_{r1}	Duration of the first ramp
i	Time interval between first and second ramps
t_{r2}	Duration of the second ramp

6.3.4 Strength Parameter Scaling Factors

The strength of torque-driven simulation model is dependent on the strength parameters governing the torque generators used to drive the motion. In order to successfully evaluate a simulation model it must be able to reproduce realistic movements, so the strength parameters governing the performance of the torque generators must be able to closely represent the capabilities of the subject.

In order to accurately represent the strength of the subject using strength parameters measured from different individuals, the isometric torque parameters were scaled so that the model was able to achieve the torques required to match the recorded performances (King *et al.*, 2009). During the matching procedure used to evaluate the torque-driven model, the isometric torque parameters T_0 were multiplied by a scaling factor x to give a subject-specific, scaled isometric torque sT_0. A common value for x was used for both the extensors and flexors at each joint, so that the relative strength of the extensors and flexors about a joint was maintained. Whilst performing this process, it was necessary to force the extensor torque generators to use maximal activation and reduce the level of co-contraction of the flexor to a minimum, so that the matching procedure was not able to use the scaling factor to compensate for sub-maximal activation levels or unnecessary co-contraction:

$$sT_0 = T_0 \cdot x \quad \text{when} \quad a_{max} = 1.0 \qquad (6.3.11)$$

During the model evaluation three trials were matched, providing three values of x for each of the pairs of torque generators about each joint. From the three values the highest scaling factor was selected as this represented the largest value of the isometric torque parameter required by the simulation model in order for it to be able to perform the movements recorded during the collection of kinematic data. After the strength scaling factor for each joint had been determined, this value was fixed and the model was re-evaluated allowing each torque generator to peak at sub-maximal activation.

6.3.5   Metatarsal-Phalangeal Joint

The metatarsal-phalangeal joint is angle-driven and is governed by a function that relates the joint angle to the depression of the trampoline suspension system. The movement of the MTP joint during the performances was found to be related to depression of the trampoline through observation of the recorded performances. During the depression phase of the contact there it was observed that the relationship between MTP joint angle and trampoline depression was consistent (Figure 6.3.5). Whilst during the recoil phase it was observed that the MTP joint angle was only consistent between skills rotating in the same direction (Figure 6.3.6 and Figure 6.3.7)
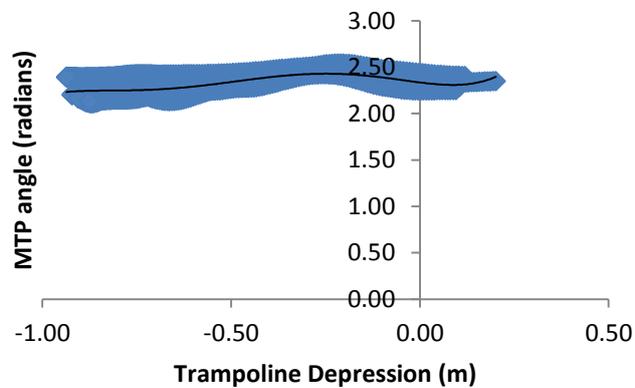
Figure 6.3.5 Illustration of the relationship between MTP joint angle and trampoline depression during the depression phase of the trampoline contact.
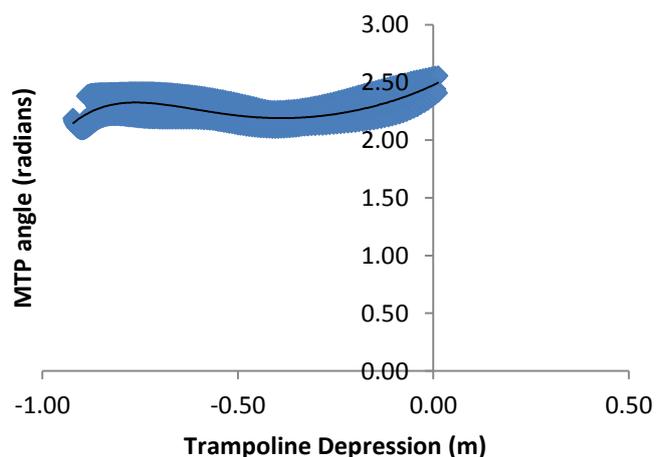
Figure 6.3.6 Illustration of the relationship between MTP joint angle and trampoline depression in forward rotating skills during the recoil phase of the trampoline contact.
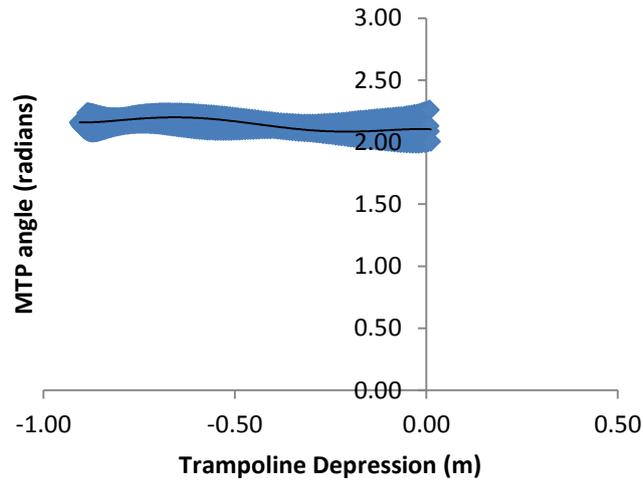
Figure 6.3.7 Illustration of the relationship between MTP joint angle and trampoline depression in backward rotating skills during the recoil phase of the trampoline contact.

A quintic polynomial was fit to each of the data sets to describe the MTP joint angle as a function of trampoline depression. The polynomials describing the depression phase for all skills and recoil phases for forward skills achieved R^2 values of 0.456 and 0.365 respectively. The polynomials were used to drive the MTP joint angle throughout the simulations whilst the first and second derivatives were used to calculate the angular velocity and acceleration.

Using two functions to describe the MTP joint angle during one simulation meant that at the transition between the two functions at the lowest point there was a small discontinuity in the MTP angle and velocity. This small discontinuity was avoided by subtracting a quadratic function from the polynomial describing the recoil phase so that at maximum depression the quadratic function was equal to the difference between the MTP joint angles given by the two functions and the gradient equal to the difference between the MTP joint angular velocities.

6.4   Model Evaluation

The torque-driven model was evaluated in order to ensure its validity and reliability. A successful evaluation proves that a simulation model is capable of accurately reproducing realistic human movement, and can be achieved by

comparing simulations to actual performances. Once a simulation model has been successfully evaluated, and good agreement between simulated and actual performance has been shown, the model can be used for further analysis and to simulate motion. The model evaluation was concurrently conducted along with the process to determine strength parameter scaling factors detailed in Section 6.3.4.

The model was evaluated in a two-step procedure. The first step, a maximal activation protocol, was carried out to discover the strength scaling parameters required to enable the simulation model to perform the skills by forcing the extensors of the supporting joints to be fully activated during the simulations whilst allowing the strength scaling factors to vary. The second step, a fixed strength protocol, used a fixed isometric strength for each joint and allowed submaximal activation of each joint during the simulations.

Three trials were selected to be used in the matching procedure. These trials covered a broad range of forward rotational requirements. The selected skills were a single straight forward somersault F_1, a piked 1¾ forward somersault F_2, and a piked triffus F_3; the same trials as used in the matching of the angle-driven model.

6.4.1 Model Input

The inputs of the torque-driven model were the initial conditions of the trampolinist immediately prior to first contact with the trampoline, body segmental inertias, the visco-elastic parameters governing the foot-suspension system interactions, and the strength parameters governing the each torque generator. The initial conditions prior to contact were the horizontal and vertical position and velocities of the toe, orientation angle and angular velocity, and joint angles and angular velocities determined from the kinematic data. The torques produced by the torque generators were doubled in order to represent both the left and right limbs acting symmetrically.

6.4.2 Model Variables

Fifty-five parameters were varied within the initial matching procedure; forty-seven activation parameters, four strength scaling factors, and four parameters to vary initial conditions.

There were 15 parameters governing the actions of each pair of torque generators, seven activation parameters each and a strength scaling factor. However because the strength were being scaled, as described in Section 6.3.4, each of the ankle, knee, and hip extensors were forced to reach maximal activation, reducing the number of parameters by three. The flexor torque generators of the ankle and hip were also forced to reach zero activation to prevent co-contraction artificially inflating the strength required at the joints, removing a further two parameters. It was also possible to eliminate four initial activation parameters, a_0, as it was observed from the data that each of the torque-driven joints had a low angular velocity at the moment of impact with the trampoline. It was reasoned that the initial extensor and flexor torques must be similar. On this basis the initial activation level of the extensor was related to the initial activation level of the flexor in an inverse ratio of their respective isometric strengths, so that the co-contraction at the joint caused zero net torque at impact.

Based on the torques generated about each joint in the angle-driven simulations (Appendix 4) the activation profiles of the ankle, knee, and hip torque generators were constrained so that the extensor torques ramped down and then up, and the flexor torques ramped up and then down. The activation profiles maintained flexibility though as the activation level was permitted to remain constant throughout the simulation or only ramp in one direction if the start times of each ramp were delayed.

The 47 muscle activation parameters varied within the matching procedures were limited to values based on information found in the literature.

Yeadon *et al*. (2010) demonstrated that prior to a landing the muscles of the legs are activated. The onset of pre-landing activation has been shown to begin up to 139 ms prior to landing dependent on the vertical velocity at impact (Arampatzis

et al., 2003), thus the it was decided to set the initial starting time t_s to between - 150 and 0 ms, where touchdown occurred at 0 ms.

All joints were given pre-landing activation levels, a_0, greater than zero to ensure co-contraction at all joints and prevent rapid joint accelerations at the beginning of the simulation. The level of pre-landing activation in a drop jump has been found to be about 50% of maximal activation (Horita *et al.*, 2002) or higher (Arampatzis *et al.*, 2003), therefore the pre-landing activation level was set to between 0.2 and 0.6.

Freund and Budingen (1978) showed that the required time to ramp from zero to maximal activation in voluntary contractions was 70 ms, however it has been shown that in jumping and landing activities ramp times of between 100 and 200 ms have been required to reach maximal activation (Arampatzis *et al.*, 2003; Duncan & McDonough, 2000; Jacobs *et al.*, 1996). The lower limit for ramping durations t_{r1} and t_{r2} therefore was set to 100 ms and whilst there is no theoretical upper limit for the ramp time it was set to 0.55 s for t_{r1} and 0.3 s for t_{r2} as by those times takeoff will have occurred.

The time interval between the two rampings, i, was allowed to vary between 0.0 to 0.15 s. If the second ramp started after takeoff then no second ramp would take place.

Each of the torque generators were allowed to vary the isometric torque parameter, by multiplying it by a scaling factor, in order to match the maximum torques used by the trampolinist during the recorded performances. The scaling factors were allowed to vary between 0.35 and 2.0 based on the torque values achieved during the angle-driven simulations.

Four additional parameters were allowed to vary the initial horizontal and vertical velocity of the toe, the initial orientation angle of the trunk, and the initial angular velocity of the shoulder.

Table 6.4.1 Upper and lower bounds for muscle activation parameters.

Parameter		LB	UB
a_0		0.005	0.6
a_1		0.0	1.0
a_2		0.0	1.0
t_s	(s)	-0.02	0.02
t_{r1}	(s)	0.1	0.55
i	(s)	0.1	0.4
t_{r2}	(s)	0.1	0.3
Extensors			
a_1		0.0	a_0
a_2		a_1	1.0
Flexors			
a_1		a_0	1.0
a_2		0.0	a_1

After the initial matching procedure the strength scaling parameters that were determined to be required for the simulation model to perform the skills were used in a second matching procedure that allowed submaximal activation of the torque generators whilst the isometric strength of each torque generator was now fixed.

During the fixed strength matching procedure sixty parameters were varied; seven activation parameters for each torque generator, and four parameters allowing the initial conditions to vary. There were no longer the constraints of the extensors maximal activation, the ankle and hip flexors reaching minimal activation, and the initial activation levels of each pair of torque generators were no longer constrained to produce zero net torque.

6.4.3 Cost Function

The torque-driven model was evaluated using a cost function developed to objectively assess the agreement between the torque-driven simulation and the recorded performance. The cost function was a root mean square of component

scores designed to measure the discrepancies in three different aspects of the simulation. The three aspects covered the difference in joint and orientation angles throughout the simulation S_{RMS}, the difference in joint and orientation angles at the end of the simulation S_{ABS}, and the differences in the movement outcomes at the end of the simulation S_{MOV}.

$$COST = \sqrt{S_{RMS}{}^2 + S_{ABS}{}^2 + S_{MOV}{}^2 + P^2} \qquad (6.4.1)$$

Where: S_{RMS} = component score for orientation and configuration angles during contact

S_{ABS} = component score for orientation and configuration angles at takeoff

S_{MOV} = component score for movement outcomes

P = joint angle penalties (°)

The component score for orientation and configuration angles during contact S_{RMS} was the mean square RMS difference between the simulation and recorded performance, measured in degrees, of the trunk orientation angle θ_t and the four joint angles: ankle θ_a, knee θ_k, hip θ_h, and shoulder θ_s.

$$S_{RMS} = \sqrt{\frac{\theta t_{RMS}^2 + \theta a_{RMS}^2 + \theta k_{RMS}^2 + \theta h_{RMS}^2 + \theta s_{RMS}^2}{5}} \qquad (6.4.2)$$

Where: θt_{RMS} = RMS difference in trunk orientation (°)

θa_{RMS} = RMS difference in ankle angle (°)

θk_{RMS} = RMS difference in knee angle (°)

θh_{RMS} = RMS difference in hip angle (°)

θs_{RMS} = RMS difference in shoulder angle (°)

The component score for orientation and configuration angles at takeoff S_{ABS} was calculated as the mean square absolute difference between the simulation and recorded performance of the orientation and four joint angles measured in degrees.

91

$$S_{ABS} = \sqrt{\frac{\theta t_{ABS}^2 + \theta a_{ABS}^2 + \theta k_{ABS}^2 + \theta h_{ABS}^2 + \theta s_{ABS}^2}{5}}$$ (6.4.3)

Where: θt_{ABS} = RMS difference in trunk orientation (°)

θa_{ABS} = RMS difference in ankle angle (°)

θk_{ABS} = RMS difference in knee angle (°)

θh_{ABS} = RMS difference in hip angle (°)

θs_{ABS} = RMS difference in shoulder angle (°)

The component score for the movement outcomes was the mean square of individual component scores measuring the discrepancies in four areas; horizontal and vertical linear momentum, angular momentum and the duration of the contact phase. The horizontal linear momentum and vertical linear momentum scores S_1 and S_2 were calculated as the difference in horizontal and vertical takeoff velocities as a percentage of recorded resultant velocity at takeoff. The angular momentum score S_3 was calculated as the percentage difference in angular momentum at takeoff between the recorded and simulated performance. The contact duration score S_4 was calculated as the percentage difference between the simulated contact duration and the recorded contact duration as a percentage of the recorded contact duration.

$$S_{MOV} = \sqrt{\frac{S_1^2 + S_2^2 + S_3^2 + S_4^2}{4}}$$ (6.4.4)

Where: S_1 = percentage difference in horizontal linear momentum (%)

S_2 = percentage difference vertical linear momentum (%)

S_3 = percentage difference angular momentum (%)

S_4 = percentage difference contact duration (%)

The simulations were also penalised if the joint angles of the hip, knee, and ankle exceeded the range of motion demonstrated by the trampolinist during the data collection. A penalty was incurred when the simulations exceeded these ranges of motion, this penalty was equal to the square of the cumulative number of degrees

the range of motion was exceeded by across the three joints. The limits of the ranges of motion for each joint are described in Table 6.4.2.

Table 6.4.2 Limits of the range of motion of the joints, as used for penalties.

Joint	Lower Limit (°)	Upper Limit (°)
Ankle	93	152
Knee	133	196
Hip	106	213

6.4.4 Strength Scaling Matching Results

The four trials were matched using the simulated annealing algorithm optimising the parameter values so that the average difference across the three trials was just 4.4%. The individual simulations matched the recorded performances with scores of 3.3% (F_1), 4.9% (F_2), and 5.0% (F_3). The mean score of 4.4% across the three selected trials shows that the simulation model was capable of adequately replicating the motion of a trampolinist both throughout the contact phase and at takeoff in forward somersaulting skills. Table 6.4.3 shows the component scores achieved by the combined matching procedure for each of the four skills and the mean value of each component score.

Table 6.4.3 Cost function component scores resulting from the strength scaling matching protocol.

| | Component Score | | | | | | | Score |
	S_{RMS} (°)	S_{ABS} (°)	S_1 (%)	S_2 (%)	S_3 (%)	S_4 (%)	P (°)	(%)
F_1	2.8	1.5	0.2	1.7	0.0	0.3	–	3.3
F_2	4.0	1.0	2.4	3.2	0.3	3.0	–	4.9
F_3	4.8	0.9	2.0	1.2	1.2	0.3	–	5.0
Mean	3.9	1.2	1.5	2.0	0.5	1.2	0.0	4.4

S_1 – average RMS difference in orientation and configuration angles during contact (°), S_2 - average difference in orientation and configuration angles at takeoff (°), S_3 - percentage difference in horizontal linear momentum (%), S_4 - percentage difference vertical linear momentum (%), S_5 - percentage difference angular momentum (%), S_6 - percentage difference contact duration (%), P - joint angle penalties

The torque-driven model was able to closely match the performance of the trampolinist in all three forward rotating skills. The angles at takeoff (1.2°), horizontal linear momentum (1.5%), vertical linear momentum of the trampolinist (2.0%), and angular momentum at takeoff (0.5%) and the duration of contact (1.2%) were all closely matched by the simulation model. None of the simulations received penalties for exceeding the observed ranges of motion.

Figure 6.4.1 and Figure 6.4.2 show visual representations of the trampoline contact phase during the recorded performances and the matched torque-driven simulations for a single straight front somersault F_1 and a piked triffus F_3 respectively.
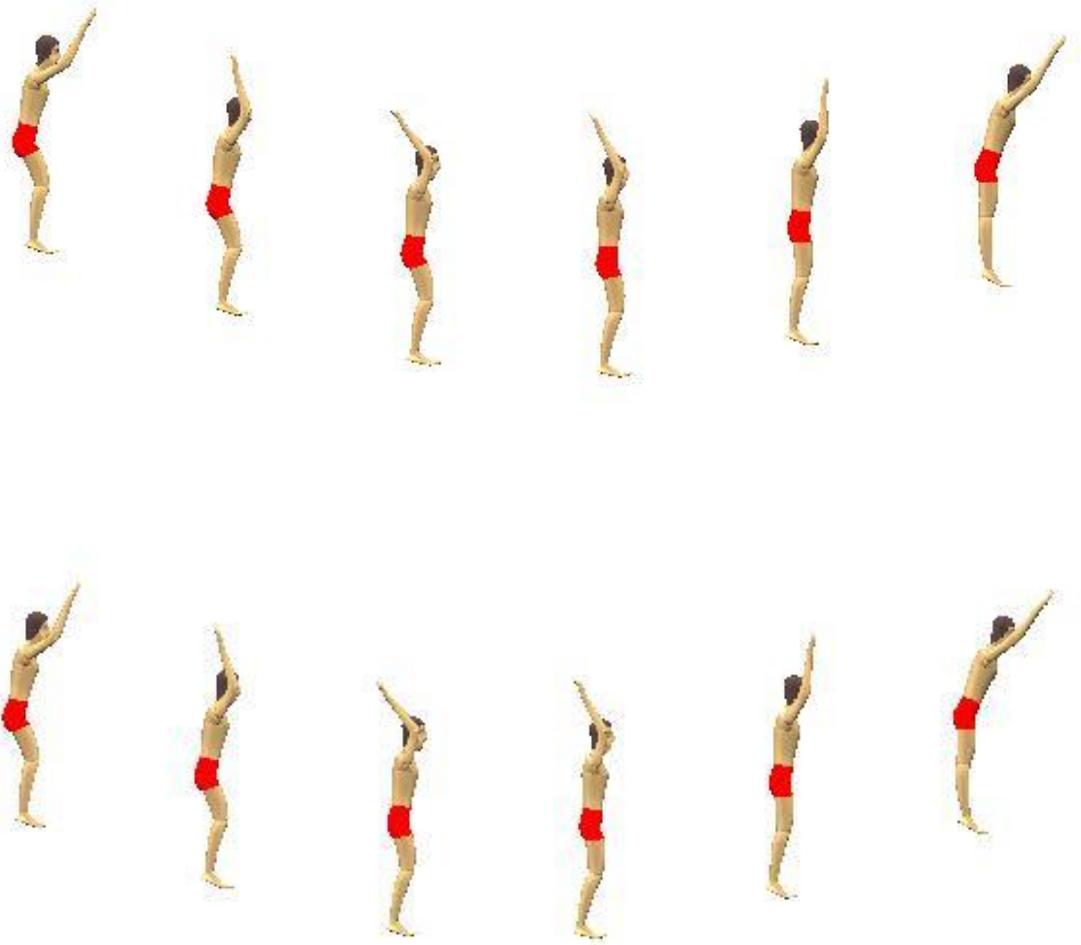
Figure 6.4.1 Comparison of F_1 trampoline contact phase performance (above) and torque-driven simulation (below).
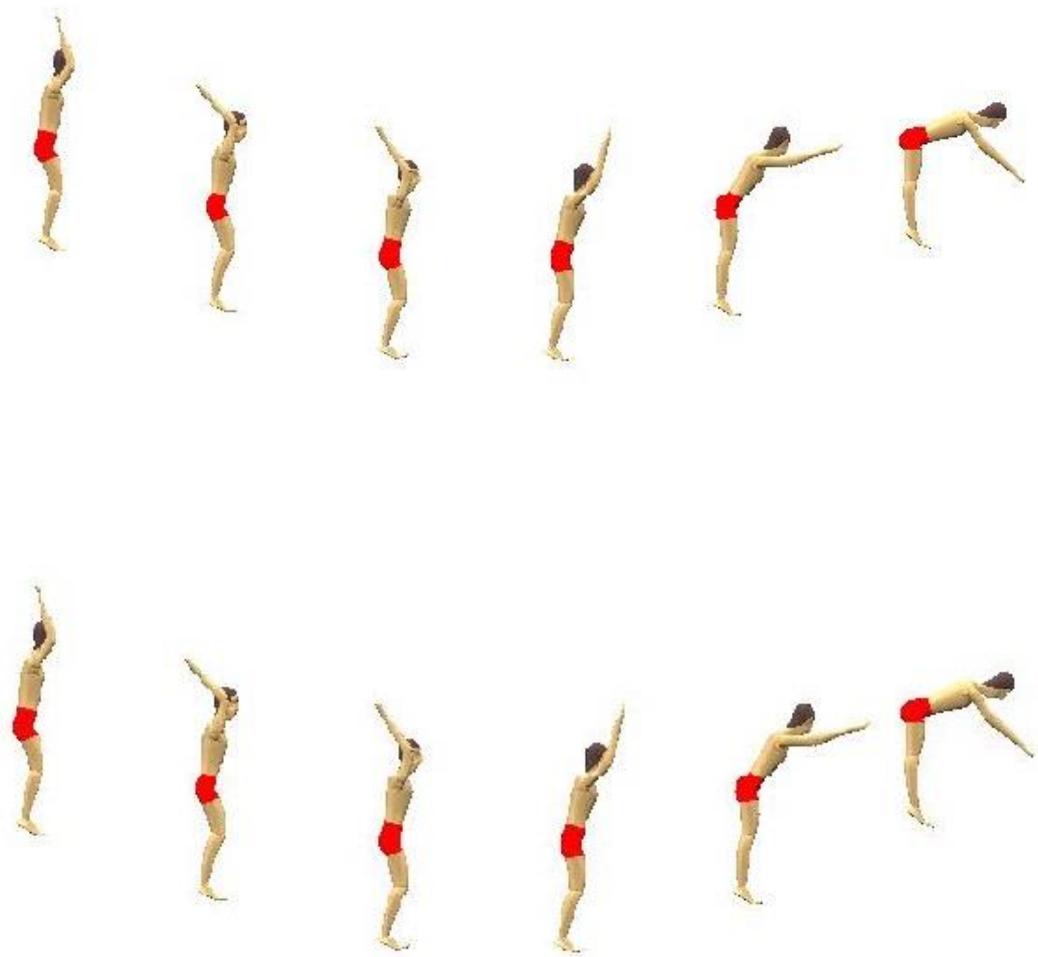
Figure 6.4.2 Comparison of F_3 trampoline contact phase performance (above) and torque-driven simulation (below).

6.4.4.1 Joint Angles

The difference between the joint angles of the recorded and simulated performance was weighted heavily in the evaluation of the simulation model; one component of the cost function quantified the difference between the simulation and performance throughout the contact phase and another quantified the difference at the moment of takeoff. The simulation model was able to reasonably reproduce the joint movements throughout the contact phase and closely matched the joint angles at takeoff. Figure 6.4.3 compares the joint angles of the ankle, knee, hip, and shoulder during the skills F_1 and F_3.

It can be seen that generally the model was able to closely match the joint angles throughout the contact, although the ankle shows greater plantar flexion during the depression phase of F_1 and the shoulder angle during the depression phase of F_3 is less flexed. It can also be seen that upon reaching maximum depression at the midpoint of the contact phase and during the recoil phase all the joint angles follow the recorded performances closely.
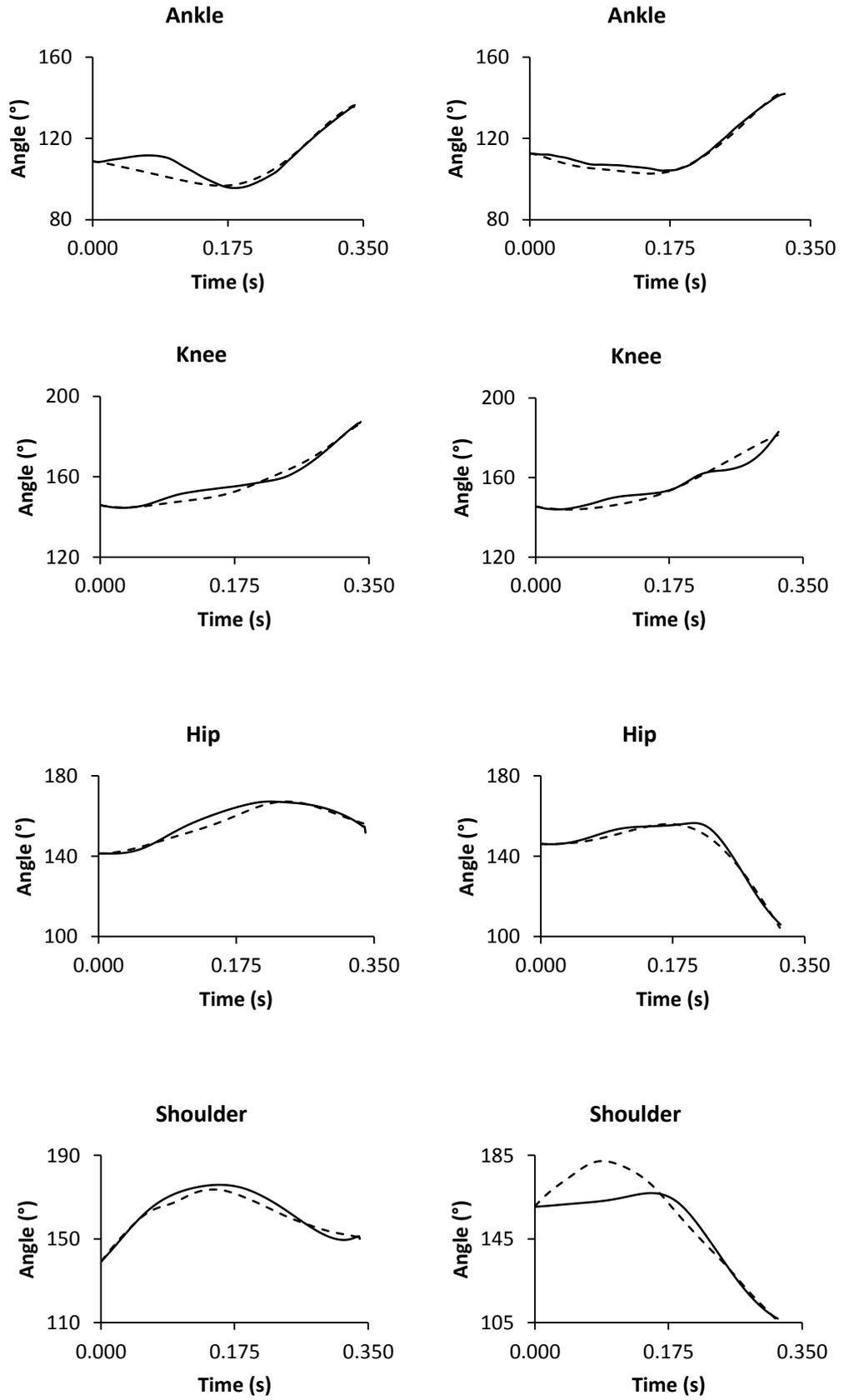
Figure 6.4.3 Comparison of the joint angles during matched simulations (solid line) and performance (dashed line) of F_1 (left) and F_3 (right).

98

<u>6.4.4.2</u> <u>Joint Torque Activation Profiles</u>

The activation profiles for the six torque generators for the skills F_1 and F_3 are shown in Figure 6.4.4, and the parameter values describing the activation profiles can be found in Appendix 5. The activation time histories show that the ankle plantar flexors reached maximal activation after both the hip and the knee extensors in both skills, and the hip extensors ramped the activation level down earlier than both the knee and ankle. All of the matching simulations used both the available ramps, up and down, for both the flexor and extensor at the ankle, hip, and shoulder, however the knee flexor did not ramp the activation back up in either F_2 or F_3.

The hip activation profiles are very different to each other during the recoil phase. In F_1 co-contraction is maintained throughout, however during the recoil phase of F_3 the hip extensors switch off completely and immediately before takeoff the hip flexors ramp up quickly, in order to promote hip flexion and initiating the forward motion of the centre of mass in order to produce somersault rotation. This effect can be seen in Figure 6.4.3 the hip angle in F_3 the hip angle quickly decreases before takeoff, requiring a lower extensor torque.
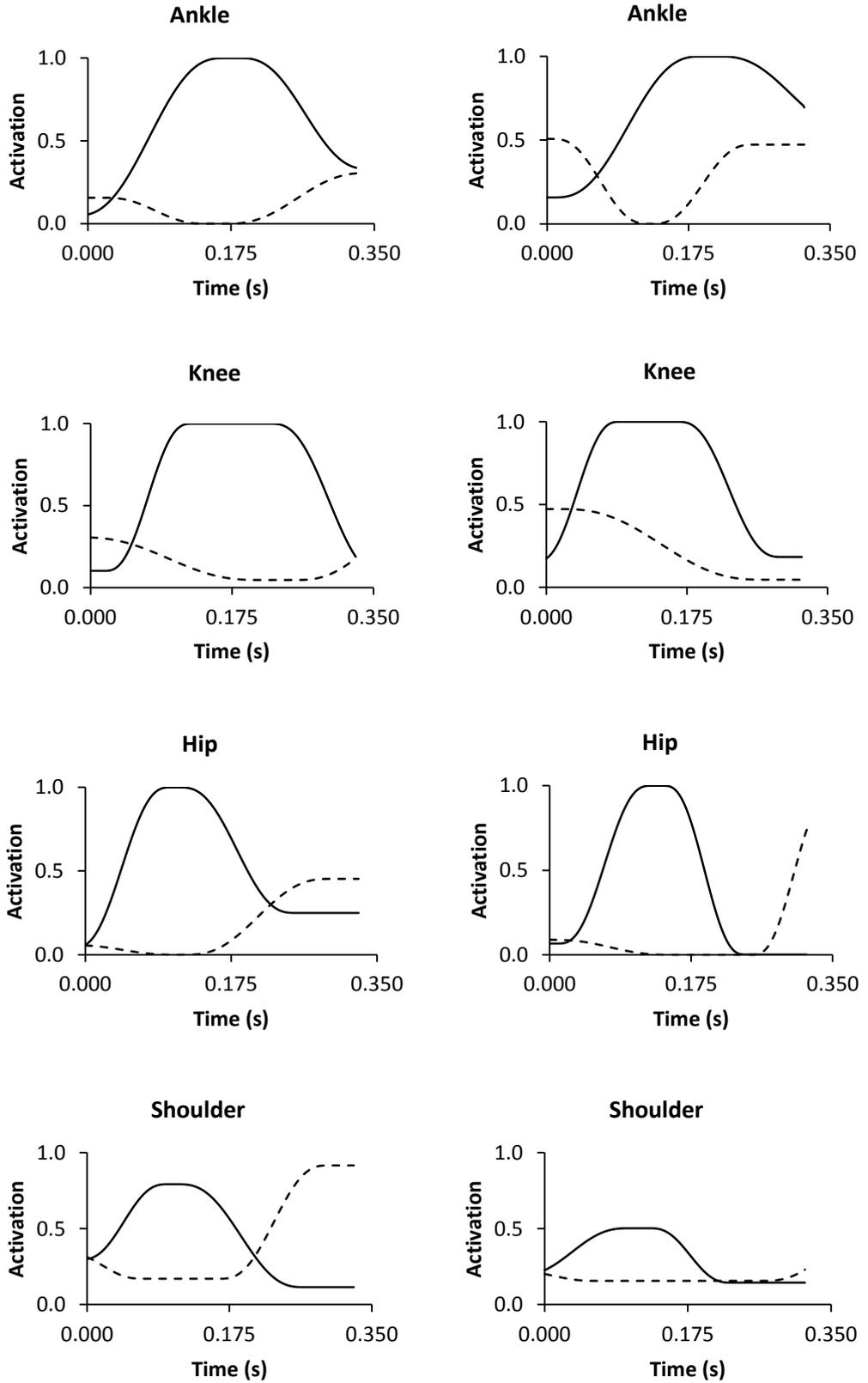
Figure 6.4.4 Activation time histories of the extensors (solid line) and flexors (dashed line) of F_1 (left) and F_3 (right).

100

<u>6.4.4.3</u> <u>Joint Torques</u>

The net joint torque time histories obtained from the torque driven simulations for the skills F_1 and F_3 are detailed in Figure 6.4.5, with negative torques representing extension and positive torques representing flexion.

There are similarities between the shapes of the different joint torque; each supporting joint steadily increased the extensor torque to a maximum point at around the time of maximum depression of the trampoline before decreasing during the recoil phase. The joint torque profiles at each joint have similar shapes for both of the skills but there were some differences in the magnitude and timing of the torques. The magnitude of the peak extensor torque is greater at each supporting joint in the triffus with differences in the shape of the torque profiles in the recoil phase displaying how the joint angles are changed for produce angular momentum as histories shown in Figure 6.4.3.

During the recoil phase of the triffus the hip extensor torque quickly decreases due to the sharp deactivation of the hip extensors, whilst also causing a step in the knee torque as it decreases. The change in the hip torque and the resulting decrease in the hip angle, also leads to the shoulder flexor torque being maintained throughout the recoil phase, as a greater torque is required to keep the arms overhead and produce the necessary arm action when the upper body is leaning forward.
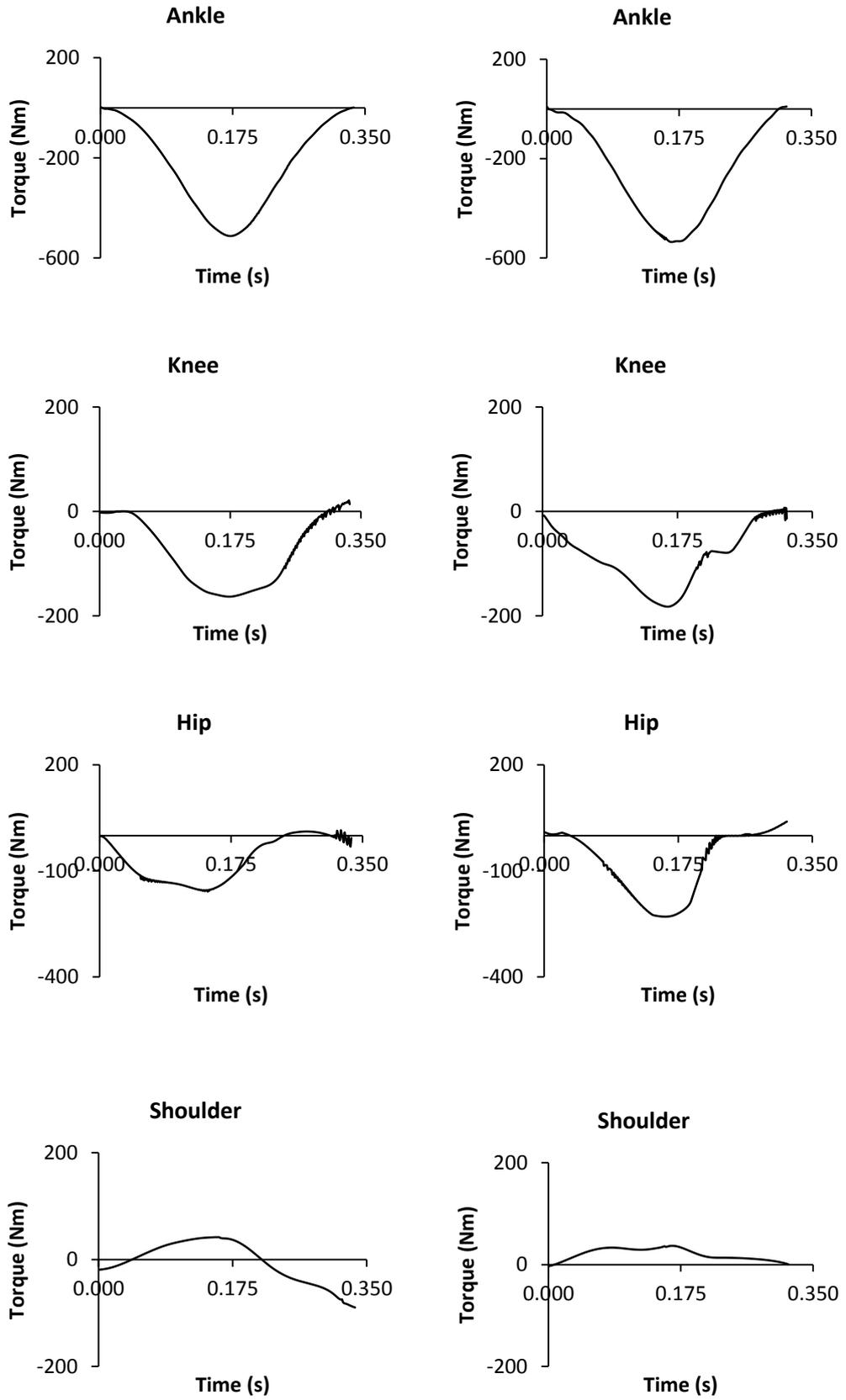
Figure 6.4.5 Comparison of the joint torques during matched torque-driven simulations of F_1 (left) and F_3 (right).

102

6.4.4.4 Strength Scaling Factors

The matching procedure varied the strength scaling factors resulting in three different values, one from each skill, for the scaling factor at each joint. The resulting strength scaling factors are shown in Table 6.4.4. None of the scaling factors pushed against the limits of the bounds set during the matching procedure demonstrating that the strengths of each pair of torque generators was not too closely constrained to the values measured from the studies of Allen (2009) and Jackson (2010).

Table 6.4.4 Strength scaling factors.

	ankle	knee	hip	shoulder
	Strength Scaling Factors			
F_1	1.04	0.75	1.26	0.47
F_2	1.55	0.44	1.34	0.57
F_3	1.77	0.93	0.99	0.69
Maximum	1.77	0.93	1.34	0.69

The maximum value of each of the strength scaling factors found across the four matching simulations was assumed to represent the maximal functional strength of the trampolinist about each joint whilst trampolining. These values were then used in a second matching procedure, the results of which are detailed in Section 6.4.5. Three of the maximum values, for the ankle, knee, and shoulder, were obtained from the matching simulation of the triffus skill; the maximum scaling factor for the hip came from the 1¾ somersault.

The largest strength scaling factor required in the matching process was 1.77 for the ankle in F_3. This is a large increase over the measured isometric strength of a triple jumper's ankle, however given the difficulties in collecting maximal torque data from the ankle joint this was not deemed to be unreasonable.

6.4.5 Fixed Strength Matching Results

The same three trials that were matched previously were subsequently matched using the simulated annealing algorithm to optimise only the parameter values governing the activation profiles. This procedure resulted in an average difference across the 3 trials of just 4.4%. The individual simulations matched the recorded performances with scores of 3.2% (F_1), 4.8% (F_2), and 5.3% (F_3). The mean score of 4.4% across the three selected trials shows that the simulation model was capable of adequately replicating the motion of a trampolinist both throughout the contact phase and at takeoff. Table 6.4.5 shows the component scores achieved by the combined matching procedure for each of the three skills and the mean value of each component score.

Table 6.4.5 Cost function component scores resulting from the fixed strength matching.

	Component Score							Score
	S_{RMS} (°)	S_{ABS} (°)	S_1 (%)	S_2 (%)	S_3 (%)	S_4 (%)	P (°)	(%)
F_1	2.7	1.5	0.2	1.3	0.2	0.0	–	3.2
F_2	4.1	1.2	1.4	2.8	0.1	3.0	–	4.8
F_3	4.9	1.2	1.7	2.2	1.2	0.6	–	5.3
Mean	3.9	1.3	1.1	2.1	0.5	1.2	0.0	4.4

S_1 – average RMS difference in orientation and configuration angles during contact (°), S_2 - average difference in orientation and configuration angles at takeoff (°), S_3 - percentage difference in horizontal linear momentum (%), S_4 - percentage difference vertical linear momentum (%), S_5 - percentage difference angular momentum (%), S_6 - percentage difference contact duration (%), P - joint angle penalties

In the fixed strength protocol the torque-driven simulation model was capable of matching the performance of the trampolinist to the same level as during the strength scaling matching protocol (4.4% v 4.4%). The fixed strength protocol achieved the same results largely by reproducing similar average values for each of the component scores with only some small variation in each of the trials. In

both protocols the component scores were evenly balanced and showed a strong match across the different aspects of the simulation.

Figure 6.4.6 and Figure 6.4.7 show visual representations of the trampoline contact phase during the recorded performances and the matched torque-driven simulations for skills F_1 and F_3 respectively.
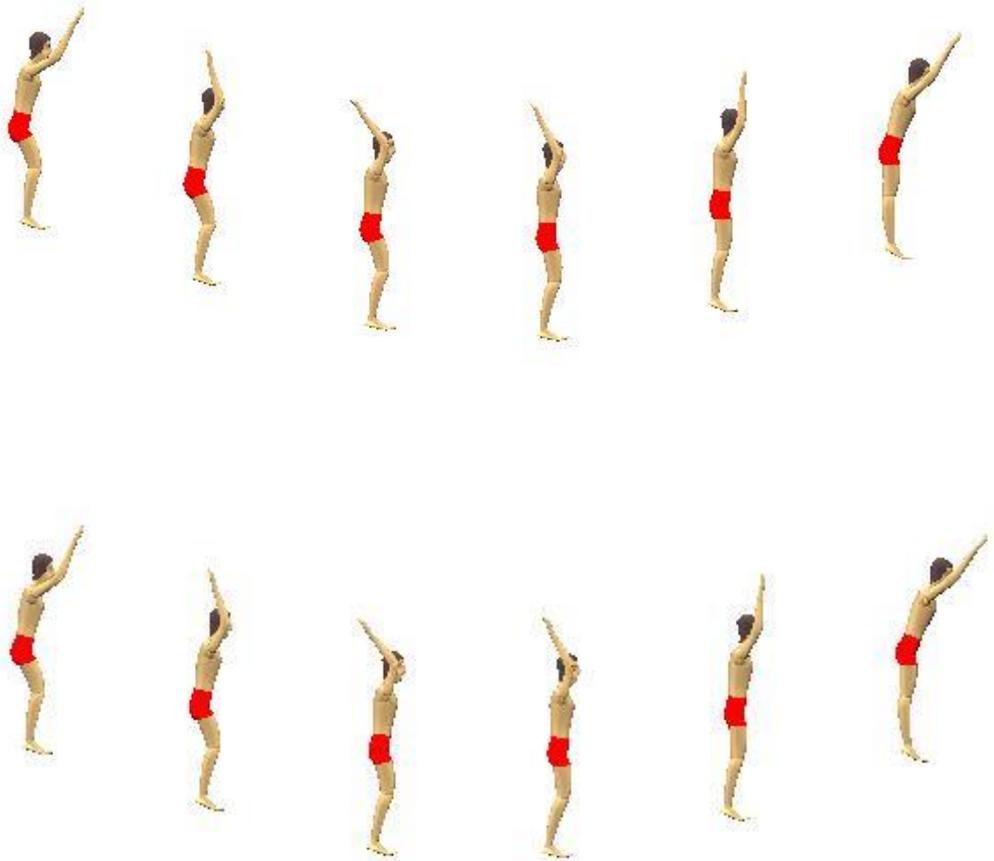
Figure 6.4.6 Comparison of F_1 trampoline contact phase performance (above) and fixed strength torque-driven simulation (below).
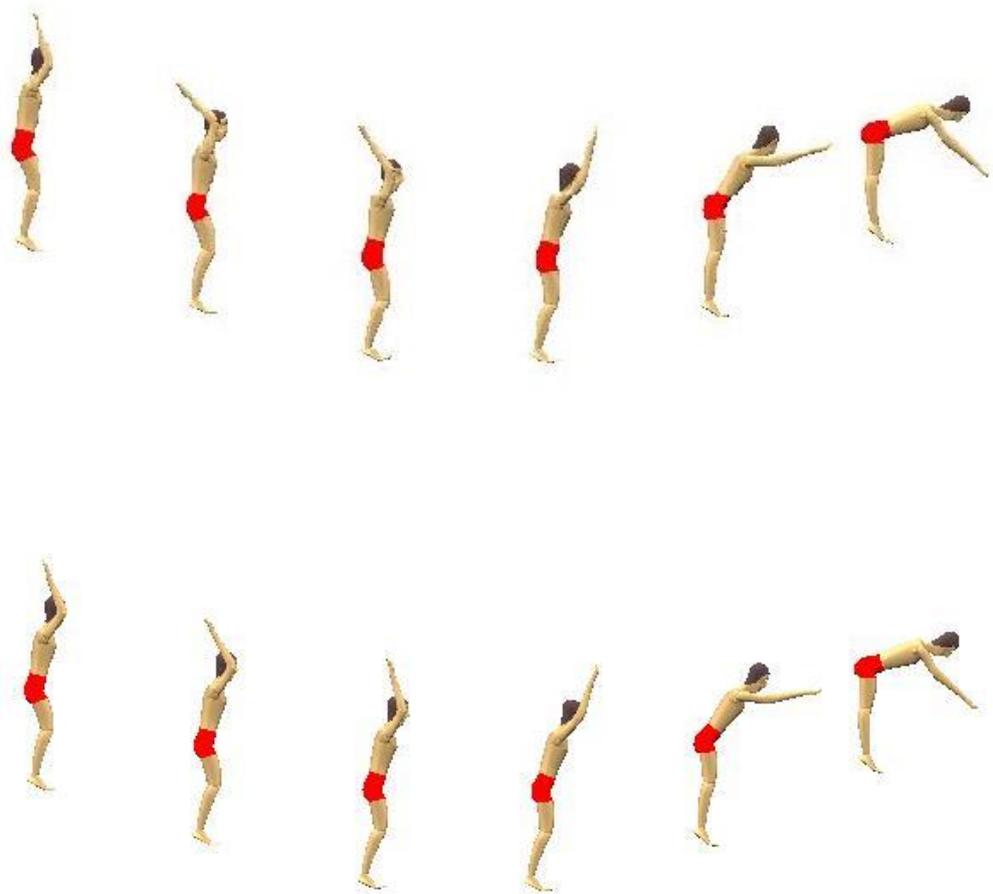
Figure 6.4.7 Comparison of F_3 trampoline contact phase performance (above) and fixed strength torque-driven simulation (below).

6.4.5.1 <u>Joint Angles</u>

Figure 6.4.8 compares the joint angles of the ankle, knee and hip throughout the performance and fixed strength matched simulations of skills F_1 and F_3. The fixed strength matching procedure was able to match the joint angles throughout the whole duration of the simulations, and showed very similar patterns to the joint angles in the matched simulations in the protocol. The shoulder angle during the simulation of F_3 followed the same pattern, reducing the initial shoulder velocity and not matching well in the first half of the contact phase in favour of matching closely throughout the recoil phase and at takeoff.

Ankle

Ankle

Knee

Knee

Hip

Hip

Shoulder

Shoulder
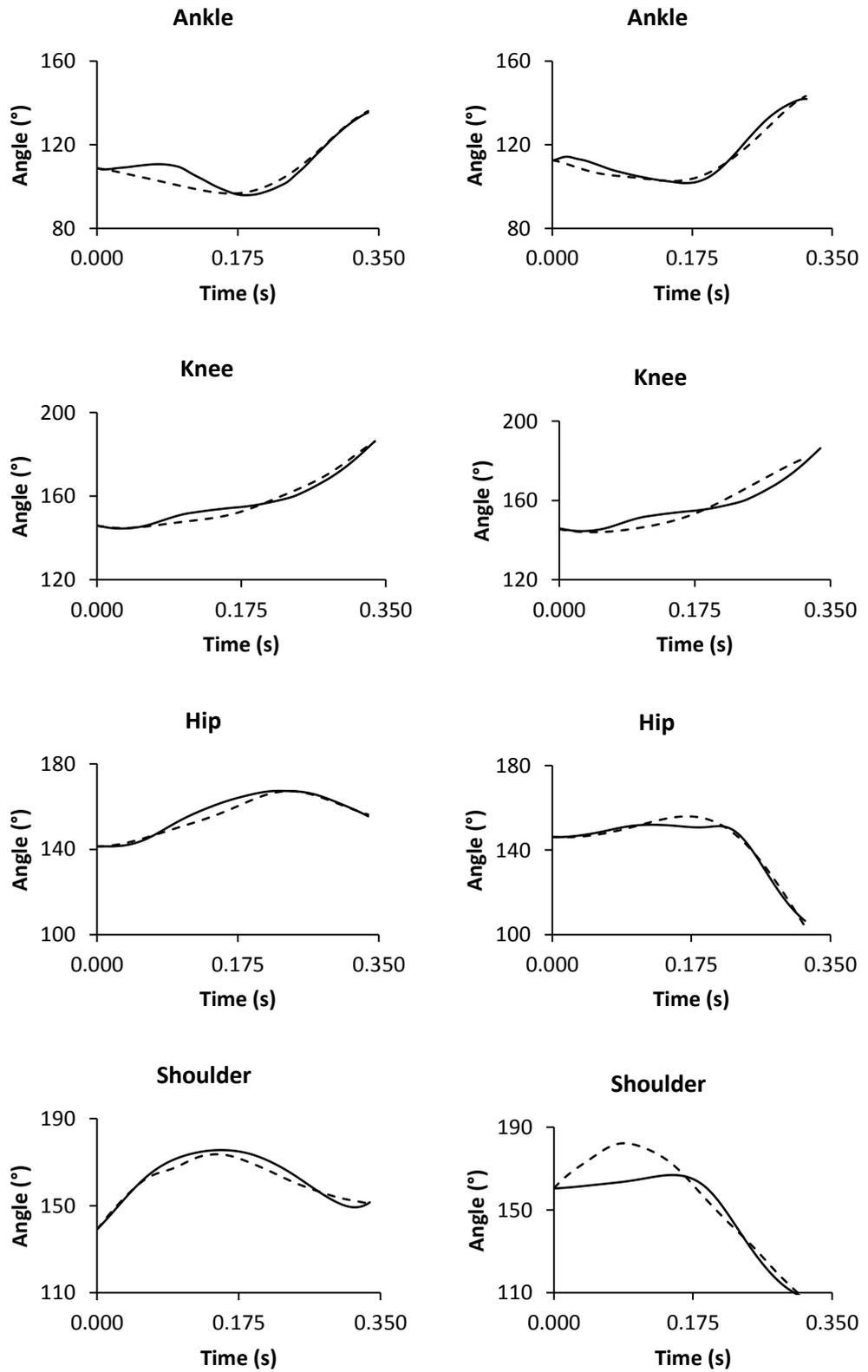
Figure 6.4.8 Comparison of the joint angles during fixed strength matched simulations (solid line) and performance (dashed line) of F_1 (left) and F_3 (right).

<u>6.4.5.2</u> <u>Joint Torque Activation Profiles</u>

The activation profiles for the six torque generators for the fixed strength matching simulations of skills F_1 and F_3 are shown in Figure 6.4.9, and the parameter values describing the activation profiles can be found in Appendix 6. Whilst generally the shapes of the activation profiles are similar to the activation profiles resulting from the strength scaling matching protocol, due to the strength of each torque generator having been scaled and the removal of other constraints the absolute activation levels and relative activation levels of extensors and flexors have changed. The most pronounced changes were made in the activation profiles of the ankle joint; in F_1 the plantar flexor ramped down activation minimally in the recoil phase, and in F_3 the dorsi flexors only slowly ramped up their activation through the contact phase instead of ramping off and on.

However, the largest difference in the activation profiles between the strength scaling matching and the fixed strength matching protocols is the disappearance of the increase in hip flexor activation immediately prior to takeoff in the triffus, F_3, instead opting to slowly ramp up in a similar profile to the dorsi flexors.
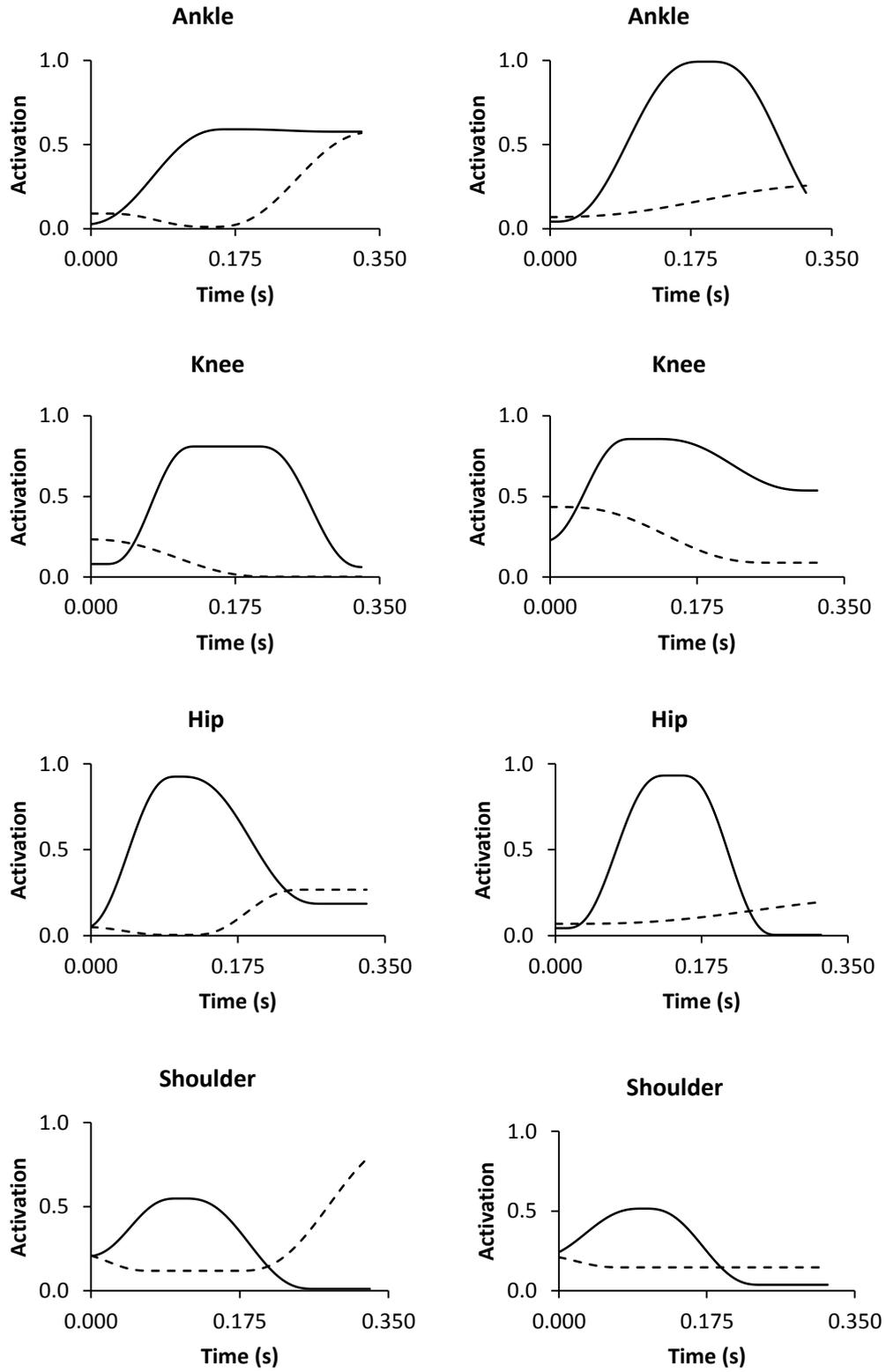
Figure 6.4.9 Matched activation time histories of the extensors (solid line) and flexors (dashed line) of F_1 (left) and F_3 (right) from the fixed strength protocol.

The net joint torque time histories obtained from the fixed strength torque-driven simulations for the skills F_1 and F_3 are compared to the joint torque time histories from the strength scaled matched simulations in Figure 6.4.10, with negative torques representing extension and positive torques representing flexion.

Each of the joint torque profiles have very similar shapes from both matching protocols with the only notable difference being the hip torque profile in the triffus. The fixed strength matching simulation utilised a greater peak hip extensor torque in the contact phase than the strength scaling matching simulation whilst the overall shape of the joint torque profiles remained consistent with the strength scaling protocol.
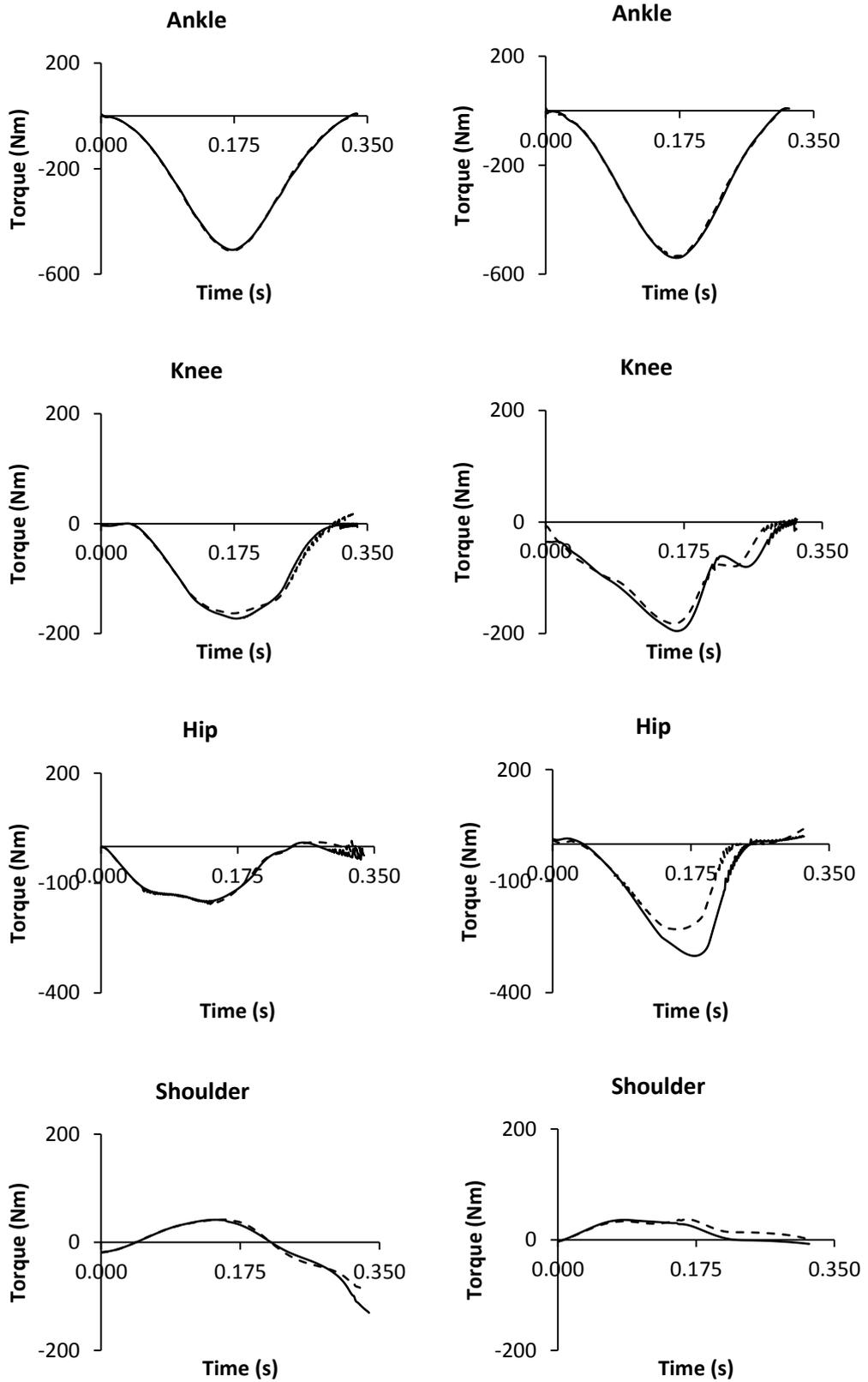
Figure 6.4.10 Comparison of the joint torques during fixed strength matched torque-driven simulations (solid line) and strength scaling matched simulations (dashed line) of F_1 (left) and F_3 (right).

111

6.4.6   Discussion

The evaluation of the torque-driven model has shown that the simulation is capable of closely representing the performance of forward rotating somersault skills on the trampoline. After scaling the strength parameters governing the torque generators to the performance of the subject, the simulation model matched the performance of the trampolinist well with a mean difference between the simulations and performances of 4.4%.

6.4.6.1 Joint Angles

The evaluation of the torque-driven model was able to match the joint angles well throughout the contact phase with the only exception being found at the shoulder during the depression phase of the triffus. The shapes of the joint angle time histories were reproduced with only small deviations from the recorded angles in the majority of cases. The matching simulations seemed to match the joint angles more closely during the recoil phase than the depression phase of contact, this most likely arose due to the large weighting of differences in both joint angles and movement outcomes at takeoff compared to throughout the whole duration of the movement.

In both of the matching protocols it can be seen that the root mean square difference in joint angles throughout the contact phase increases as the angular rotation requirement of the somersaulting skill increases. It can also be seen that the absolute difference in joint angles at takeoff decreases as the angular rotation requirement of the somersaulting skill increases. These results also in agreement with the idea that the composition of the cost function caused the optimisation algorithm to more closely match the movements of the simulation model to the complex performances at the moment of takeoff, rather than throughout the whole duration of the movements.

6.4.6.2 Movement Outcomes at Takeoff

Both matching protocols were able to recreate the movement outcomes of horizontal and vertical linear momentum, and angular momentum at takeoff, as well as the duration of the contact phase, to a high degree, with no individual

score exceeding 3.3% difference in any of these criteria. Angular momentum was matched particularly closely in both protocols with no difference greater than 1.2%, whilst the simulation model found it most difficult to match vertical linear momentum at takeoff, but even this achieved an average difference of almost 2%.

6.4.6.3 Summary

The torque-driven simulation model was demonstrated to be capable of realistically simulating forward somersaulting trampolining performances. Whilst the simulation model did not employ any strength parameters that were specific to the subject, the model was able to accurately represent the strength capabilities of the subject through the scaling of strength parameters taken from the literature. The model simulated the performances of the subject and was able to replicate key performance outcomes of the performances including the linear and angular momenta at takeoff, and so the model is considered to be suitable to be applied to optimise performance of forward somersaulting skills.

6.5   Chapter Summary

This chapter described the torque-driven simulation model, the method used to determine strength scaling factors to be used in conjunction with the simulation model, and the method used to evaluate the torque-driven simulation model. The model was able to simulate the performances of the subject well with a mean difference of 4.4% observed over three different skills, and so is considered suitable to be employed to answer the research questions. The following chapter will apply the simulation model of trampolining to answer the research questions.

Chapter 7: Optimisation and Applications

7.1   Chapter Overview

The present chapter describes the methods employed to apply the torque-driven simulation model of trampolining to answer the research questions presented at the beginning of this thesis. The results are then described and discussed.

7.2   Application to Research Questions

The research questions presented at the beginning of this thesis concerned the optimal techniques used by a trampolinist during the contact phase with the trampoline. Specifically:

For specific skills with a fixed rotational requirement what is the optimal takeoff technique to produce the required angular momentum with maximum peak height and minimum travel?

and

What is the optimal takeoff strategy to produce maximal somersault rotation potential in forward somersaults?

Within the present study the trampolinist performed a range of forward rotating skills with different rotation requirements, ranging up to a piked triffus. Could the subject perform a straight triffus or possibly a greater number of somersaults by using a different technique?

In order to perform skills with a larger amount of rotation the trampolinist must be able to either remain airborne for a longer period of time or takeoff with a greater amount of angular momentum, or a combination of both. A technique which produces more angular momentum is likely to reduce the height reached and the time spent airborne. An optimal technique for producing rotation will enable the trampolinist to takeoff with a high amount of both angular and vertical linear momenta.

7.3   Calculation of Kinematic Variables

7.3.1   Jump Height

The height of the jump h_j, was defined as the maximum height of the trampolinist's centre of mass above the level of the trampoline suspension system during the flight phase following the trampoline contact phase. Jump height comprises two constituent components; the height of the centre of mass at takeoff h_1, and the height gained by the centre of mass during flight h_2. Jump height was calculated as the sum of h_1 and h_2.

$$h_2 = \frac{v_z{}^2}{-2g} \qquad (7.3.1)$$

$$h_j = h_1 + h_2 \qquad (7.3.2)$$

Where: g = acceleration due to gravity (-9.81 ms^{-2})

h_j = jump height (m)

h_1 = height of CM at takeoff (m)

h_2 = height gained by the centre of mass during flight (m)

v_z = trampolinist's CM vertical takeoff velocity (ms^{-1})

7.3.2   Flight Time

The flight time t, was defined as the time between the last instant of contact between the feet of the trampolinist and the trampoline suspension system until the trampolinist's centre of mass was 0.936 m above the trampoline, *i.e.* the average height of the centre of mass at the moment of touchdown across all recorded trials. Using constant acceleration equations t was defined as:

$$t = \frac{v_z + \sqrt{(v_z{}^2 - 2g(0.936 - h_1))}}{g} \qquad (7.3.3)$$

Where: t = flight time (s)

g = acceleration due to gravity (-9.81 ms^{-2})

v_z = trampolinist's CM vertical takeoff velocity (ms^{-1})

h_1 = height of CM at takeoff (m)

7.3.3 Rotation Potential

Rotation potential is a measure of the trampolinist's potential to rotate in the flight phase following takeoff, accounting for the trampolinist's orientation and angular momentum at takeoff, as well as the duration of the flight phase following takeoff. Rotation potential is a normalised product of angular momentum and flight time, and is expressed as the number of somersaults the trampolinist would be capable of completing in a straight position.

The somersault angle at takeoff θ_i, was based on the orientation of the trunk and thigh at takeoff, and was weighted to represent the relative masses of the upper and lower body:

$$\theta_i = m_u\theta_u + m_l\theta_l \qquad (7.3.4)$$

Where: m_l = lower body mass ratio

m_u = upper body mass ratio

θ_i = initial somersault angle (°)

θ_l = angle of the thigh from vertical (°)

θ_u = angle of the trunk from vertical (°)

The amount of rotation the trampolinist is capable of during flight θ_f, was calculated as the product of angular velocity ω, and flight time t.

$$\theta_f = \omega t \qquad (7.3.5)$$

Where: θ_f = flight rotation angle (°)

ω = angular velocity (ms^{-1})

t = flight time (s)

Angular velocity was calculated using the angular momentum at takeoff H, and the moment of inertia of the trampolinist in a straight position I_s. The moment of inertia of the trampolinist in a straight position (arms adducted) was calculated to be 10.6 kg.m^2 using the inertia model of Yeadon (1990b.).

$$\omega = \frac{H}{I_s} \qquad (7.3.6)$$

Where: ω = angular velocity (ms^{-1})

H = angular momentum at takeoff (kg.m^2.s^{-1})

I_s = moment of inertia when straight (kg.m^2)

The rotational potential θ, was calculated as the sum of the initial somersault angle θ_i, and the flight rotation angle θ_f, converted to give the number of straight somersaults that could be achieved:

$$\theta = \frac{\theta_i + \theta_f}{360} \qquad (7.3.7)$$

Where: θ = rotation potential

θ_i = initial somersault angle (°)

θ_f = flight rotation angle (°)

7.4   Optimisation Method

7.4.1   Maximum Height Method

The optimisation procedure maximised the height reached during the flight phase for the three skills employed in the evaluation of the model; a straight single forward somersault F_1, a piked 1¾ forward somersault F_2, and a piked triffus F_3.

The 56 joint torque activation parameters of the torque-driven model were optimised to determine the optimal technique to produce jump height during the flight phase. The strength scaling factors determined during the matching procedure were maintained, whilst the initial conditions (excluding vertical velocity), and elbow joint angle time histories for the simulations were taken from the recorded data. The initial vertical velocity was normalised to -7.5 ms^{-1} but the initial horizontal velocity of the trampolinist was also allowed to vary so that the optimisation procedure could use this as a mechanism to reduce horizontal

117

velocity at takeoff. The simulated annealing algorithm varied these 57 parameters to maximise an objective score function that was designed to maximise height whilst minimising the difference between the simulated rotation potential and that required to complete the specified skill; effectively to produce the highest possible jump height for a given rotation potential.

During the optimisation the joint angle penalties described in Section 6.4.3 remained in place to ensure that the resulting simulated techniques were realistic to the subject. Simulations also incurred penalties for every millimetre of horizontal travel during the subsequent flight phase over a distance of 1.075 m; half the length of the jumping zone.

$$SCORE = 100.h_j - \Delta\theta^2 - P_a^2 - P_t^2 \qquad (7.4.1)$$

Where: h_j = jump height (m)

    $\Delta\theta$ = rotation potential difference (°)

    P_a = joint angle penalties (°)

    P_t = horizontal travel penalties (mm)

7.4.2 Maximum Rotation Method

The optimisation procedure maximised the rotation potential achieved for the flight phase following the contact under two different conditions dependent on horizontal travel; one optimisation was permitted to travel the full length of the trampoline's jump zone, 2.15 m, whilst the second optimisation was only allowed to travel half this distance, 1.075 m.

The optimisation procedure for maximum rotation varied the 56 parameters governing the activation profiles of the 8 torque generators as in the optimisation for height. The initial conditions were based on the movements of the piked triffus F_3, and a final parameter varied the initial horizontal velocity whilst the other initial conditions were not allowed to vary. The elbow joint angle time history of the simulation was also taken from the F_3 trial that was used in the matching procedure. The simulated annealing algorithm varied the 57 parameters in order to maximise an objective score function that quantified the rotation potential of the flight phase following the simulated contact phase, once again with penalties

constraining the joint movements to within the observed range of motion and for exceeding the permitted amount of horizontal travel.

$$SCORE = 100.\theta - P_a^2 - P_t^2 \qquad (7.4.2)$$

Where: θ = rotation potential (rev)

P_a = joint angle penalties (°)

P_t = horizontal travel penalties (mm)

7.5 Optimisation Results

7.5.1 Maximum Jump Height Results

The optimisation procedure was able to increase jump height in each of the skills by 14%, 9%, and 14% for the single straight forward somersault F_1, piked 1¾ forward somersault F_2, and piked triffus F_3 respectively over the matched simulations. The simulation model was able to perform a single straight somersault at a height of 4.16 m, a piked 1¾ somersault at 4.07 m and a piked triffus at a height of 3.91 m. This was achieved by increases in centre of mass height at takeoff of 5%, 2%, and 12% respectively and increases in vertical velocity at takeoff of 8%, 5% and 7% respectively, leading to respective increases in the time of flight of 9%, 6%, and 8%. The optimal techniques to produce height in each skill were also capable of matching the rotation potential required to perform the skills very closely with an average difference of just -0.02% over the three trials.

Table 7.5.1 Differences between matched simulations (M) and the optimal simulation (O) for maximum jump height in the skills F_1, F_2, and F_3.

		F_1			F_2			F_3		
		M	O	% Diff	M	O	% Diff	M	O	% Diff
h_1	(m)	0.97	1.02	5	0.94	0.96	2	0.81	0.90	12
v_z	(ms^{-1})	7.2	7.8	8	7.4	7.8	5	7.2	7.7	7
t	(s)	1.48	1.61	9	1.51	1.60	6	1.44	1.56	8
H	(kgm^{2}s^{-1})	34.1	33.5	-2	45.5	42.2	-7	70.1	69.1	-1
θ	(rev)	0.84	0.84	1	1.07	1.07	0	1.74	1.73	-1
tr	(m)		0.35			0.14			1.07	
h_j	(m)	3.64	4.16	14	3.74	4.07	9	3.42	3.91	14

h_1 = height of CM at takeoff, v_z = trampolinist's CM vertical takeoff velocity, t = flight time, H = angular momentum at takeoff, θ = rotation potential measured in straight somersaults, tr = travel, h_j = jump height

The optimised single somersault only resulted in 0.35 m of horizontal travel and the optimised 1¾ somersault travelled just 0.14 m but the triffus resulted in over one metre of travel, travelling 1.07 m horizontally. It is possible the triffus could be performed at a greater height if it was allowed to travel more than half the length of the jumping zone.

Figures 7.5.1, 7.5.2, 7.5.3 compare the optimal techniques to achieve height to the technique employed by the matching simulations in the somersaulting trials F_1, F_2, and F_3 respectively.
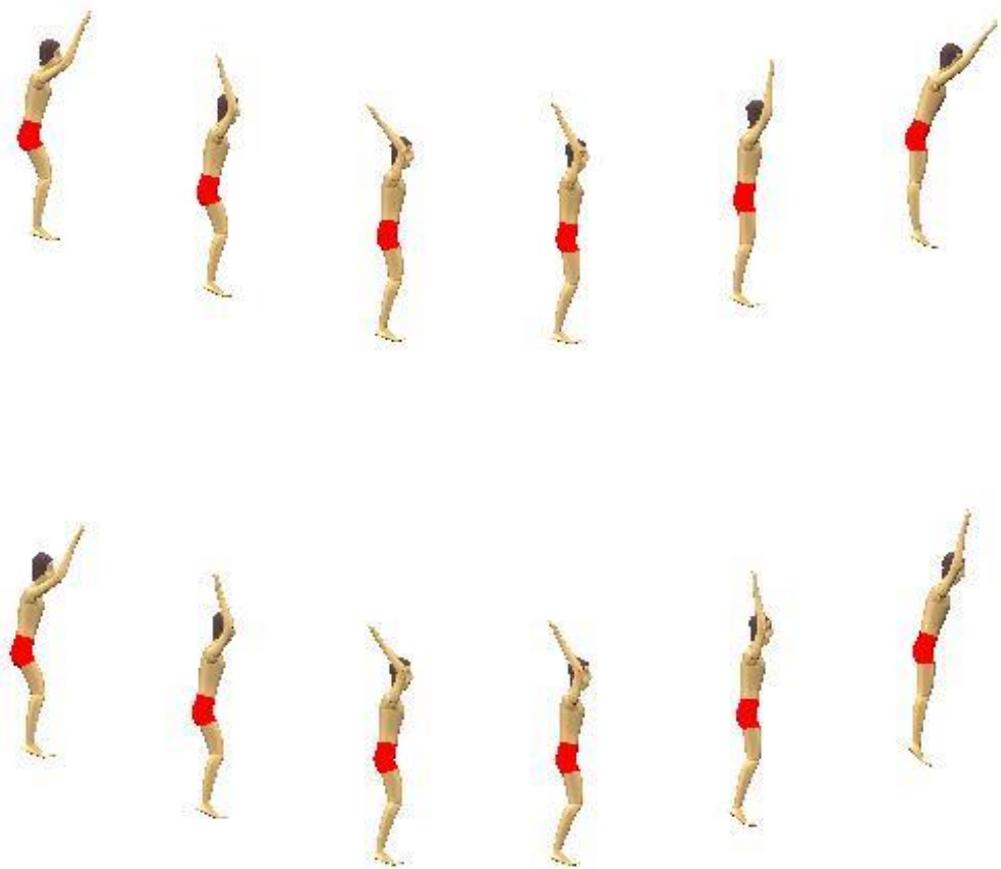
Figure 7.5.1 Comparison of fixed strength torque-driven simulation of F_1 (above) and optimal technique to produce jump height in a single straight front somersault (below).
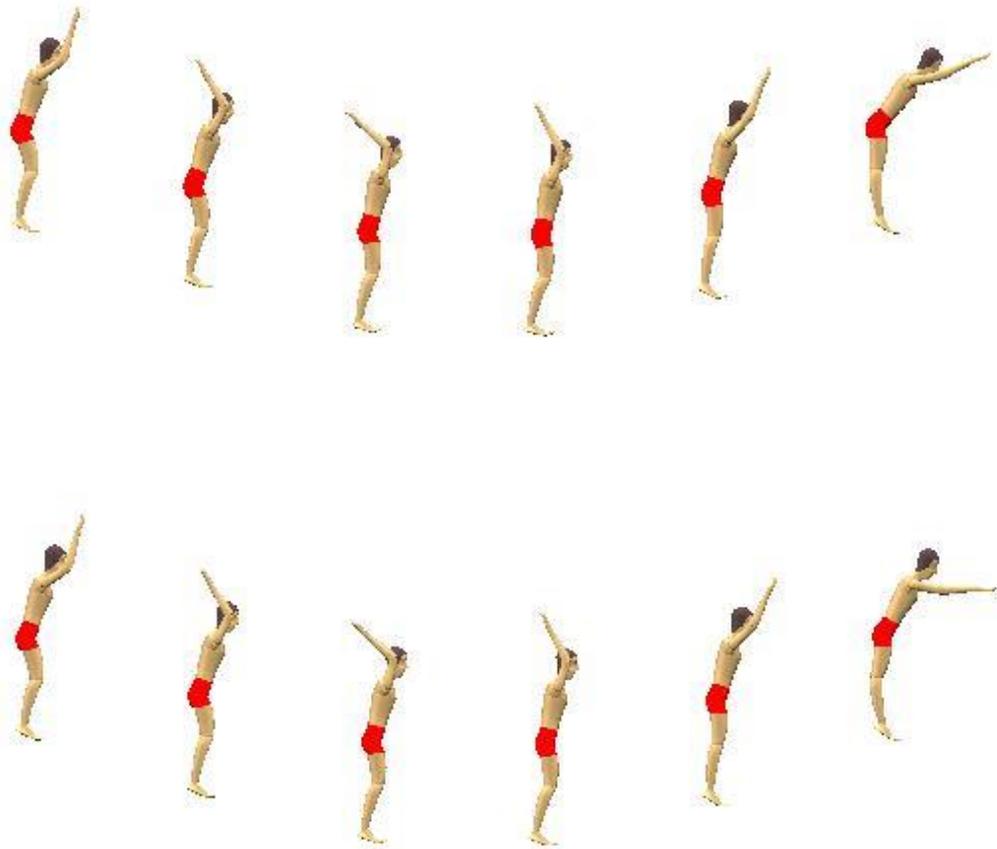
Figure 7.5.2 Comparison of fixed strength torque-driven simulation of F_2 (above) and optimal technique to produce jump height in a 1¾ piked front somersault (below).
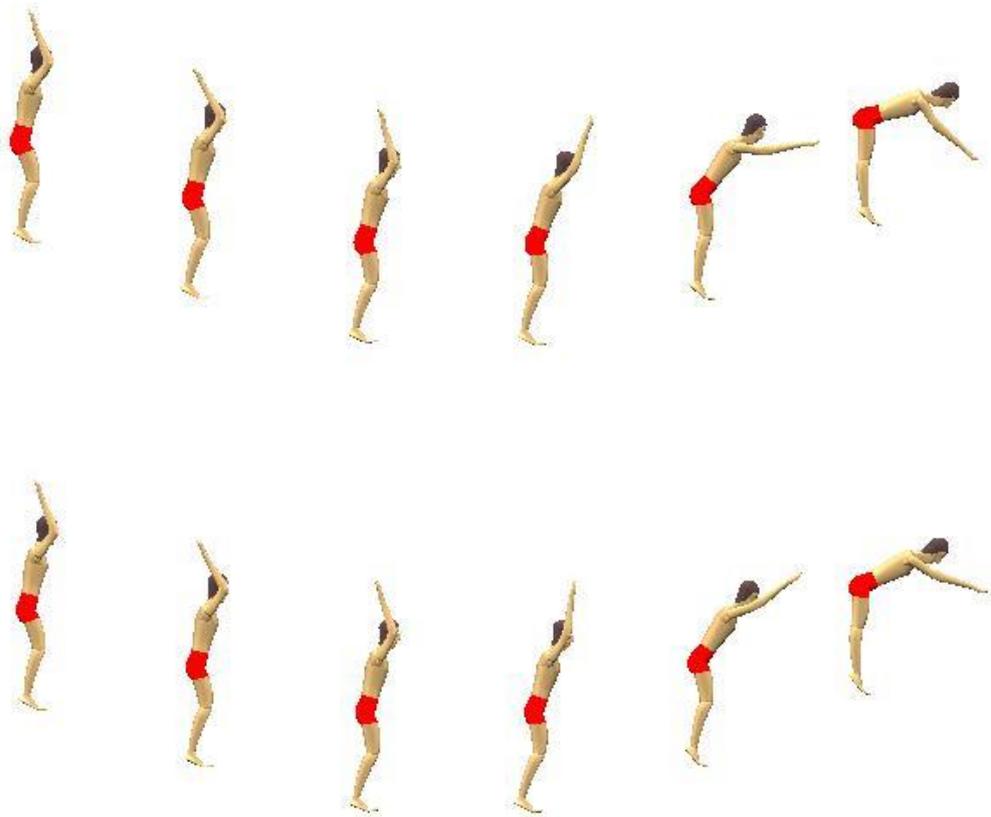
Figure 7.5.3 Comparison of fixed strength torque-driven simulation of F_3 (above) and optimal technique to produce jump height in a piked triffus (below).

7.5.1.1 Joint Angles

Figure 7.5.4 compares the joint angle time histories of the ankle, knee, hip, and shoulder during the optimal solutions for jump height to the fixed strength matched simulations of the forward somersaulting skills. During the depression phase the joint angles of the ankle, hip, and shoulder are not much different to the techniques of the matching simulation whilst the knee angles for the optimal simulations of the single straight somersault and the piked triffus extend more slowly than the matched simulations during the second half of the trampoline's depression. As the trampoline recoils knee extension occurs later than in the matching simulations but, in the 1¾ somersault and triffus, extends more quickly after the delayed onset of the movement. The shoulder also shows differences in the optimal technique when compared to the matched simulations; the single somersault maintains a flexed shoulder throughout the recoil phase, the 1¾

somersault displays extra extension of the shoulder prior to takeoff, and the triffus technique shows shoulder extension occurring much slower than during the matched simulation. During the recoil phase the ankle plantar flexes to a greater degree than the matched simulations in each of the optimised techniques, the hip shows some additional extension immediately prior to takeoff in the 1¾ somersault and triffus, whilst the hip extends to a greater degree. Immediately before takeoff there is an additional plantar flexion of the ankle to provide a last boost of vertical linear momentum.
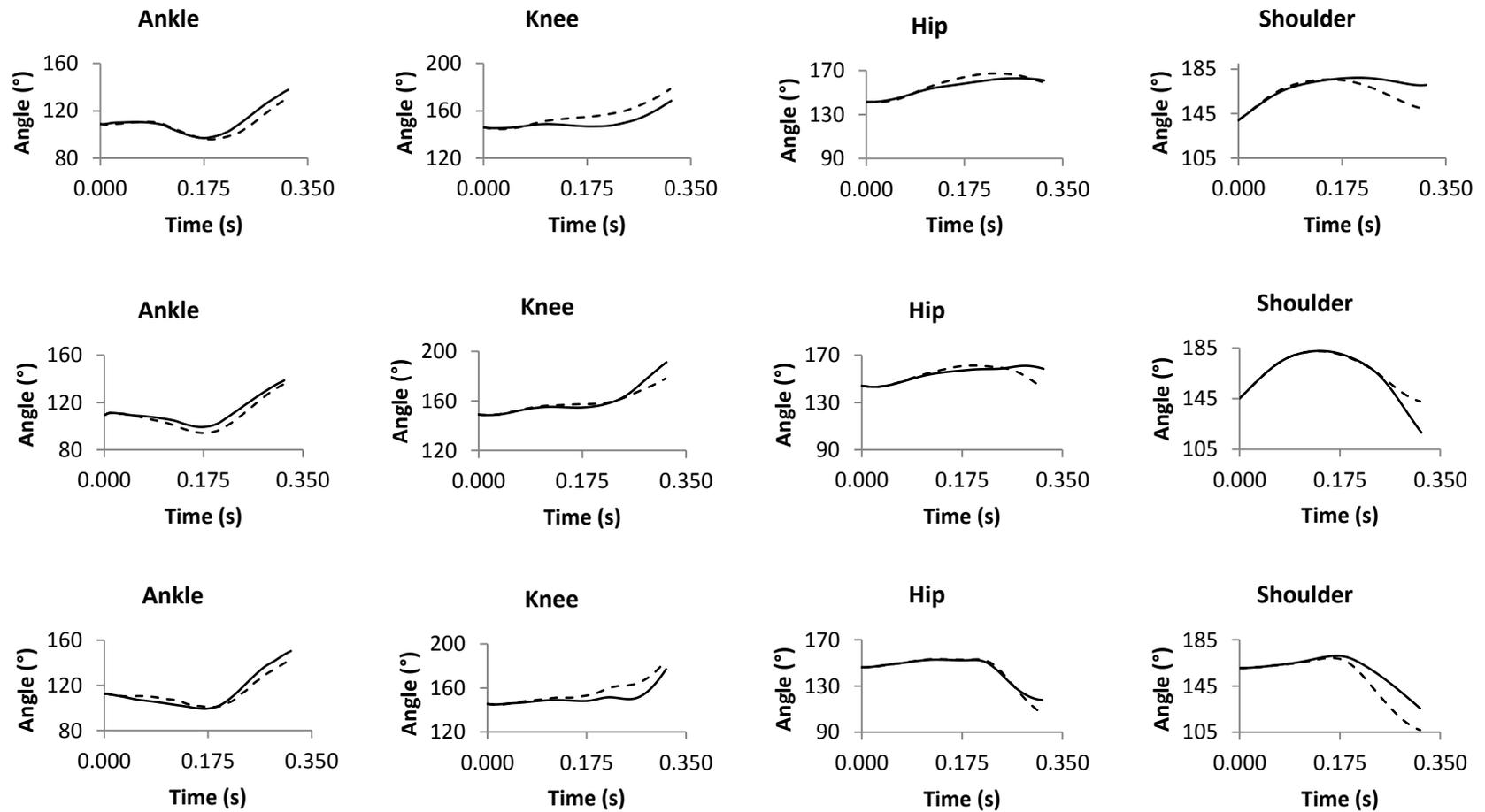
Figure 7.5.4 Comparison of the joint angle time histories during optimal jump height technique (solid lines) and the fixed strength matched simulation (dashed lines) of F_1 (top), F_2 (middle), and F_3 (bottom).

7.5.1.2 Joint Torque Activation Profiles

Figures 7.5.5, 7.5.6, and 7.5.7 compare the joint torque activation profiles utilised at the ankle, knee, hip, and shoulder during the optimal techniques to produce jump height and the matching simulations of F_1, F_2, and F_3.

The optimal solution for the single straight somersault shows each of the torque generator activation profiles follow similar shapes to the activation profiles from the matching simulation. The knee flexor activation profile is very similar to the matching simulation whilst the other profiles show combinations of slightly different activation levels and delayed ramp times. The plantar flexors and knee extensors ramp up to a greater activation level; whilst in the recoil phase the knee extensors ramp down later and more slowly. The shoulder flexors meanwhile show more moderate activation levels, and the shoulder extensors activate more slowly before takeoff.

The optimal technique for the production of height during a 1¾ piked somersault was accomplished using activation profiles very similar to the matched simulation throughout the depression phase, and throughout the whole contact phase the activation profiles of the knee and shoulder showed only small alterations to those used by the matching simulations, with only a small difference in the final activation of the shoulder flexors. The ankle plantar flexors also used a similar activation profile, but the activation of the dorsi flexors ramped up later and to a lower level than in the matched solution, whilst the hip extensors ramped down to an increased level and the hip flexors delayed ramping up to a decreased level.

Optimal height in a piked triffus was achieved by using different activations at all joints than in the matching solution, with the most notable differences being a greater level of activation of the hip extensors throughout the contact phase, the knee flexors decreasing to minimal activation in the recoil phase, and a much lower amount of plantar flexor activity at takeoff. After the initial ramp down the shoulder extensors maintained a constant activation through the contact phase instead of ramping up before takeoff, and the dorsi flexors also employed a similar activation profile.

126
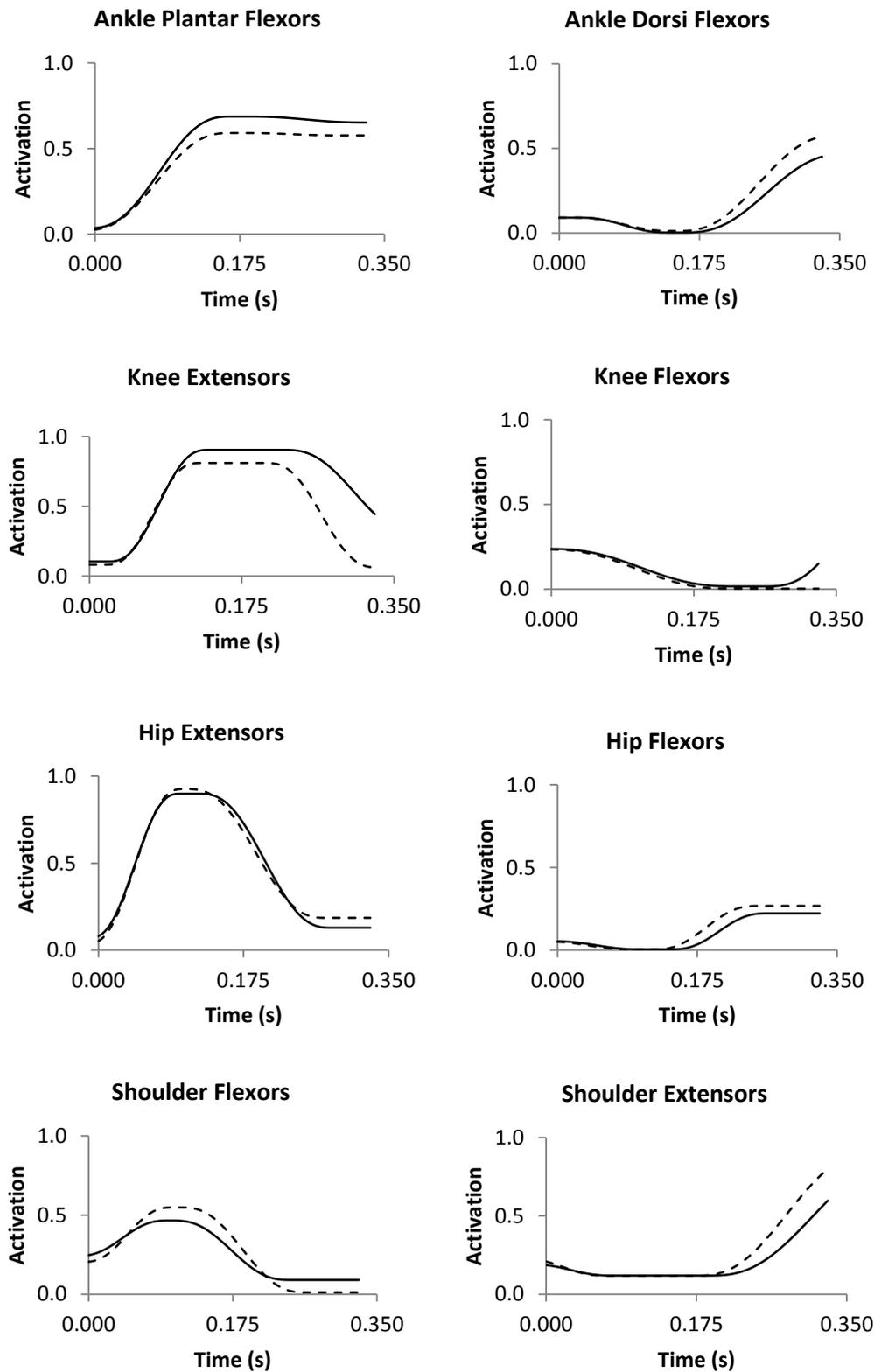
Figure 7.5.5 Comparison of activation time histories of the optimal solution for jump height (solid line) and matched simulation (dashed line) of F_1.
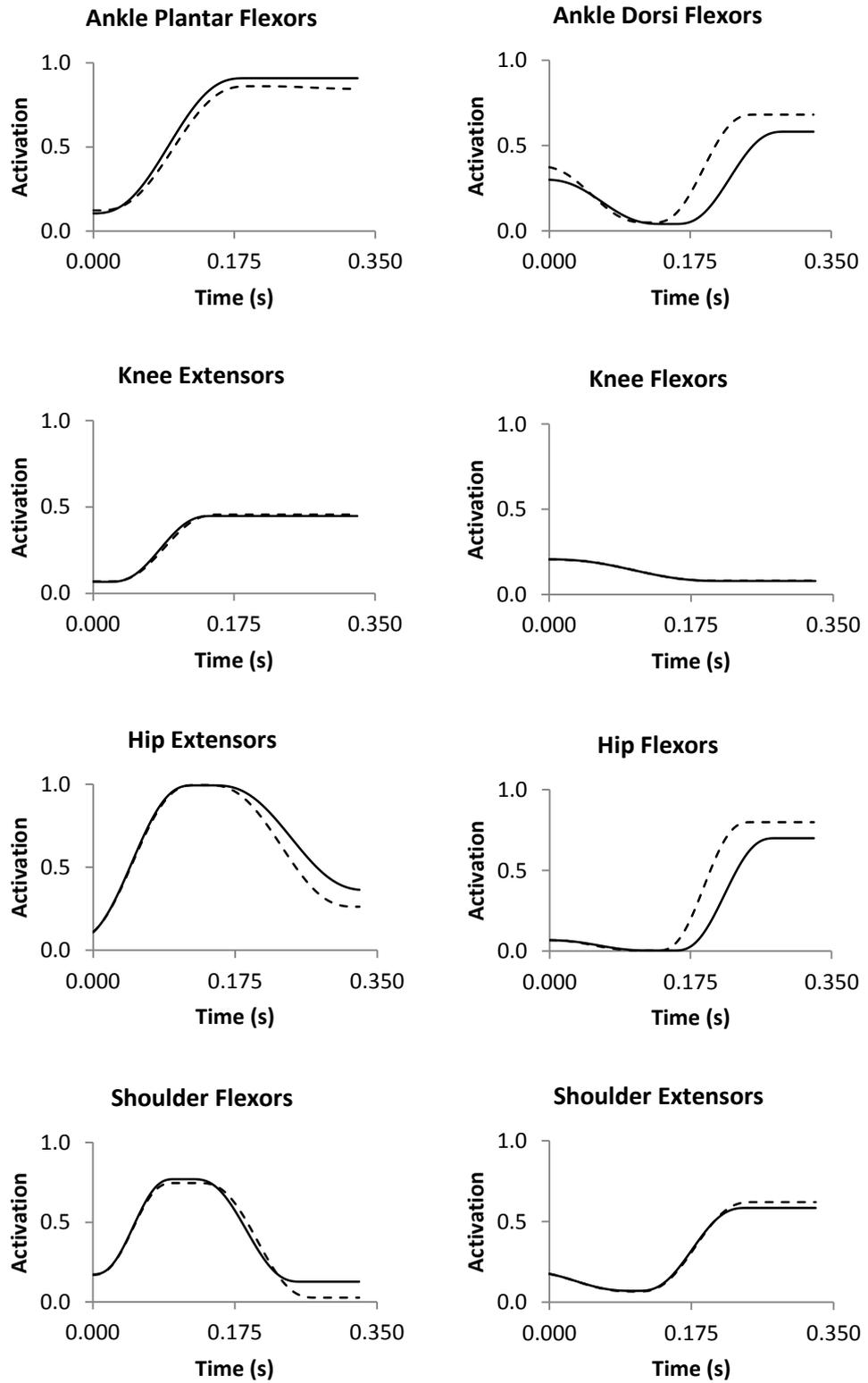
Figure 7.5.6 Comparison of activation time histories of the optimal solution for jump height (solid line) and matched simulation (dashed line) of F_2.
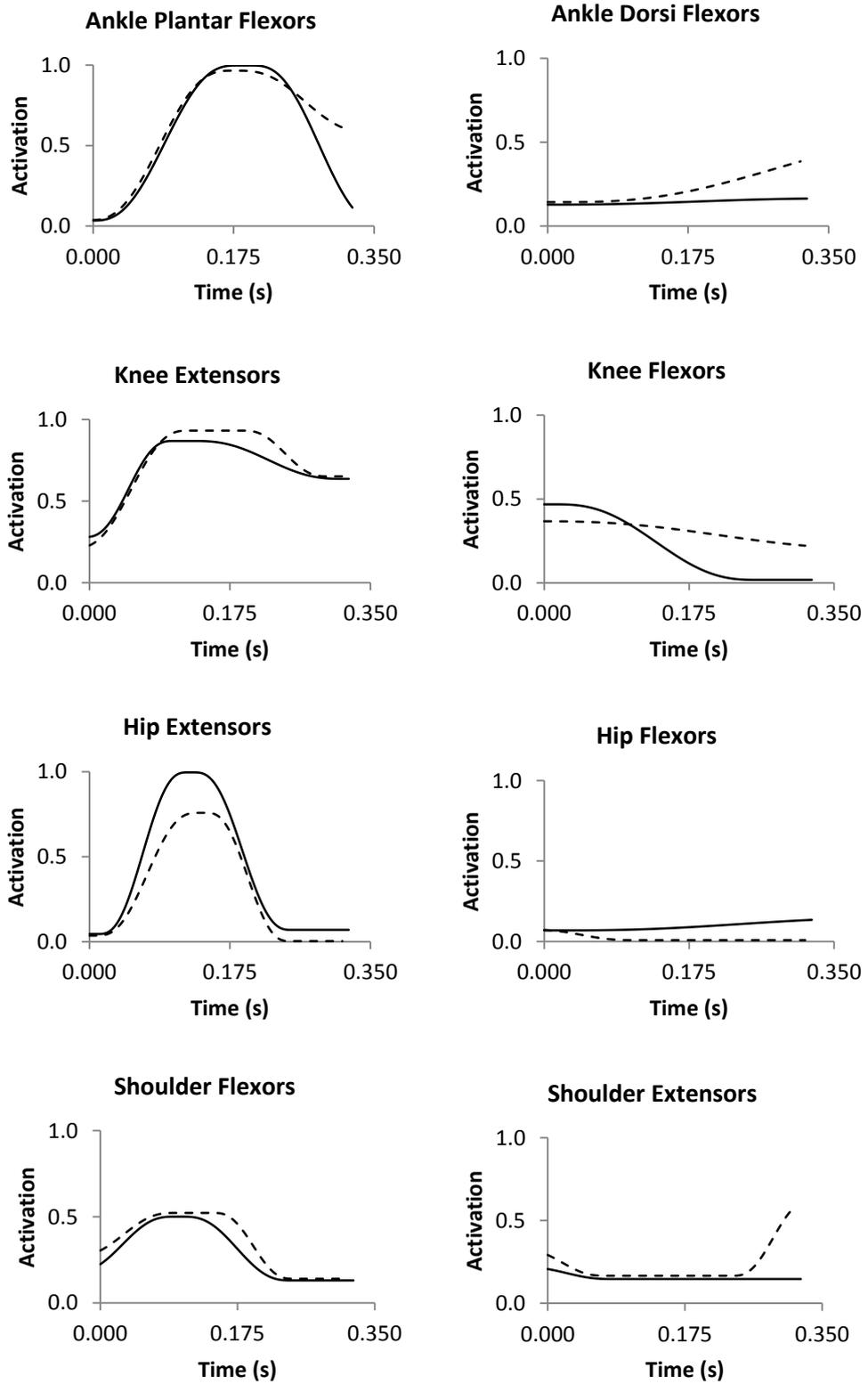
Figure 7.5.7 Comparison of activation time histories of the optimal solution for jump height (solid line) and matched simulation (dashed line) of F_3.

7.5.1.3 Joint Torques

Figure 7.5.8 compares the joint torque time histories of the ankle, knee, hip, and shoulder to the optimal solutions for jump height to the fixed strength matching simulations of the skills F_1, F_2, and F_3.

The differences in the activation profiles of the optimal and matched solutions for the single straight somersault led to greater extensor torques at the ankle, knee, and hip in the depression phase, throughout the movement and around the time of maximal depression respectively. During the recoil phase the net torque at the hip switched to a flexor torque whereas the matched simulation only used extensor torques. The shoulder torque showed a smaller extensor torque during the depression phase.

The optimal solution for the production of height during a 1¾ piked somersault used similar joint torques at the ankle and knee to the matched solution throughout the contact phase, whilst the knee employed a significantly greater extensor torque around the time of maximal trampoline depression. The shoulder torque during the optimal solution is very similar to the matched solution until the trampolinist has begun the recoil phase, then the shoulder flexor torque decreases instead of increasing before takeoff.

The ankle and hip joint torques employed by the simulation model to optimise jump height in the piked triffus skill were very similar to the matched simulation, and the shoulder torque followed a similar pattern but did not peak the extensor torque around maximal depression and maintained an extensor torque through to takeoff. The major difference in joint torques during the optimal triffus technique was the magnitude of the hip extensor torques throughout the recoil phase. The hip extensor torque followed a similar pattern as the matching simulation the torque was more than twice as large during the recoil phase.
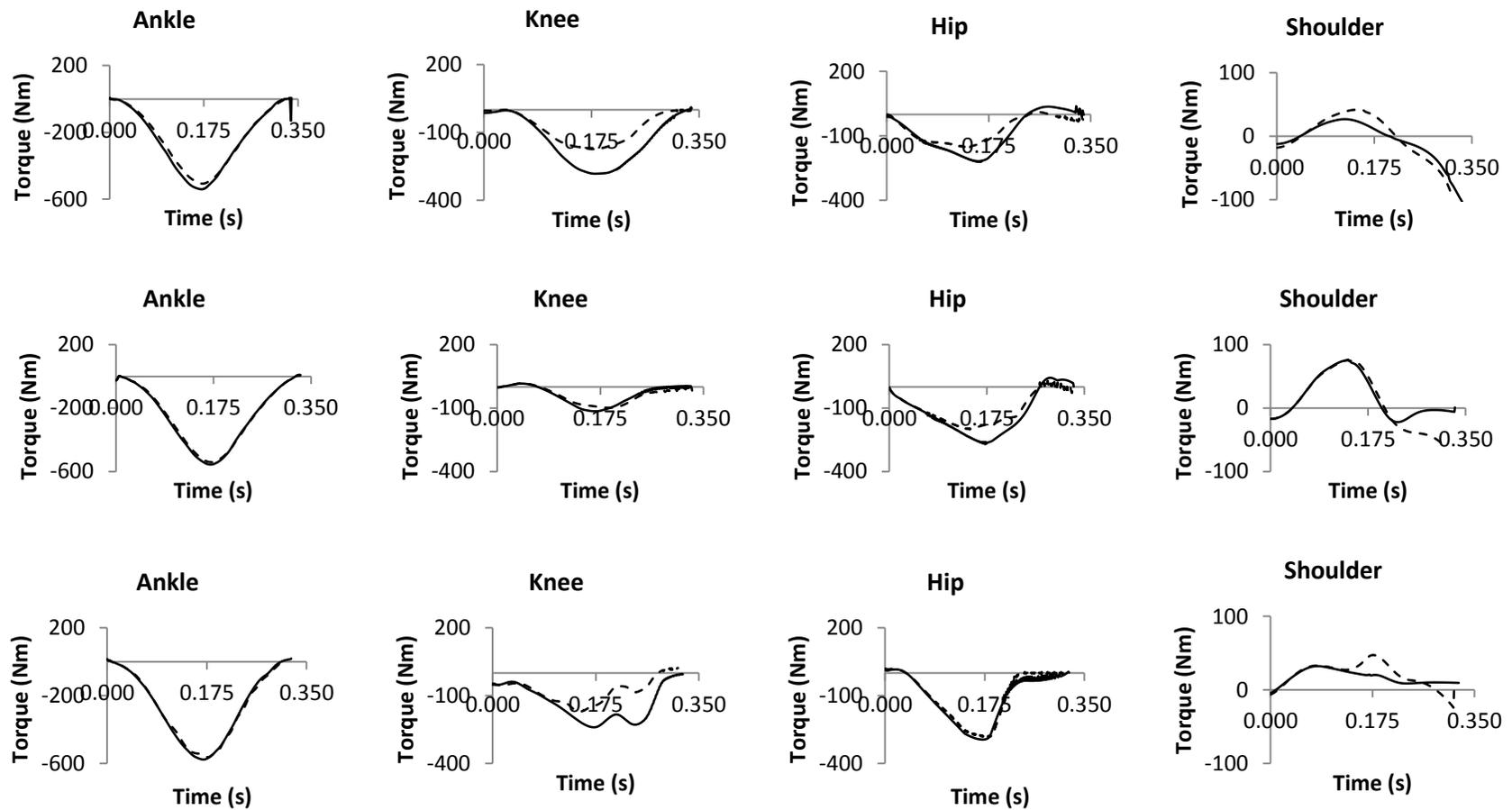
Figure 7.5.8 Comparison of the joint torques during optimal jump height technique (solid lines) and the fixed strength matched simulation (dashed lines) of F_1 (top), F_2 (middle), and F_3 (bottom).

The optimal solutions achieved jump heights of 4.16 m, 4.07 m and 3.91 m above the trampoline, decreasing as the rotational requirement increased. This represented increases of 14%, 9% and 14% over the matched solutions.

The optimal techniques to produce jump height utilised a larger hip and knee extensor torques around the point of maximal depression and during the recoil phase than the matched solutions. This was caused by combinations of increased extensor activation and decreased flexor activation.

During the optimal solutions the both the ankle and hip extensors reach maximal or near maximal activation (1.000 and 0.997 respectively), possibly indicating that hip extensor and ankle plantar flexor strength are two of the limiting factors for the production of jump height in forward rotating somersault.

7.5.2 Maximum Rotation Results

The optimisation of technique to produce rotation potential for the two different amounts of permissible horizontal travel was able to produce a flight phase during which 1.91 straight somersaults could be completed whilst only travelling half the length of the jumping zone *0.5L*, and 2.00 straight somersaults whilst travelling the whole length of the jumping zone *1L*. These optimal results represented a 10% and 15% increase in rotation potential over the matched solution for F_3 respectively. The optimal rotation potential was achieved by taking off having already rotated through 48° and 57°, representing increases of 13% and 33%, and angular momenta of 83 kg.m^2.s^{-1} and 90 kg.m^2.s^{-1}, respective increases of 19% and 28%. This increased angular momentum was combined with slightly shorter time in the air to result in increased angles rotated through during flight, as the flight times achieved by the optimal technique were 1% and 5% shorter than the matched solution of F_3 but during flight the optimal techniques rotated through angles of 640° and 662° respectively, representing increases of 17% and 21%.

Both optimised techniques used the limits of their permitted horizontal travel. When allowed to travel half the length of the jumping zone the optimal solution reached within 4 mm of the limit, whilst when allowed to travel the full length of

the jumping zone the optimal solution travelled to within 3 cm of the limit, however no penalties were incurred by the optimised simulations.

Table 7.5.2 Differences between matched simulations (M) and the optimal simulation (O) for maximum rotation potential for two limits of travel *0.5L* and *1L*.

		0.5L			1L		
		M	O	% Diff	M	O	% Diff
θ_i	(°)	42.7	48.3	13	42.7	56.6	33
v_z	(ms^{-1})	7.2	7.1	-1	7.2	6.8	-5
t	(s)	1.44	1.42	-1	1.44	1.37	-5
H	(kgm^{2}s^{-1})	70.1	83.4	19	70.1	89.5	28
θ_f	(°)	546	640	17	546	662	21
tr	(m)		1.07			2.12	
θ	(rev)	1.74	1.91	10	1.74	2.00	15

θ_i = initial somersault angle, v_z = trampolinist's CM vertical takeoff velocity, t = flight time, H = angular momentum at takeoff, θ_f = flight rotation angle, tr = travel, θ = rotation potential measured in straight somersaults

Figures 7.5.9 and 7.5.10 compare the optimal techniques to achieve maximum rotation to the fixed strength matching simulation of skill F_3.
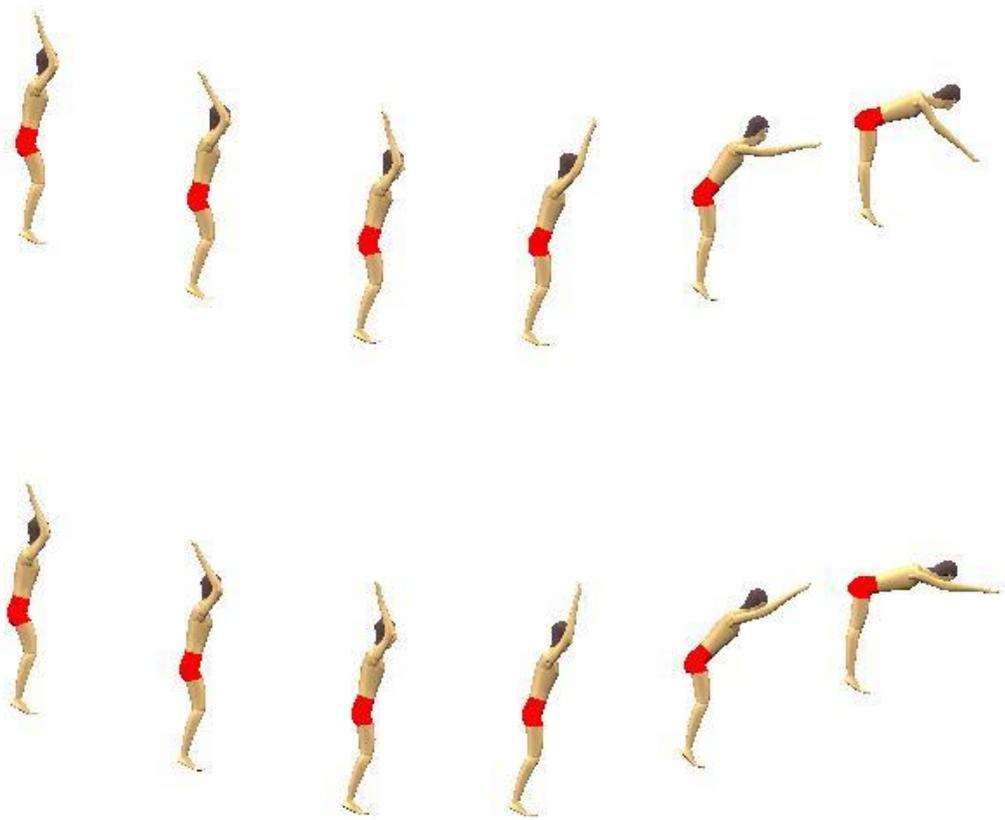
Figure 7.5.9 Comparison of fixed strength torque-driven simulation of F_3 (above) and optimal technique to produce rotation potential with up to 1.075 m of travel (below).
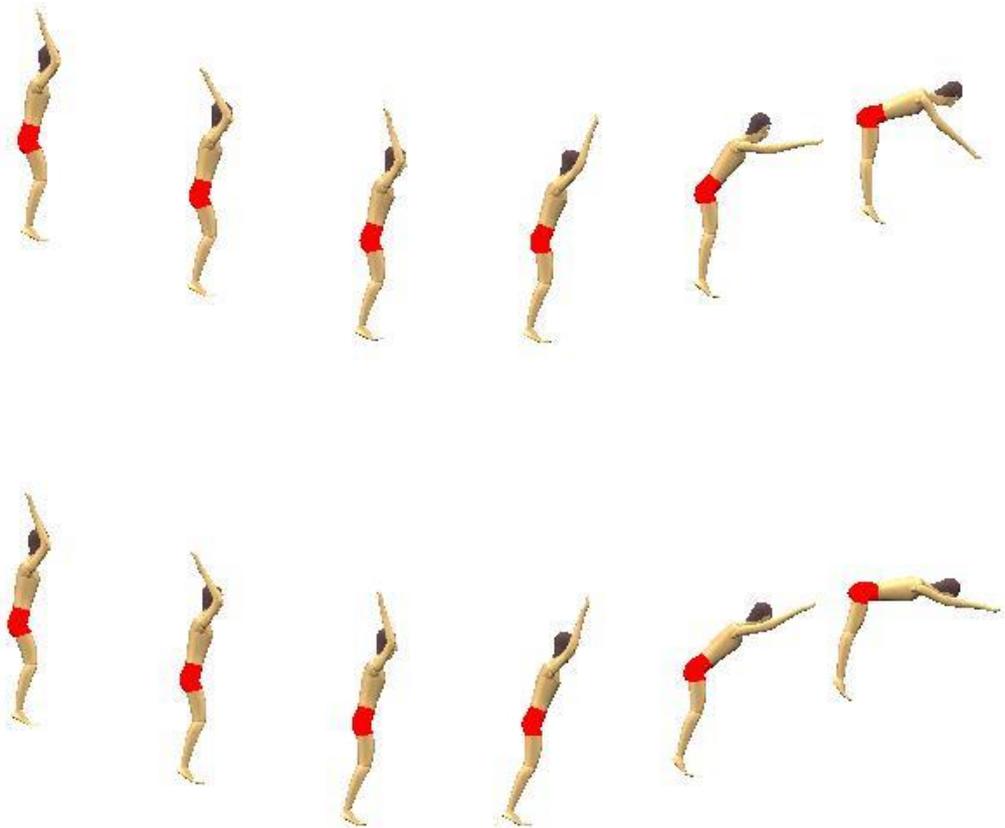
Figure 7.5.10 Comparison of fixed strength torque-driven simulation of F_3 (above) and optimal technique to produce rotation potential with up to 2.15 m of travel (below).

7.5.2.1 Joint Angles

The joint angles of the ankle, knee, and hip follow similar patterns to those used in the matching simulation of skill F_3; however there are major differences in the movements of the shoulder during the recoil phase in both optimised techniques. Both optimised techniques show significantly less shoulder extension throughout the recoil phase than the technique used by the trampolinist, this will result in moving the centre of mass further forwards and increasing the torque created about the mass centre by the vertical force. During the optimised technique of *1L* the shoulders actually flex further immediately prior to takeoff.

In addition to this, optimal solutions also show greater hip extension throughout the depression phase, with the difference in hip angle peaking around the time of maximum depression of the trampoline. The greater rigidity of the body during the depression phase can exploit the elasticity of the trampoline by helping to depress the trampoline further and storing more elastic energy for the recoil phase. The knee angle also follows a similar pattern to the technique used by the trampolinist, but during the recoil phase the knee flexes then extends before takeoff, so that at takeoff the knee angle is similar but it has a greater angular velocity of extension at this time. Figure 7.5.11 compares the joint angle time histories of the optimal technique for the production of rotation to the fixed strength matching simulation of skill F_3.
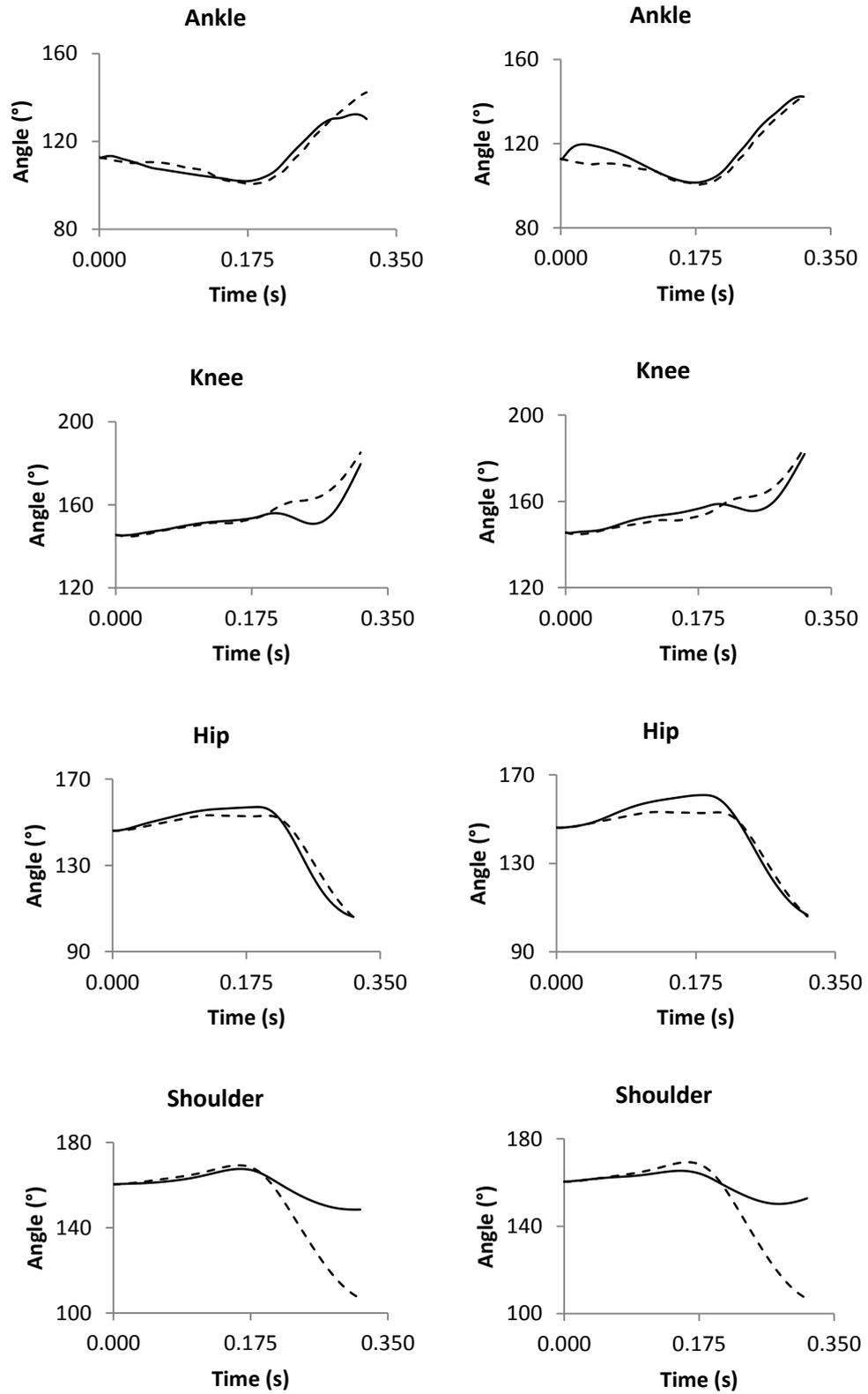
Figure 7.5.11 Comparison of the joint angle time histories of the 0.5L (left) and 1L (right) optimal techniques to and the fixed strength matching simulation of skill F_3.

Joint Torque Activation Profiles

Figures 7.5.12 and 7.5.13 compare the joint torque activation profiles utilised at the ankle, knee, hip and shoulder during the optimal techniques to produce rotation to those used during the matched simulation of F_3.

In the *0.5L* optimisation there are major differences in the activation profiles of all the joint torque generators except the dorsi flexors and the shoulder flexors. The plantar flexor activation profile is very similar throughout the depression phase but during the recoil phase the activation ramps down to a much lower level. At the knee, the extensors do not reach the same level of activation during the middle of the contact phase and the flexors ramp down much earlier and to a minimal level. The hip extensors utilise a significantly larger peak activation level in the depression phase, the hip flexors use a slowly increasing activation throughout the contact phase instead of the minimal activation used in the matching simulation, and the shoulder extensors employed a constant activation level throughout the recoil phase instead of ramping up prior to takeoff.

The optimal activation profiles for the production of rotation potential using the full length of the jump zone, *1L*, were different to those of the matched simulation in similar ways to the *0.5L* optimisation but differed from the matched solution for F_3 less. The dorsi flexor activation profile was once again very similar to the matched solution, but the shoulder flexor showed greater disparity, ramping down from peak activation earlier, before maximal depression. The plantar flexor still ramps down to a lower level than the matching simulation, however not as low as the *0.5L* optimal technique. The knee extensor activation profile reached the same level as in the matching simulation however the initial ramp up was shorter and the ramping down of the activation level began earlier, around maximal depression, and took longer, whilst the knee flexors followed the same pattern but ramped down to a higher activation level during the recoil phase. At the hip, the extensors again use a greater peak activation level and ramp up to that level and ramp down earlier but the peak activation level is closer to that used by the matching solution than the *0.5L* optimal solution. The hip flexors and shoulder extensors follow very similar activation profiles to the *0.5L* solution.
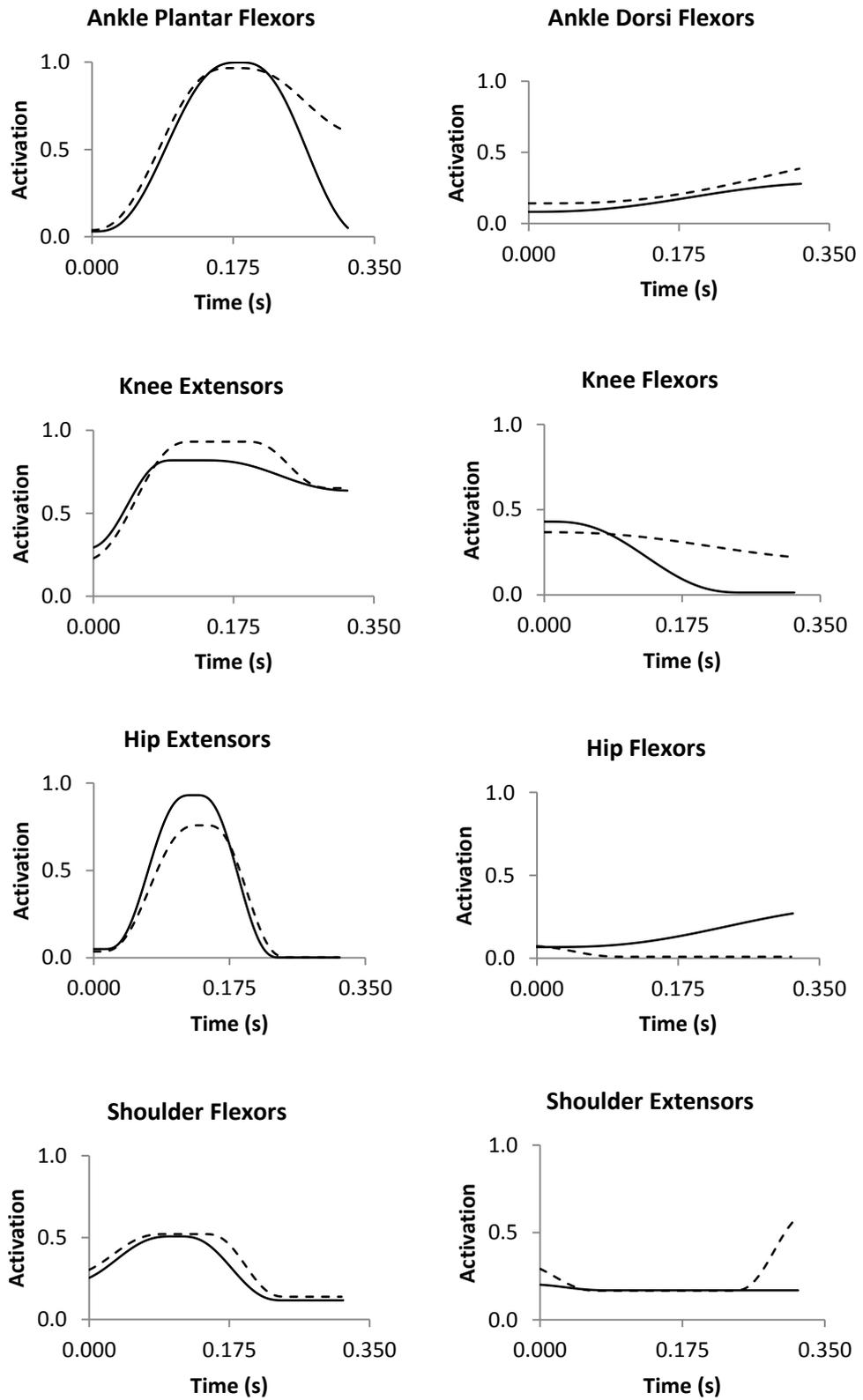
Figure 7.5.12 Comparison of activation time histories of the *0.5L* optimal solution for rotation potential (solid line) and matched simulation of F_3 (dashed line).

139
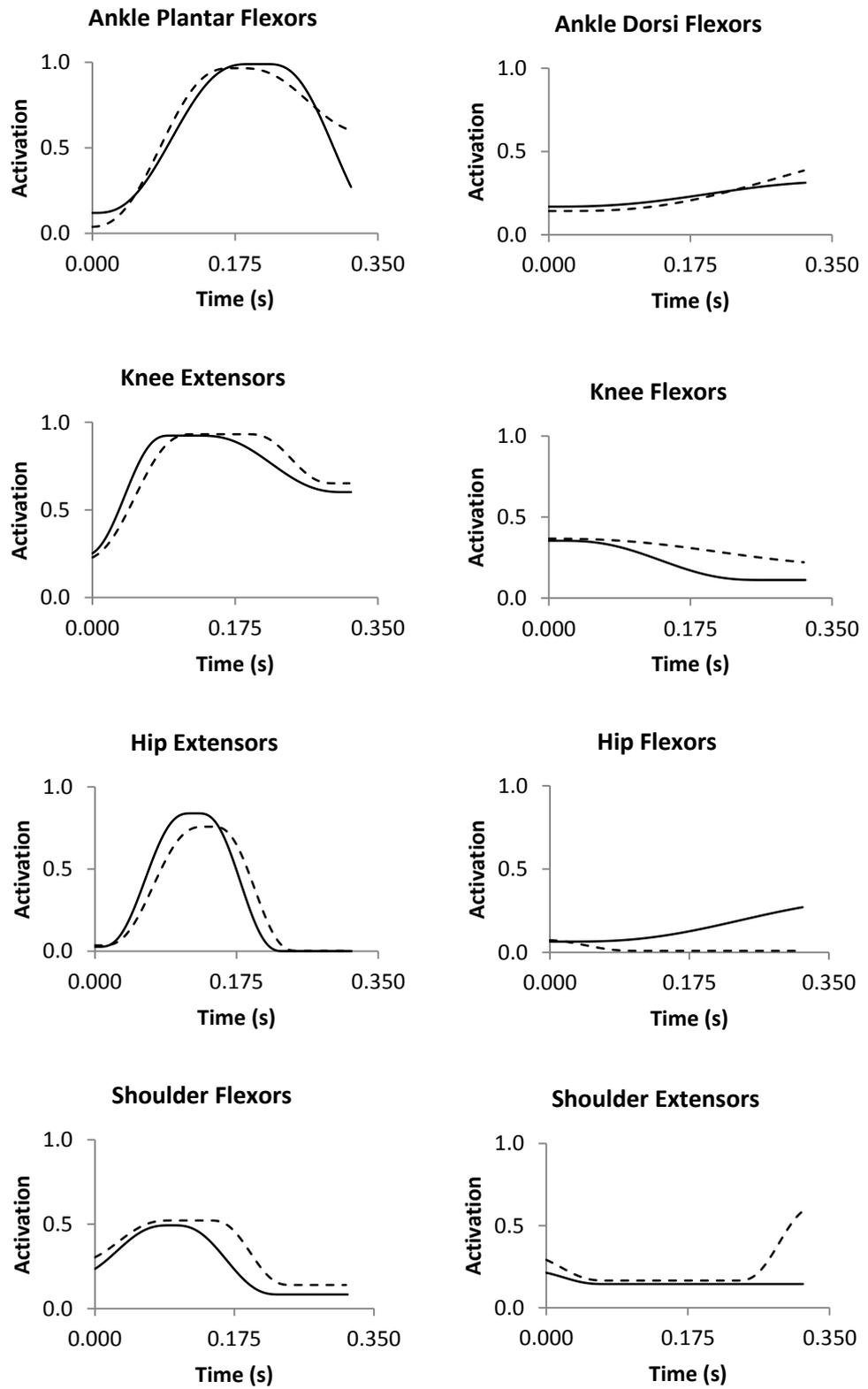
Figure 7.5.13 Comparison of activation time histories of the *IL* optimal solution for rotation potential (solid line) and matched simulation of *F₃* (dashed line).

140

7.5.2.3 Joint Torques

Figure 7.5.14 compares the joint torque time histories of the optimal techniques to produce rotation, *0.5L* and *1L*, to the fixed strength matching simulation of skill *F₃*. Both the optimal techniques utilise ankle torques very similar to those of the matching simulation, knee extensor torques that are much greater during the recoil phase, lower peak hip extensor torques around maximal depression and hip flexor torques immediately prior to takeoff, and shoulder torques that move from an extensor torque to a flexor torque during the recoil phase.

Whilst both optimal techniques use larger knee extensor torques and smaller hip extensor torques than the matched simulation, as well as similarly different shoulder torques, the *0.5L* solution uses greater knee and hip extensor torques than the *1L* solution, whilst the *1L* technique achieves a net shoulder flexor torque earlier in the contact phase.
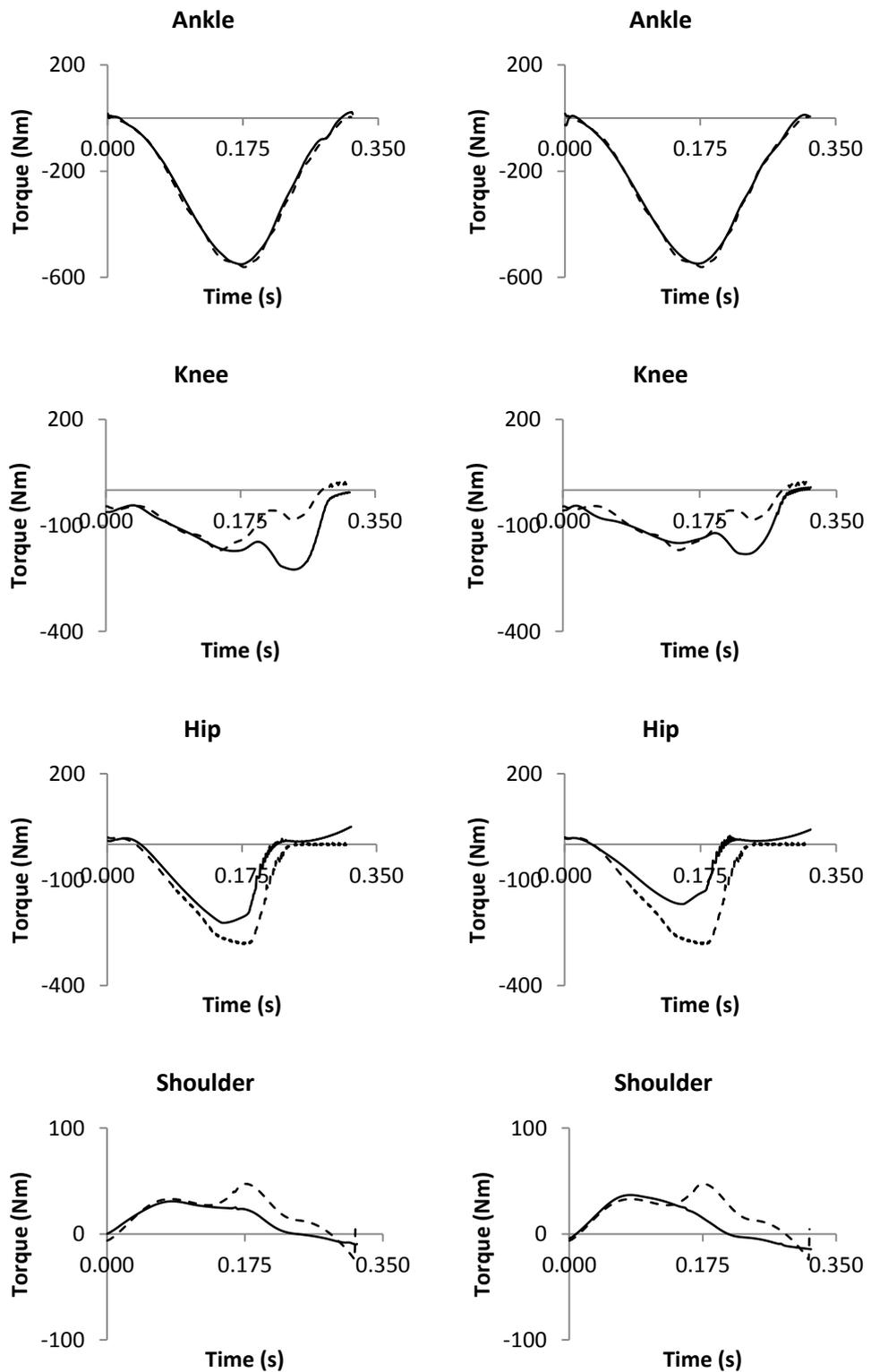
Figure 7.5.14 Comparison of the joint torque time histories of the optimal techniques, *0.5L* (left) and *1L* (right) for the production of rotation potential (solid line) and the fixed strength matched simulation of skill *F₃* (dashed line).

The optimal techniques produced a flight phase during which 1.9 and 2.0 straight somersaults could be completed for *0.5L* and *1L* respectively, representing increases of 10% and 15% over the matched solution for F_3.

The optimal techniques to produce rotation potential utilised a larger knee extensor torques during the recoil phase and lesser hip extensor torques around peak depression than the matched solution, although the hip extensor activations were greater and the knee extensor activation being lower than the matching solution. This effect was caused by the relative activations of the antagonists; the knee flexor activation levels were lower, and the hip flexors were activated to a greater level.

During the optimal solutions the ankle plantar flexors reach near maximal activation (0.999 and 0.990), possibly indicating that plantar flexor strength is one of the limiting factors for the production of forward somersault rotation.

7.6   Discussion

The optimisation of the technique employed by the simulation model of trampolining to produce maximum jump height and rotation potential showed that the trampolinist was employing suboptimal techniques during the data collection. The optimal techniques were able to increase jump height by up to 14% and rotation potential by up to 15% over the matched simulations. It was also seen that even though jump height directly effects the rotation potential, the optimal technique for rotation potential only achieved a jump height 86% as high as the optimal technique for jump height, underlining the compromise between the production of angular and linear momenta.

The optimal techniques used near maximal activations, this possibly demonstrates that the hip and ankle strength are limiting factors for jump height and ankle strength is a limiting factor for the production of rotation.

7.7   Chapter Summary

This chapter described how the simulation model was applied to answer the research questions. Optimisation demonstrated that there was potential for the trampolinist to improve performance by up to 15% by employing changes to his technique. The findings of the present study, the methods used and future applications of the model will be discussed in Chapter 8.

Chapter 8: Discussion and Conclusions

8.1 Chapter Overview

This chapter summarises the main findings of the present study. The methodology will be discussed, highlighting the limitations of the current method and suggesting possible improvements for future research. Finally the potential future applications of the simulation model of the trampolining contact phase developed during the present study will be addressed.

8.2 Research Questions

Q1. For specific skills with a fixed rotational requirement what is the optimal takeoff technique to produce the required angular momentum with maximum peak height and minimum travel?

The results of this study found that as the rotational requirement of the skill increased, less height was able to be achieved in the flight phase; this was in agreement with the findings of previous studies (Miller & Munro, 1984; Sanders & Wilson, 1988). The optimisation of the simulation model was able to produce increases in jump height of up to 14% for forward rotating skills with specified rotation requirements, with increases of up to 8% in vertical takeoff velocity, identified as the primary factor in increasing jump height by Feltner *et al.* (1999) and Sander & Wilson (1992).

For the optimisation of forward rotating trampoline skills to produce maximum jump height, the optimal techniques utilised were very similar to one another during the depression phase. The optimised techniques typically showed increased hip flexion at takeoff and a later and quicker extension of the knee during the recoil phase as the rotational requirement increased. As well as these characteristics the optimal techniques for jump height also used greater plantar flexion during the recoil phase and a less flexed shoulder angle but with slower rates of extension as the rotational requirement increased. These characteristics of

the techniques could cause the angular momentum required for the skills to be produced later in the contact phase, so that during the early portion of the contact phase maximum elastic potential energy can be stored in the trampoline bed, and then in the recoil phase the elastic energy can be used to create maximum vertical linear momentum before the trampolinist flexes, moving out of the line of action of the vertical force to create the required rotation.

The differences in technique are primarily the result of changes in the activation profiles of the ankle, knee, and hip flexors, rather than the extensors, with the main result being a larger peak hip extensor torque decreasing more quickly during the recoil phase.

Q2. What is the optimal takeoff strategy to produce maximal somersault rotation potential in both forward somersaults?

When the takeoff strategy was optimised for maximal somersault rotation, the simulation model was able to produce up to 15% more rotation potential. The optimal techniques managed to achieve substantial increases in angular momentum, up to 28%, with only small reductions in flight time of up to 5%.

The optimal techniques to produce rotation potential both utilised a technique that involves a large amount of hip flexion and much less shoulder extension during the recoil phase, and even small amounts of shoulder flexion immediately prior to takeoff. These movements increase the horizontal displacement of the centre of mass, increasing the moment arm of the vertical force acting on the feet and enabling the production of greater quantities of angular momentum. The techniques also showed greater hip extension at the time of maximal trampoline depression, and small degrees of knee flexion in the recoil phase followed by a quick extension of the knee in the moments before takeoff, that could increase the total vertical force during the recoil phase, and also when the moment arm of the vertical force is at its largest, utilising the vertical force with the optimum strategy (Ollerenshaw, 2004; Vaughan, 1980).

These optimal techniques were produced by smaller shoulder flexor and larger knee extensor torques during the recoil phase, and smaller hip extensor torques during the depression phase that decreased to a minimal amount earlier in the

recoil phase. These torques were the results of not increasing the activation of the shoulder extensors prior to takeoff, increased activation of the hip extensors during the depression phase and of the hip flexors during the recoil phase, and decreased activation of the knee flexors during the recoil phase.

8.3   Discussion

8.3.1   Simulation Model

The simulation model developed in the present study represented a simplification of trampolining and human motion based on assumptions that may have limited the capabilities of the model to accurately simulate the performance of a trampolinist. The trampolinist was modelled by a planar representation assuming bilateral symmetry. This representation neglects any movements that take place outside the primary plane of motion, most notably of the arms, and assumes that the motion is symmetrical when reflected in the plane of motion. The method of projecting the three dimensional coordinates of the arms onto a plane to calculate two dimensional joint angles could misrepresent the configuration of the upper limb and the resulting inaccuracies in the torque time histories may have affected the orientation and angular momentum of the trampolinist.

The trampolinist was represented by seven rigid segments with the head and trunk represented by a single rigid segment, assuming that the curvature of the spine remained constant. This is a major assumption as it was witnessed during the data collection that prior to takeoff for forward rotating skills flexion of the spine occurs and hyperextension of the spine occurs before takeoff for backward rotation skills, such motions could play a major role in the production of angular momentum. The advantage of modelling the spine as a single rigid segment is that the torque acting across the length of the spine is much more easily measured than measuring the torque between multiple spinal segments. The angle-driven simulations showed hyperextension of the hip and this was also allowed by the torque-driven model to facilitate the matching process and the production of angular momentum during the optimisation procedure.

The model also did not include any representation of the soft tissue as it had previously been shown not to be necessary in the simulation of impacts with compliant surfaces. The inclusion of wobbling masses in the simulation model would likely have taken a lot of time and resulted in very little effect on the outputs of the simulations.

8.3.2   Foot-Suspension System Interface

The foot-suspension system interface was modelled by a damped, two dimensional force-displacement relationship which was non-linear vertically and linear horizontally. The force-displacement relationship also accounted for the force required to accelerate the mass of the suspension system. The reaction force was distributed between the heel, metatarsal-phalangeal joint and toe based on the relative depressions of the three points compared to the natural slope of the trampoline around the most depressed point. The trials were selected to be located centrally on the trampoline, however the impacts were not located in the very centre of the trampoline and the location has been shown to affect the force-displacement relationship. The representation of the foot-suspension system did not take into account the location of impact on the trampoline however the force-displacement relationship was able to represent the foot-suspension system interface satisfactorily as the angle-driven model was capable of closely matching the performance data.

8.3.3   Performance Data

The trampolining performances were recorded using an automatic motion capture system recording at 300 Hz. The motion of the trampolinist was tracked by opto-reflective markers placed along the midline of the torso and the joints of the right limbs. In only recording the movements of the right limbs it was assumed that the movements of the trampolinist would be symmetrical and the movement of the right limb would represent the average motion during each trial. An alternate method could record the motion of both limbs and take an average position of both of the limbs as an input for a planar simulation model, however due to the spatial constraints of the available trampolining facility the automatic motion

capture system could only be arranged in a configuration suitable to reliably record the motion of one side of the body.

8.3.4   Anthropometric Data

Anthropometric data was taken from direct measurements of the subject's body and body segmental inertia parameters were calculated using the model of Yeadon (1990b). Inertia parameters calculated using this method have been used in various rigid body simulation models that have been evaluated and shown to accurately reproduced human motion King *et al*., 2009; Wilson *et al*., 2006; Yeadon & Hiley, 2000). The method is of limited ability to accurately estimate the mass of the torso without knowing the volume of air in the lungs however the effect of this limitation has been shown to be small given the success it has achieved in simulating a variety of different sporting motions.

Distances between marker locations and joint centres were measured in the frontal and lateral axes; the distance between each of the markers on the foot and the floor were also measured. In measuring the joint centre offsets, the precise location of the joint centre was not clear however reliable estimates of the centre of rotation were found using manual joint rotation and the assumption that the joint centre lies along the longitudinal axis of two connecting segments.

8.3.5   Kinematic Data Processing

The kinematic data was processed by transposing the recorded marker locations to the joint centre locations by adjusting the position data according to the offset measurements taken from the subject. The elbow, shoulder, hip, knee, and ankle positions were transposed toward the midline of the body in the frontal plane, and the metatarsal-phalangeal joint and toe were transposed at right angles to the vector between that marker and the ankle in the sagittal plane. This process assumed that the movements of the trampolinist were confined to the sagittal plane and movements outside of this plane would have affected the kinematic data used in the matching procedures.

8.3.6 Determination of Suspension System Interface Parameters

The parameters governing the force interactions of the foot-suspension system interface were determined by a combined matching procedure using seven trials of varying rotation requirements. The matching procedure used a simulated annealing algorithm to minimise the difference between the angle-driven simulation model and the recorded performances. The parameter set was then evaluated by using it to simulate two independent skills, one forward rotating and one backward rotating, and was found to be applicable to trampoline contacts in general.

8.3.7 Torque Parameters

The parameters governing the performance of the torque generators were taken from the previous studies of Allen (2009) and Jackson (2010) who modelled the motion of triple jumping and gymnastic vaulting respectively. The torque parameter sets were then scaled to the recorded performances of the trampolinist, whilst forcing maximal activation to reach 1.0, by multiplying the isometric torque parameter by a scaling factor which was allowed to vary in the matching procedure in the evaluation of the torque-driven model using the method described by (King *et al*., 2009). The activities of gymnastics and triple jumping were considered to be reasonably similar to trampolining to assume that the torque-angle-angular velocity profiles of the individuals to be sufficiently similar.

The method of scaling torque parameters measured from third parties has limited ability to match the angle and angular velocity dependent aspects of the torque, as only the isometric torque was scaled to match the maximum torque required by the recorded performances. Despite this limitation the torque-driven model was able to simulate the performance of the trampolinist closely and realistically using the scaled torque parameters and the optimised performance only allowed for a modest improvement in jump height and reasonable improvement in rotation potential, suggesting that the torque parameters were realistic assuming the subject was already using near optimal technique. Ideally accurate torque parameters could be measured from the subject directly using isovelocity dynamometry, however measuring torque parameters accurately from a subject is time consuming. The subject should go through a familiarisation protocol in order

to be able to produce maximal effort during the testing procedure, greatly increasing the time involvement of the subject in the data collection procedure.

Bilateral symmetry was assumed once again, as the torques produced about each joint were simply doubled to represent the activity of both limbs. The model did not incorporate any bilateral deficit is the phenomena has been shown to be primarily caused by increased velocity of shortening (Bobbert *et al*., 2005) which is already incorporated by the simulation model.

8.3.8   Evaluation of the Torque-driven Model

The torque-driven model was evaluated by varying the activation parameters and a scaling factor for each of the torque generators using a simulated annealing algorithm whilst minimising the difference between the simulations and recorded performances of forward somersaults. The torque-driven simulations were able to closely match the recorded performances and so the model was considered to be suitable for the purpose of simulating forward rotating trampolining skills.

8.3.9   Cost Scores and Penalties

The structure and components of a cost score, that is minimised or maximised within an optimisation procedure, are the most important factors in the optimisation process. The constituent components and the weighting of those components dictate which aspects of the simulation outcomes the optimisation process focusses on matching to the greatest extent.

The cost scores used in the matching procedures were taken as a root mean square of multiple component scores describing the difference of many variables between the simulations and recorded performances. These variables described differences at the beginning, the end, and throughout simulations, and examined positions, velocities, orientations and configurations.

In the angle-driven matching procedure the standard deviation of the average component scores was 0.72 and in the torque driven matching procedure the standard deviation was 1.91. This shows RMS function was able to distribute the scores evenly amongst each of the components.

The optimisation scores for height and rotation potential heavily weighted the primary scores of height and rotation potential respectively, and both penalised the simulations for unrealistic joint angles and unwanted horizontal travel, whilst the height score also penalised the simulations for differences to the desired rotation potential. Joint angle penalties were squared, weighting them heavily, so that unrealistic techniques were not rewarded by the optimisation procedure.

The weighting of the penalty scores applied to each simulation will also heavily influence the solutions found during the optimisation procedure. If penalties are weighted too lightly compared to the cost score simulations that violate the constraints applied might be accepted as long if the overall simulation is still a good match. During the matching of the torque driven models none of the matching simulations incurred penalties whilst the optimal techniques were able to improve on the performance of the subject suggesting the penalties were weighted correctly.

8.4   Future Research

After a simulation model has been successfully evaluated it can be applied to answer research questions. The torque-driven model developed in the present study could be further applied to investigate wider aspects of the trampoline contact phase and trampoline takeoff techniques including some of the areas detailed below.

8.4.1   Robustness

Trampolinists are not able to perfectly coordinate movements time after time and yet they are capable of reliably performing complex skills time after time. It follows that they are able to use slightly different techniques to accomplish the same movement outcomes and to make adjustments in order to compensate for variations in movement characteristics between touchdown and takeoff as well as during the following flight period. The evaluated simulation model can be used to investigate how sensitive the simulated motion is to perturbations in the activation profiles. For example if the trampolinist mistimed the extension of the hips by 10

ms would they still be able to perform a piked triffus, or if the optimal technique used to complete 3 somersaults was perturbed slightly would they still be able to complete those somersaults or would they lose enough angular momentum to make attempting the skill dangerous.

8.4.2 Initial Conditions

Maximal depression of an elastic surface has been shown to result in maximal jump height in both trampolining (Shvartz, 1967) and diving (Cheng & Hubbard, 2004), and increased touchdown velocity has also been associated with increased jump height (Sanders & Wilson, 1988). Variations in joint configurations at touchdown will also affect the effectiveness of certain techniques to produce the desired movement outcomes. Varying the initial horizontal and vertical velocity of the centre of mass, the initial orientation and angular velocity of the trunk, and the initial joint configurations would allow the model to investigate optimal takeoff techniques given variations in initial conditions and examine how those optimal techniques differ according to the changes in initial conditions.

8.4.3 Subject-Specific Parameters

Throughout time the bodies of athletes can change through training and natural growth, effecting the strength capabilities and body size of an individual. As the body grows and changes the optimal takeoff techniques for that athlete will change to allow them to exploit strength gains or changes in the distribution of their body mass. Such changes in the optimal techniques can be investigating through the application of the simulation model with altered strength and body segmental inertia parameters. The results could have strong implications for coaching as strength and conditioning programs could be designed to specifically fit the needs of a given trampolinist, there may also be implications for talent identification as specific body types may be better suited to trampolining than others.

8.4.4 Sensitivity to Model Parameters

The parameters governing the foot-suspension system interface in the present study were determined to be specific to the trampolinist and the trampoline that

was used during the data collection. Trampoline beds can have varying degrees of elasticity and the construction of the suspension system has changed during the past few decades. The sensitivity of the simulation model to changes in the model parameters could be assessed by varying the individual parameter values and investigating the resulting changes in the performance of the model.

8.4.5   Application to Different Trampoline Contacts

Trampolinists perform skills that involve contact between the trampoline and parts of the body other than the feet. The contact between the trampoline and the anterior or posterior aspects of the torso could be represented by a simulation model based upon the model used in the present study to allow the simulation of skills where a trampolinist lands on their front or back. The primary change to the model required to simulate these skills would be to alter the distribution of force between different points along the interacting surfaces.

8.5   Conclusions

The torque-driven simulation model developed and successfully evaluated during the present study has been applied to optimise trampoline takeoff techniques for height and rotation potential in both forward rotating and backward rotating somersaults. The assumptions made during the development of the model and the limitations of the data collection, parameter determination and optimisation processes have been discussed, and improvements for future simulation models of trampolining have been suggested. Future applications of the simulation model have been considered, including investigations of questions that cannot be investigated by experimental methods and possible extensions of the present study.

References

Aaron, G.S. (1970). The science of trampolining. John Jones Cardiff Ltd: Cardiff

Abdel-Aziz, Y.I. & Karara, H.M. (1971). Direct linear transformation from computer coordinates into object space coordinates in close range photogrammetry. In: *Proceedings of the American Society of Photogrammetry Symposium on Close Range Photogrammetry*, pp. 1-18, American Society of Photogrammetry: Falls Church.

Ait-Haddou, R., Jinha, A., Herzog, W. & Binding, P. (2004). Analysis of the force-sharing problem using an optimization model. *Mathematical Biosciences*, 191, 111-122.

Alexander, R.McN. (1990). Optimum take-off techniques for high and long jumps. *Philosophical Transactions of the Royal Society of London. Series B: Biological Sciences*, 329(1252), pp.3-10.

Alkner, B.A., Tesch, P.A. & Berg, H.E. (2000). Quadriceps EMG/force relationship in knee extension and leg press. *Medicine and Science in Sports and Exercise*, 42(2), 459-463.

Allen, S.J. (2009). Optimisation of performance in the triple jump using computer optimisation. Unpublished Doctoral Thesis. Loughborough University.

Anderson, F.C. & Pandy, M.G. (1999). A dynamic optimization solution for vertical jumping in three dimensions. *Computer Methods in Biomechanics and Biomedical Engineering*, 2(3), 201-231.

Arampatzis, A., Morey-Klapsing, G. & Bruggemann, G.P. (2003). The effect of falling height on muscle activity and foot motion during landings. *Journal of Electromyography and Kinesiology*, 13(6), 533-544.

Bayer, H. & Flechtenmacher, R.C. (1950). Ermiidung und Aktionstromspannung bei der isometrischen Muskelkontraktion des Menschen. *Arbeitsphysiologie*, 14, 261-270.

Black, G.B. & Amadeo, R. (2003). Orthopaedic injuries associated with backyard trampoline use in children. *Canadian Journal of Surgery*, 46, 199-201.

Blajer, W. & Czaplicki, A. (2001). Modeling and inverse simulation of somersaults on the trampoline. *Journal of Biomechanics*, 34, 1619-1629.

Blajer, W. & Czaplicki, A. (2003). Contact modeling and identification of planar somersaults on the trampoline. *Multibody System Dynamics*, 10, 289-312.

Blajer, W. & Czaplicki, A. (2005). An alternative scheme for determination of joint reaction forces in human multibody models. *Journal of Theoretical and Applied Mechanics*, 43(4), 813-824.

Bobbert, M.F., De Graaf, W.W., Jonk, J.N. & Casius, L.J.R. (2005). Explanation of the bilateral deficit in human vertical squat jumping. *Journal of Applied Physiology*, 100, 493-499.

Bobbert, M.F., Huijing, P.A. & van Ingen Schenau, G.J. (1986). A model of the human triceps surae muscle-tendon complex applied to jumping. *Journal of Biomechanics*, 19(11) 887-898.

Bobbert, M.F. & van Ingen Schenau, G. (1988). Coordination in vertical jumping. *Journal of Biomechanics*, 21, 249-262.

Boda, W. (1992). Modelling the springboard and diver as an oscillating spring system. Unpublished Doctoral Thesis. University of Massachusetts.

Brüggemann, G.P. (1983). Kinematics and kinetics of the backward somersault take-off from the floor. In: Matsui, H. & Kobayashi, K. (Eds.), Biomechanics VII-B. Human Kinetics: Champaign, IL., pp. 793-800.

Brüggemann, G.P. (1987). Biomechanics in gymnastics. In: van Gheluwe, B. & Atha, J. (Eds.), Current Research in sports biomechanics. Medicine and Sport Science. Karger: Basel, pp.142-176.

Buchegger, J., Fritsch, R., Meier-Koll, A. & Riehle, H. (1991). Does trampolining and anaerobic physical fitness affect sleep? *Perceptual & Motor Skills*, 73(1), 243-252.

Buchegger, J & Meier-Koll, A. (1988). Motor learning and ultradian sleep cycle: an electroencephalographic study of trampoliners. *Perceptual & Motor Skills*, 67(2), 635-645.

Bunn, J.W. (1955). Scientific principles of coaching. Prentice-Hall, Inc: New York.

Cavagna, G.A. (1970). Elastic bounce of the body. *Journal of Applied Physiology*, 29(3), 279-282.

Challis, J.H. & Kerwin, D.G. (1988). An evaluation of splines in biomechanical data analysis. In: *Biomechanics XI-B*, de Groot, G *et al.* (Eds.), pp. 1057-1061. Free University Press: Amsterdam.

Chandler, R.F. (1975). Investigation of inertial properties of the human body. In: *Proceedings of the Aerospace Medical Research Laboratories* (AD-A016-485), Wright-Patterson Air Force Base: Dayton, OH.

Cheng, K.B. & Hubbard, M. (2004). Optimal jumping strategies from compliant surfaces: A simple model of springboard standing jumps. *Human Movement Science*, 23, 35-48.

Cheng, K.B. & Hubbard, M. (2005). Optimal compliant surface jumping: a multi-segment model of springboard standing jumps. *Journal of Biomechanics*, 38, 1822-1829.

Cheng, K.B. & Hubbard, M. (2008). Role of arms in somersaulting from compliant surfaces: A simulation study of springboard standing dives. *Human Movement Science*, 27, 80-95.

Clarys, J.P. & Marfell-Jones, M.J. (1986). Anthropometric prediction of component tissue mass in the minor limb segments of the human body. *Human Biology*, 58(5), 761-769.

Corana, A., Marchesi, C. & Ridella, S. (1987). Minimizing multimodal functions of continuous variables with the "Simulated Annealing" algorithm. *ACM Transactions on Mathematical Software*, 13(3), 262-280.

Cramer, J.T., Housh, T.J., Evetovich, T.K., Johnson, G.O., Ebersole, K.T., Perry, S.R. & Bull, A.J. (2002). The relationships among peak torque, mean power output, mechanomyography, and electromyography in men and women during maximal, eccentric isokinetic muscle actions. *European Journal of Applied Physiology*, 86, 226-232.

Craven, P. & Wahba, G. (1979). Smoothing noisy data with spline functions. *Numerische Mathematik*, 31, 377-403.

Dapena, J. (1993). Biomechanical studies in the high jump and implications for coaching. *Modern Athlete and Coach*, 31(4), 7-12.

Dapena, J. (1999). A biomechanical explanation of the effect of arm actions on the vertical velocity of a standing jump. In: *Proceedings of the XVIIth Congress of the International Society of Biomechanics*, Calgary Canada.

Dapena, J. & Chung, C.S. (1988). Vertical and radial motions of the body during the take-off phase of high jumping. *Medicine and Science in Sports and Exercise*, 20(3), 290-302.

Davis, L. (1991). Handbook of Genetic Algorithms. Van Nostrand Reinhold, New York.

Davis, R. & Macdonald, A. (1980). Better Trampolining. Kaye & Ward: London.

De Leva, P. (1996). Adjustments to Zatsiorsky-Seluyanov's segment inertia parameters. *Journal of Biomechanics*, 29(9), 1223-1230.

Dempster, W.T. (1955). Space requirements of the seated operator (WADC TR 55-159). Wright-Patterson Air Force Base: Dayton, OH.

Doane, J.E. & Quesada, P.M. (2006). Subject specific body segment parameter estimation using 2D work and energy principles. *Gait and Posture*, 245, s123-125.

Duncan, A. & McDonough, M.J. (2000). Stretch reflex distinguished from pre-programmed muscle activations following landing impacts in man. *Journal of Physiology*, 526 (Pt. 2), 457-468.

Durkin, J.L. & Dowling, J.J. (2006). Body segment parameter estimation of the human lower leg using an elliptical model with validation from DEXA. *Annals of Biomedical Engineering*, 34(9), 1483-1493.

Dyson, G.H. (1964). The mechanics of athletics, 3rd Ed. University of London Press: London.

Edman, K.A. (1988). Double-hyperbolic force velocity relation in frog muscle fibres. *Journal of Applied Physiology*, 404, 301-321.

Edman, K.A.P. and Regianni, C. (1987). The sarcomere length-tension relation determined in short segment of intact muscle fibres of the frog. *Journal of Physiology*, 385, 709-732.

Feltner, M.E., Fraschetti, D.J. & Crisp, R.J. (1999). Upper extremity augmentation of lower extremity kinetics during countermovement vertical jumps. *Journal of Sports Sciences*, 17, 449-466.

Federation Internationale de Gymnnastique, (2013). FIG 2013-2016 code of points – trampoline gymnastics. FIG

Flynn, A. & Simms, C. (2003). Multibody modelling of trampoline kinematics. In: Proceedings Madymo Users Conference, Brussels, pp.1-8.

Forrester, S.E., Yeadon, M.R., King, M.A. and Pain, M.T. (2011). Comparing different approaches for determining joint torque parameters from isovelocity dynamometer measurements. *Journal of Biomechanics*, 44(5), 955-961.

Forwood, M.R., Neal, R.J. & Wilson, B.D. (1985). Scaling segmental moments of inertia for individual subjects. *Journal of Biomechanics*, 18(10), 755-761.

Frohlich, C. (1979). Do Springboard divers violate angular momentum conservation? *American journal of physics*, 47(7), 583-592.

Furnival, R.A., Street, K.A. & Schunk, J.E. (1999). Too many pediatric trampoline injuries. *Pediatrics*, 103(5), e57-62.

Goffe, W.L., Ferrier, G.D. & Rogers, J. (1994). Global optimization of statistical functions with simulated annealing. *Journal of Econometrics*, 60, 65-99.

Gordon, A.M., Huxley, A.F. & Julian, F.J. (1964). The length-tension diagram of single vertebrate striated muscle fibres. *Journal of Physiology*, 171, 28-30.

Gordon, A.M., Huxley, A.F. & Julian, F.J. (1966). Tension development in highly stretched vertebrate muscle fibres. *Journal of Physiology*, 184, 143-169.

Gordon, A.M., Huxley, A.F. & Julian, F.J. (1966). The variation in isometric tension with sacromere length in vertebrate muscle fibres. *Journal of Physiology*, 184, 170-192.

Griswold, L. (1948). Trampoline tumbling. Barnes: New York.

Gruber, K., Ruder, H., Denoth, J. & Schneider, K. (1998). A comparative study of impact dynamics: wobbling mass models versus rigid body models. *Journal of Biomechanics*, 31, 439-444.

Hagueneuer, M., Legreneur, P. & Monteil, K.M. (2006). Influence of figure skating skates on vertical jumping performance. *Journal of Biomechanics*, 39, 699-707.

Hamill, J., Ricard, M.D. & Golden, D.M. (1986). Angular momentum in multiple rotation nontwisting platform dives. *International Journal of Sports Biomechanics*, 2, 78-87.

Hanavan, E.P. (1964). A mathematical model of the human body. *AMRL Technical Report*, 64-102. Wright-Patterson Air Force Base: Dayton, OH.

Hara, M., Shibayama, A., Takeshita, D. & Fukashiro, S. (2006). The effect of arm swing on lower extremities in vertical jumping. *Journal of Biomechanics*, 39(13), 2503-2511.

Hara, M., Shibayama, A., Takeshita, D., Hay, D.C. & Fukashiro, S. (2008). A comparison of the effect of arm swing and countermovement on the lower extremities in vertical jumping. *Human Movement Science*, 27(4), 636-648.

Harik, G., Cantau-Paz, E., Goldberg, D.E., and Miller, B.L. (1999). The gambler's ruin problem, genetic algorithms, and the sizing of populations. *Evolutionary Computation*, 7(3), 231-253.

Harman, E.A., Rosenstein, M.T., Frykman, P.N. & Rosenstein, R.M. (1990). The effects of arms and countermovement on vertical jumping. *Medicine and Science in Sports and Exercise*, 22, 825-833.

Hatze, H. (1980). A mathematical model for the computational determination of parameter values of anthropomorphic segments. *Journal of Biomechanics*, 13, 833-843.

Hatze, H. (1981a). A comprehensive model for human motion simulation and its application to the take-off phase of the long jump. *Journal of Biomechanics*, 14, 135-142.

Hatze, H. (1981b). The use of optimally regularized Fourier series for estimating higher order derivatives of noisy biomechanical data. *Journal of Biomechanics*, 14, 13-18.

Hatze, H. (2005). Parameter identification for human body segment models. *Theoretical Issues in Ergonomics Science*, 6(3-4), 331-334.

Hawkins, D. & Smeulders, M. (1998). Relationship between knee joint torque, velocity, and muscle activation: consideration for musculoskeletal modelling. *Journal of Applied Biomechanics*, 14, 141-157.

Hawkins, D. & Smeulders, M. (1999). An investigation of the relationship between hip extension torque, hip extension velocity, and muscle activation. *Journal of Applied Biomechanics*, 15, 253-269.

Hennessey, J.T. (1969). The Trampoline: As I see it, 2nd Ed. International Publications of Lafayette: Louisiana.

Herzog, W. (1988). The relation between the resultant moments at a joint and the moments measured by an isokinetic dynamometer. *Journal of Biomechanics*, 21(1), 5-12.

Hiley, M.J. & Yeadon, M.R. (2007). Optimization of backward giant circle technique on the asymmetric bars. *Journal of Applied Biomechanics*, 23, 300-308.

Hill, A.V. (1938) The heat of shortening and the dynamic constants of muscle. *Proceedings of the Royal Society Series B*, 126, 136-195.

Hinrichs, R.N. (1985). Regression equations to predict segmental moments of inertia from anthropometric measurements: an extension of Chandler *et al.* (1975). *Journal of Biomechanics*, 18(8), 621-624.

Hof. A.L. & van den Berg, J.W. (1981a). EMG to force processing, I: An electrical analogue of the Hill muscle model. *Journal of Biomechanics*, 14. 747-758.

Hof, A.L. & van den Berg, J.W. (1981b). EMG to force processing, II: Estimation of the parameters of the Hill muscle model for the human triceps surae by means of a calfergometer. *Journal of Biomechanics*, 14. 759-770.

Hof. A.L. & van den Berg, J.W. (1981c). EMG to force processing, III: Estimation of model parameters for the human triceps surae muscle and assessment of the accuracy by means of a torque plate. *Journal of Biomechanics*, 14, 771-785.

Hof, A.L. & van den Berg, J.W. (1981d). EMG to force processing, IV: Eccentric-concentric contractions on a spring-flywheel set-up. *Journal of Biomechanics*, 14, 787-792.

Horita, T., Komi, P.V., Nicol, C. & Kyrolainen, H. (2002). Interaction between pre-landing activities and stiffness regulation of the knee joint musculoskeletal system in the drop jump: implications to performance. *European Journal of Applied Physiology*, 88(1-2), 76-84.

Horne, D.E. (1968). Trampolining. Faber and Faber: London & Boston.

Huxley, A.F. (1957). Muscle structure and theories of contraction. *Progress in Biophysics and Biophysical Chemistry*, 7, 225-318.

Hwang, I., Seo, G. & Liu, Z.C. (1990). Takeoff mechanics of the double backward somersault. *International Journal of Sport Biomechanics*, 6, 177-186.

Jacobs, R., Bobbert, M.F. & van Ingen Schenau, G.J. (1996). Mechanical output from individual muscles during explosive leg extensions: the role of biarticular muscles. *Journal of Biomechanics*, 29(4), 513-523.

Jackson, M.I. (2010). The mechanics of the table contact phase of gymnastics vaulting. Unpublished Doctoral Thesis. Loughborough University.

Jaques, H.P. (2008). Determining and modelling the forces exert by a trampoline suspension system. Unpublished Masters Thesis. Loughborough University.

Jensen, R.K. (1976). Model for body segment parameters. In: *Biomechanics V-B*. Komi, P.J. (Ed), 380-386, University Park Press: Baltimore, MD.

Kane, T.R. & Levinson, D.A. (1985). Dynamics: theory and applications. 1st Ed. McGraw-Hill Book Co., New York.

Kane, T.R. & Levinson, D.A. (1996). Dynamics online: theory and implementations with AUTOLEV. 1st Ed. Online Dynamics Inc., Sunnyvale.

Kawakami, Y., Kubo, K., Kanehisa, H. & Fukunaga, T. (2002). Effect of series elasticity on isokinetic torque-angle relationship in humans. *European Journal of Applied Physiology*, 87, 381-387.

Keeney, C. (1961). Trampolining illustrated. The Ronald Press Company: New York.

Kennett, K., Lai, W. & Kelkar, R. (2001). Modeling of falls and jumps. In: The 4th MADYMO User's meeting of the America's, Detroit, MI.

Khalaf, K.A., Parnianpour, M. & Karakostas, T. (2000). Surface responses of maximum isokinetic ankle torque generation capability. *Journal of Applied Biomechanics*, 16, 52-59.

Kikuchi, S.; Nakazawa, K. (2004). Motion reconstruction of somersaults using three dimensional model matching method from its silhouette image. In: *Advanced Motion Control, 2004. AMC '04. The 8th IEEE International Workshop*, pp. 671-676.

King, M.A., Kong, P.W. & Yeadon, M.R. (2009). Determining effective subject-specific strength levels for forward dives using computer simulations of recorded performances. *Journal of Biomechanics*, 42, 2672-2677.

King, M.A. & Yeadon, M.R. (2002). Determining subject-specific torque parameters for use in a torque-driven simulation model of dynamic jumping. *Journal of Applied Biomechanics*, 18, 207-217.

King, M.A. & Yeadon, M.R. (2003). Coping with perturbations to a layout somersault in tumbling. *Journal of Biomechanics*, 36(7), 921-927.

King, M.A. & Yeadon, M.R. (2004). Maximising somersault rotation. *Journal of Biomechanics*, 37, 471-477.

Kong, P.W. (2005). Computer simulation of the takeoff in springboard diving. Unpublished Doctoral Thesis. Loughborough University.

Kooi, B.W. & Kuipers, M. (1994). The dynamics of springboards. *Journal of Applied Biomechanics*, 10, 335-351.

Kraft, M. (2001). Eine einfache Näherung für die vertikale Federkraft des Trampolinsprungtuches [online]. *http://opus.tu-bs.de/opus/volltexte/2001/214*, accessed 6/10/08.

Kwon, Y. (1996). Effects of the methods of body segment parameter estimation on airborne angular momentum. *Journal of Applied Biomechanics*, 12, 413-430.

Kwon, Y. (2000). Flexibility of the experimental simulation approach to the analysis of the human airborne movements: body segment parameter estimation. In: *proceedings of the XVIII International Symposium on Biomechanics in Sports II*, pp.507-514, The Chinese University of Hong Kong: Hong Kong.

Kwon, Y. (2001). Experimental simulation of airborne movement: applicability of the body segment parameter estimation methods. *Journal of Applied Biomechanics*, 17, 232-240.

LaDue, F. & Norman, J. (1956). This is Trampolining, 2nd Ed. Nissen Trampoline Company: Cedar Rapids, Iowa.

Larson, B.J. & Davis, J.W. (1995). Trampoline-related injuries. *Journal of Bone and Joint Surgery*, 77, 1174-1178.

Lees, A., Vanrenterghem, J. & De Clerq, D. (2004). Understanding how an arm swing enhances performance in the vertical jump. *Journal of Biomechanics*, 37, 1929-1940.

Leite de Barros, R.M., Russomanno, T.G., Brenzikofer, R. & Figeuroa, P.J. (2006). A method to synchronise video cameras using the audio band. *Journal of Biomechanics*, 39, 776-780.

Lephart, S.A. (1971). The design of the force mechanism in rebound tumbling and its influence on teaching methods. *The Australian Journal of Physical Education*, 52, 8-10.

Lephart, S.A. (1972). A Mechanical analysis of forward somersaulting skills in rebound tumbling. Unpublished Doctoral Thesis. Ohio State University.

Lewis, M.G.C., King, M.A., Yeadon, M.R. and Conceição, F. (2012). Are joint torque models limited by an assumption of monoarticularity? *Journal of Applied Biomechanics*, 28, 520-529.

Loken, N.C. & Willoughby, R.J. (1967). The complete book of gymnastics, 2nd Ed. Prentice-Hall, Inc: Englewood Cliffs, NJ.

Liu, T. & Wu, X. (1989). Best instant of take-off from springboard. In: *Proceedings of the XII International Congress of Biomechanics* (Abstract 23), University of California: Los Angeles, California.

Mathiyakom, W. & McNitt-Gray, J.L. (2007). Generation of linear and angular momentum during interaction with deformable surfaces. *Journal of Biomechanics*, 40, s700.

Mesnard, M., Morlier, J. & Cid, M. (2007). An essential performance factor in pole-vaulting. *Comptes Rendus Mecanique*, 335, 382-387.

Miller, D.I. (1984). Biomechanical characteristics of the final approach step, hurdle and takeoff of elite American springboard divers. *Journal of Human Movement Studies*, 10, 189-212.

Miller, D.I. & Munro, C.F. (1984). Body segment contributions to height achieved during the flight of a springboard dive. *Medicine and Science in Sports and Exercise*, 16(3), 234-242.

Miller, D.I. & Munro, C.F. (1985). Greg Louganis' springboard takeoff: II. linear and angular momentum considerations. *International Journal of Sport Biomechanics*, 1, 288-307.

Miller, D.I. & Sprigings, E.J. (2001). Factors influencing the performance of springboard dives of increasing difficulty. *Journal of Applied Biomechanics*, 17, 217-231.

Mills, C. (2005). Computer simulation of gymnastics vault landings. Unpublished Doctoral Thesis. Loughborough University.

Mills, C., Pain, M.T.G. & Yeadon, M.R. (2008). The influence of simulation model complexity on the estimation of internal loading in gymnastics landings, *Journal of Biomechanics*, 41(3), 620-628.

Murphy, C. (2000). Trampoline Injuries. *Hazard*, 42, Victorian Injury Surveillance System.

Musker, F.F., Cassady, D. & Irwin, L. (1968). A guide to gymnastics. The Macmillan Company: New York.

Nigg, B.M. & Liu, W. (1999). The effect of muscle stiffness and damping on simulated impact force peaks during running. *Journal of Biomechanics*, 32, 849-856.

Ollerenshaw, R. (2004). Development of a method to quantify the contributions of horizontal and vertical forces and angular momentum generation in trampolining somersaults, and application to forward rotating somersaults. Unpublished Masters Thesis, University of Wales Institute, Cardiff.

Page, R.L. (1974). The mechanics of toppling techniques in diving. *Research Quarterly*, 45(2), 185-192.

Pain, M.T.G. & Challis, J.H. (2001). The role of the heel pad and shank soft tissue during impacts: a further resolution of a paradox. *Journal of Biomechanics*, 34, 327-333.

Pain, M.T.G. & Challis, J.H. (2004). Wobbling mass influence on impact ground reaction forces: a simulation model sensitivity analysis. *Journal of Applied Biomechanics*, 20, 309-316.

Pain, M.T.G. & Challis, J.H. (2006). The influence of soft tissue movement on ground reaction forces, joint torques and joint reaction forces in drop landings. *Journal of Biomechanics*, 39, 119-124.

Pandy, M.G. & Anderson, F.C. (2000). Dynamic simulation of human movement using large-scale models of the body. *Phonetica*, 57(2-4), 219-228.

Pandy, M.G., Zajac, F.E., Sim, E. & Levine, W.S. (1990). An optimal control model for maximum-height jumping. *Journal of Biomechanics*, 23(12), 1185-1198.

Pandy, M.G. & Zajac, F.E. (1991). Optimal muscular coordination strategies for jumping. *Journal of Biomechanics*, 24, 1-10.

Panjabi, M. (1979) Validation of mathematical models. *Journal of Biomechanics*, 12(3), 238.

Pavol, M.J. & Grabiner, M.D. (2000). Knee strength variability between individuals across ranges of motion and hip angles. Medicine and Science in Sports and Exercise, 32(5), 985-992.

Payne, A.H., Slater, W.J. & Telford, T. (1968). The use of a force platform in the study of athletic activities. *Ergonomics*, 11, 123-143.

Pezzack, J.C., Norman, R.W. & Winter, D.A. (1977). An assessment of derivative determining techniques used for motion analysis. *Journal of Biomechanics*, 10, 377-382.

Phelps, E. & Phelps, B. (1990). Trampolining: the skills of the game. Crowood Press: Ramsbury, UK.

Pourcelot, P., Audigie, F., Degueurce, C., Geiger, D. & Denoix, J.M. (2000). A method to synchronise cameras using the direct linear transformation technique. *Journal of Biomechanics*, 33(12), 1751-1754.

Press, W.H., Teukolsky, S., Vetterling, W. & Flannery, B. (1992). Numerical Recipes FORTRAN: The art of scientific computing (2nd Ed). Cambridge University Press: New York.

Press, W.H. (1997). Numerical Recipes C: The art of scientific computing (2nd Ed). Cambridge University Press: New York.

Rácz, L., Béres, S., Hortobágyi, T. & Tihanyi, J. (2002). Contraction history affects the in vivo quadriceps torque-velocity relationship in humans. *European Journal of Applied Physiology*, 87, 393-402.

Raikova, R.T. & Alodjov, H.T. (2005). Comparison between two muscle models under dynamic conditions. *Computers in Biology and Medicine*, 35, 373- 387.

Riehle, H. (1979). Die Biomechanik der Wirbelsäule beim Trampolinturnen. Richarz: St. Augustin

Sanders, R.H. & Allen, J.B. (1993). Changes in net joint torques during accommodation to change in surface compliance in a drop jumping task. *Human Movement Science*, 12, 299-326.

Sanders, R.H. & Wilson, B.D. (1987). Angular momentum and requirements of the twisting and nontwisting forward 1 ½ somersault dive. *International Journal of Sport Biomechanics*, 3, 47-62.

Sanders, R.H. & Wilson, B.D. (1988). Factors contributing to maximum height of dives after take off from the 3m springboard. *International Journal of Sport Biomechanics*, 4, 231-259.

Sanders, R.H. & Wilson, B.D. (1992). Modification of movement patterns to accommodate to a change in surface compliance in a drop jumping task. *Human Movement Science*, 11, 593-614.

Sarfaty, O. & Ladin, Z. 91993). A video-based system for the estimation of the inertial properties of body segments. *Journal of Biomechanics*, 26(8), 1011-1016.

Sargent, R.G. (2005). Verification and validation of simulation models. In: WSC '05: Proceedings of the 37th conference on Winter simulation. Winter Simulation Conference: Orlando, FL.

Scovil, C.Y. & Ronsky, J.L. (2006) Sensitivity of a Hill-based model to perturbations in model parameters. *Journal of Biomechanics*, 39, 2055-2063.

Selbie, W.S. & Caldwell, G.E. (1996). A simulation study of vertical jumping from different starting postures. *Journal of Biomechanics*, 29(9), 1137-1146.

Shvartz, E. (1967). Effect of impulse on momentum in performing on the trampoline. *The Research Quarterly*, 38(2), 300-304.

Smith, G.A. & Shields, B.J. (1998). Trampoline-related injuries to children. *Archives of Pediatrics & Adolescent Medicine*, 152, 694-699.

Spägele, T., Kistner, A. & Gollhofer, A. (1999). Modelling simulation and optimisation of a human vertical jump. *Journal of Biomechanics*, 32, 521-530.

Sprigings, E.J. & Miller, D.I. (2002) Searching for optimal knee extension timing in dives from the reverse group. *Journal of Applied Biomechanics*, 20, 275-290.

Sprigings, E.J., Stilling, D.S. & Watson, L.G. (1989). Development of a model to represent an aluminium springboard in diving. *International Journal of Sport Biomechanics*, 5(3), 297-307.

Sprigings, E.J. & Watson, G. (1985). A mathematical search for the optimal timing of the armswing during springboard diving take-offs. In Winter, D.A. *et al.* (Eds.), *Biomechanics IX B*, Human Kinetics: Champaign, IL, pp. 389-394.

Sprigings, E.J. Watson, G., Haseganu, E. & Derby, D. (1986). A model for optimizing the timing of the relative force patterns of the arms, torso, and legs during springboard diving take-offs. In: *Proceedings of the North American Congress on Biomechanics*, Montreal, pp.39-40.

Stojanovic, B., Kojic, M., Tsui, C.P. & Tang, C.Y. (2007). An extension of Hill's three-component model to include different fib re types in finite element modelling of muscle. *International Journal for Numerical Methods in Engineering*, 71, 801-817.

Stroup, F. & Bushnell, D.L. (1969). Rotation, translation and trajectory in diving. *Research Quarterly*, 40(4), 812-817.

Takashima, S., Unno, T., Ohara, S. & Ashikaga, K. (1998). Motion control of a trampoline gymnast robot. *1998 Japan-USA Symposium on Flexible Automation*, 1057-1060.

Tate, O.J. & Damiano, D.L. (2002). Torque-EMG relationships in normal and spastic muscles. *Electromyography and Clinical Neurophysiology*, 42(6), 347-357.

Van Soest, A.J. and Casius, L.J.R., (2003). The merits of a parallel genetic algorithm in solving hard optimisation problems. *Journal of Biomechanical Engineering*, 125, 141-146.

Van Soest, A.J., Schwab, A.L., Bobbert, M.F. & van Ingen Schenau, G.J. (1993). The influence of the biarticularity of the gastrocnemius muscle on vertical-jumping achievement. *Journal of biomechanics*, 26(1), 1-8.

Vaughan, C.L. (1980). A kinetic analysis of basic trampoline stunts. *Journal of Human Movement Studies*, 6, 236-251.

Vaughan, C.L. (1984). Simulation of human motion in sports biomechanics. In Terjung, R.L. (Ed.), Exercise and Sport Science Review Vol.2, American College of Sports Medicine Series, pp. 373-410.

Vint, P.F. & Hinrichs, R.N. (1996). Endpoint error in smoothing and differentiating raw kinematic data: an evaluation of four popular methods. *Journal of Biomechanics*, 29(12), 1637-1642.

Virmavirta, M., Isolehto, J., Komi, P.V., Schwameder, H., Pigozzi, F. & Massazza, G. (2007). Take-off analysis of the Olympic ski jumping competition (HS-106M). *Journal of Biomechanics*, 40(2), 403.

Walker, R. (1983). Trampolining: beginner to competitor. EP Publishing Limited: East Ardsley, UK.

Westing, S.H., Seger, J.Y. & Thorstensson, A. (1990). Effects of electrical stimulation on eccentric and concentric torque-velocity relationships during knee extension in man. *Acta Physiologica Scandinavica*, 140, 17-22.

Wilson, C. (2003). Optimisation of performance in running jumps. Unpublished Doctoral Thesis. Loughborough University.

Wilson, C., King, M.A. & Yeadon, M.R. (2006). Determination of subject-specific model parameters for visco-elastic elements. *Journal of Biomechanics*, 39, 1883-1890.

Winter, D.A., Wells, R.P. & Orr, G.W. (1981). Errors in the use of isokinetic dynamometers. *European Journal of Applied Physiology*, 46, 397-408.

Woltring, H.J. (1985). On optimal smoothing and derivative estimation from noisy displacement data in biomechanics. *Human Movement Science*, 4, 229-245.

Wood, G.A. (1982). Data smoothing and differentiation procedures in biomechanics. *Exercise and Sport Science Review*, 10, 308-362.

Wood, G.A. & Jennings, L.S. (1979). On the use of spline functions for data smoothing. *Journal of biomechanics*, 12, 477-479.

Xu, Y. (2000). Basic diving coaching manual. National Aquatic Centre: Beijing.

Xu, Y. & Zhang, D. (1996). Basic diving coaching manual. Fédération Internationale, de Natation Amateur: Lausanne.

Yeadon, M.R. (1989). A method for obtaining three-dimensional data on ski jumping using pan and tilt cameras. *International Journal of Sports Biomechanics*, 5, 238-247.

Yeadon, M.R. (1990a). The simulation of aerial movement--I. The determination of orientation angle from film data. *Journal of Biomechanics*, 23(1), 59-66.

Yeadon, M.R. (1990b). The simulation of aerial movement--II. A mathematical inertia model of the human body. *Journal of Biomechanics*, 23(1), 67-74.

Yeadon, M.R. (1990c). The simulation of aerial movement--III. The determination of angular momentum of the human body. *Journal of Biomechanics*, 23(1), 75-83.

Yeadon, M.R., Atha, J. & Hales, F.D. (1990). The simulation of aerial movement--IV. A computer simulation model. *Journal of Biomechanics*, 23(1), 85-89.

Yeadon, M.R. & Challis, J.H. (1994). The future of performance-related sports biomechanics research. *Journal of Sports Sciences*, 12, 3-32.

Yeadon, M.R. and Hiley, M.J. (2000). The mechanics of the backward giant circle on the high bar. *Human Movement Science*, 19(2), 153-173.

Yeadon, M.R. & King, M.A. (1999). A method for synchronising digitised video data. *Journal of Biomechanics*, 32(9), 983-986.

Yeadon, M.R., King, M., Forrester, S., Caldwell, G. & Pain, M. (2010). The need for muscle co-contraction prior to landing. *Journal of Biomechanics*, 43(2), 364-369.

Yeadon, M.R., King, M.A. & Wilson, C. (2006). Modelling the maximum voluntary joint torque/angular velocity relationship in human movement. *Journal of Biomechanics*, 39, 476-482.

Yeadon, M.R., Kong, P.W. & King, M.A. (2006b) Parameter determination for a computer simulation model of a diver and a springboard. *Journal of Applied Biomechanics*, 22, 167-176.

Yeadon, M.R. & Morlock, M. (1989). The appropriate use of regression equations for the estimation of segmental inertia parameters. *Journal of Biomechanics*, 22(6/7), 683-689.

Yu, B., Koh, T.H & Hay, J. (1993). A panning DLT procedure for three-dimensional videography. *Journal of Biomechanics*, 26, 109-124.

Zatsiorsky, V. & Seluyanov, V. (1985). Estimation of the mass and inertia characteristics of the human body by means of the best predictive regression equations. In: Winter, D.A. *et al.* (Eds.), *Biomechanics IX-B*, pp. 233-239. Human Kinetics: Champaign, IL.

Zatsiorsky, V.M. & Seluyanov, V.N. (1983). The mass and inertia characteristics of the main segments of the human body. In Matsui, H. & Kobayashi, K. (Eds.), *Biomechanics VIII-B*, pp. 1152-1159. Human Kinetics: Champaign, IL.

APPENDICES

APPENDIX 1

Informed Consent Form

DATA ACQUISITION FOR THE ANALYSIS OF HUMAN MOVEMENTS
LAY SUMMARY

The study comprises a biomechanical analysis of human movement. This analysis requires:
Kinematic (how you are moving) during human movements
Subject specific inertia parameters

The data of actual human movements are required to give detailed information about the current techniques used by humans. The subject specific parameters are required for the customisation of computer simulation models to individual humans. The simulation models will then be used to understand and explain techniques currently used, determine the contributions of different techniques to performance and also optimise performance.

The kinematic, kinetic and EMG data may be obtained in a number of different ways:
Automatic displacement acquisition system. This is similar to being videoed but reflective markers or LEDs will be taped to you and only their image recorded.

The subject specific parameters may be obtained from:
Anthropometric measurements. Measuring the size of your limbs and body.

Data will be acquired in the biomechanics research facilities in the University or in other research laboratories. Any data collection session will last no longer than two hours, with the subject actively involved for only a fraction of the total time:
Actual performance of movements: 15 minutes
Anthropometric measurements: 30 minutes

A medical history questionnaire and full written consent will be required from the parent (if the subject is under the age of 18) or the subject prior to participation in the study.

DOCUMENTS WHEN SUBJECTS ARE AT LEAST 18 YEARS OF AGE

INFORMATION FOR SUBJECTS
PRE-SELECTION MEDICAL QUESTIONNAIRE
INFORMED CONSENT FORM (SUBJECT)

INFORMATION FOR SUBJECTS

The study in which you have been invited to participate will involve a biomechanical analysis of human movement. The study will be divided into two parts; firstly, a video recording will be taken of you performing selected human movements. You will only be asked to perform movements that you are familiar with and feel comfortable performing such as those listed:

Trampolining

The second part of the study will involve measurements to determine the lengths, widths and circumferences of your body segments (e.g. your arms, legs, trunk and head). It may also be necessary to take additional measurements to estimate your strength characteristics during various activities (e.g. extending and flexing your knee or hip). The measurement procedures will be described and demonstrated in advance. It may be necessary to shave certain areas of your body to attach monitoring equipment using adhesive tape. The data collected will be used to help increase our understanding of the mechanics of human movements.

You will perform the data collection in a suitable environment. The risk of injury during the data collection will be minimal since we will only ask you to perform movements with which you are familiar and comfortable. It is considered that no increased risks, discomforts or distresses are likely to result from the data collection of human movements above those associated with the normal performance of those movements.

The information obtained from the study will be collected and stored in adherence with the Data Protection Act. Whilst certain personal and training information will be required, you will be allocated a reference number to ensure that your identity and personal details will remain confidential. Video recordings will be stored in the video analysis room to which access is restricted to members of the biomechanics research team. The video images will be digitised and only the numerical values will be used in published work, not the images themselves. On occasion video images may be required. In such an instance we will seek your written permission to use such images and you are perfectly free to decline. Video recordings will be kept for three years after publication of the study. If you agree to take part in the study, you are free to withdraw from the study at any stage, with or without having to give any reasons. A contact name and phone number will be provided to you for use if you have any queries about any part of your participation in the study.

PRE-SELECTION MEDICAL QUESTIONNAIRE

LOUGHBOROUGH UNIVERSITY
SCHOOL OF SPORT, EXERCISE AND HEALTH SCIENCES

Please read through this questionnaire, BUT DO NOT ANSWER ANY OF THE
QUESTIONS YET. When you have read right through, there may be questions you
would prefer not to answer. Assistance will be provided if you require it to discuss any
questions on this form.   In this case please tick the box labelled "I wish to withdraw"
immediately below. Also tick the box labelled "I wish to withdraw" if there is any other
reason for you not to take part.   tick appropriate box

I wish to withdraw

I am happy to answer the questionnaire

If you are happy to answer the questions posed below, please proceed. Your answers will
be treated in the strictest confidence.

1.	Are you at present recovering from any illness or operation?	YES/NO*

2.	Are you suffering from or have you suffered from or received medical treatment
for any of the following conditions?

a.	Heart or circulation condition	YES/NO*
b.	High blood pressure	YES/NO*
c.	Any orthopaedic problems	YES/NO*
d.	Any muscular problems	YES/NO*
e.	Asthma or bronchial complaints	YES/NO*

3.	Are you currently taking any medication that may affect your participation in the
	study?	YES/NO*

4.	Are you recovering from any injury?	YES/NO*

5.	Are you epileptic?	YES/NO*

6.	Are you diabetic?	YES/NO*

7.	Are you allergic to sticking plasters?	YES/NO*

8.	Do you have any other allergies? If yes, please give details below
	YES/NO*
…………………………………………………………………………………….…
…………………………………………………………………………………

9.	Are you aware of any other condition or complaint that may be affected by
participation in this study? If so, please state below;
…………………………………………………………………………………….…
…………………………………………………………………………………

* Delete as appropriate

172

INFORMED CONSENT FORM (SUBJECTS)
PURPOSE
To obtain kinematic data during human movements. To obtain subject specific inertia parameters.

PROCEDURES
The kinematic data of human movements will be obtained using:
Automatic displacement acquisition system

ACTIVITIES
Possible activities of which only those to be undertaken will be listed
Trampolining

A number of trials will be requested with suitable breaks to minimise fatigue and boredom.

The subject specific parameters will be obtained from:
Anthropometric measurements (using tape measures and specialist anthropometers)

During the measurements two researchers will be present, at least one of whom will be of the same sex as you.

QUESTIONS
The researchers will be pleased to answer any questions you may have at any time.

WITHDRAWAL
You are free to withdraw from the study at any stage, with or without having to give any reasons.

CONFIDENTIALITY
Your identity will remain confidential in any material resulting from this work. Video recordings will be stored in the video analysis room to which access is restricted to members of the biomechanics research team. The video images will be digitised and only the numerical values will be used in published work, not the images themselves. On occasion video images may be required. In such an instance we will seek your written permission to use such images and you are perfectly free to decline. Video recordings will be kept for three years after publication of the study.

I have read the outline of the procedures which are involved in this study, and I understand what will be required by me. I have had the opportunity to ask for further information and for clarification of the demands of each of the procedures and understand what is entailed. I am aware that I have the right to withdraw from the study at any time with no obligation to give reasons for my decision. As far as I am aware I do not have any injury or infirmity which would be affected by the procedures outlined.
Name …………………………………………
Signed …………………………………………. (subject)   Date ……………

In the presence of:
Name …………………………………………

APPENDIX 2

Anthropometric Measurements

Appendix 2a. Anthropometric measurements taken for use in conjunction with the inertia model of Yeadon (1990b)

Appendix 2b. Marker offset measurements

60.05 kg   168.7 cm

ALL MEASUREMENTS IN MILLIMETRES

TORSO

level →	hip	umbilicus	ribcage	nipple	shoulder	neck	→	nose	ear	top
length	0	170	225	428	515	565	0	145	200	300
perimeter	793	700	690	867	■	351		474	565	
width	297	277	254	313	352					
depth					156					

LEFT ARM

level →	shoulder	Mid-arm	elbow	forearm	wrist	→	thumb	knuckle	nails (3)
length	0		245	284	490	0	60	100	178
perimeter	313	259	249	258	165		227	224	114
width					56		92	82	56

RIGHT ARM

level →	shoulder	Mid-arm	elbow	forearm	wrist	→	thumb	knuckle	nails (3)
length	0		245	293	495	0	60	100	178
perimeter	323	260	247	261	167		232	197	114
width					56		93	82	55

LEFT LEG

level →	hip	crotch	Mid-thigh	knee	calf	ankle	→	heel	arch	ball	nails (3)	ankle → floor
length	0	105		367	515	775	0	10		145	210	73
perimeter		518	449	367	348	216		313	238	221	150	
width										88	63	
depth						116						

RIGHT LEG

level →	hip	crotch	Mid-thigh	knee	calf	ankle	→	heel	arch	ball	nails (3)	ankle → floor
length	0	112		375	532	780	0	10		145	210	67
perimeter		524	451	358	350	219		314	246	223	158	
width										92	65	
depth						117						

Marker Offset Measurements				
	Axis			
	x	y	z	z → floor
sternal		75		
shoulder	45			
elbow	45			
wrist	45			
hip	100			
knee	68			
ankle	40			78
ball	0		39	60
toe	0		27	36

APPENDIX 3

Autolev^{TM} 4.1 Command Files

Appendix 3a. Autolev^{TM} commands used to create the Fortran code for the angle-driven simulation model of a trampolinist

Appendix 3b. Autolev^{TM} commands used to create the Fortran code for the torque-driven simulation model of a trampolinist

```
% TRAMPANG.AL

% ANGLE-DRIVEN 7-SEGMENT MODEL OF A TRAMPOLINE TAKEOFF
% -TRIANGULAR 2-SEGMENT FOOT
% -FORCE RELATIONSHIP TO BE REPLACED IN FORTRAN CODE

%---------------------------------------------------------------------
% PHYSICAL DECLARATION

NEWTONIAN N
FRAMES T                                        % TRIANGULAR FOOT
BODIES A,B,C,D,E,F,G
POINTS CM,O,P1,P2,P3,P4,P5,P6,P7,P8,P9,P10

AUTOZ ON

%---------------------------------------------------------------------
% MATHEMATICAL DECLARATION

MASS      A=MA,B=MB,C=MC,D=MD,E=ME,F=MF,G=MG

INERTIA   A,0,0,IA
INERTIA   B,0,0,IB
INERTIA   C,0,0,IC
INERTIA   D,0,0,ID
INERTIA   E,0,0,IE
INERTIA   F,0,0,IF
INERTIA   G,0,0,IG
SPECIFIED QBAL'',QANK'',QKNE'',QHIP'',QSHO'',QELB'',&
          TBAL,TANK,TKNE,THIP,TSHO,TELB,&      % TORQUE
          RX{3},RZ{3}                          % REACTION FORCES

CONSTANTS THETA,G,&                  % TRIANGULAR FOOT ANGLE,GRAVITY
          L{18}                               % LENGTHS
VARIABLES Q{3}',U{9}'                         % DEGREES OF FREEDOM
VARIABLES POAOX,POAOZ,POBOX,POBOZ,POCOX,POCOZ,PODOX,PODOZ,&
          POEOX,POEOZ,POP1X,POP1Z,POP10X,POP10Z,&
          POP2X,POP2Z,POP3X,POP3Z,POP4X,POP4Z,POP5X,POP5Z,&
          POP6X,POP6Z,POP7X,POP7Z,POP8X,POP8Z,POP9X,POP9Z
VARIABLES VOAOX,VOAOZ,VOBOX,VOBOZ,VOCOX,VOCOZ,VODOX,VODOZ,&
          VOEOX,VOEOZ,VOP1X,VOP1Z,VOP10X,VOP10Z,&
          VOP2X,VOP2Z,VOP3X,VOP3Z,VOP4X,VOP4Z,VOP5X,VOP5Z,&
          VOP6X,VOP6Z,VOP7X,VOP7Z,VOP8X,VOP8Z,VOP9X,VOP9Z
VARIABLES AOP1X,AOP1Z,AOP2X,AOP2Z,AOP4X,AOP4Z
VARIABLES POCMX,POCMZ,VOCMX,VOCMZ,AOCMX,AOCMZ,&
          KET,KECM,KEA,KEB,KEC,KED,KEE,KEF,KEG,&
          PET,PECM,PEA,PEB,PEC,PED,PEE,PEF,PEG,&
          M,ANGMOM,HORMOM,VERMOM

ZEE_NOT = [RX1,RX2,RX3,RZ1,RZ2,RZ3,TBAL,TANK,TKNE,THIP,TSHO,TELB]

M = MA + MB + MC + MD + ME + MF + MG

QBAL = T^3             % CALL JANGLES IN .F FILE FOR ANGLE VEL AND
QANK = T^3             % ACC TO OVER-WRITE THE Q VALUES HERE
QKNE = T^3
QHIP = T^3
QSHO = T^3
QELB = T^3

%---------------------------------------------------------------------
% GEOMETRICAL RELATION

SIMPROT(N,E,3,Q3)                               % TRUNK/HORIZONTAL
SIMPROT(D,E,3,QHIP)                             % TRUNK/THIGH
SIMPROT(D,C,3,QKNE)                             % THIGH/SHANK
SIMPROT(B,C,3,QANK)                             % SHANK/FOOT
SIMPROT(A,B,3,QBAL)                             % FOOT/TOES
```

```
SIMPROT(B,T,3,THETA)                              % FIXED TRIANGULAR FOOT
SIMPROT(E,F,3,QSHO)                               % TRUNK/UPPER ARM
SIMPROT(G,F,3,QELB)                               % UPPER ARM/FOREARM


%-------------------------------------------------------------------
% POSITION

P_O_P1> = Q1*N1> + Q2*N2>
P_P1_AO> = (L1-L2)*A1>
P_P1_P2> = L1*A1>
P_P2_P3> = -L3*B1>
P_P3_BO> = L4*B1> - L5*B2>
P_P3_P4> = -L6*T1> - L7*T2>
P_P3_CO> = (L8-L9)*C1>
P_P3_P5> = L8*C1>
P_P5_DO> = -(L10-L11)*D1>
P_P5_P6> = -L10*D1>
P_P6_EO> = L13*E1>
P_P6_P7> = L12*E1>
P_P6_P8> = L14*E1>
P_P8_FO> = -L16*F1>
P_P8_P9> = -L15*F1>
P_P9_GO> = L18*G1>
P_P9_P10> = L17*G1>
P_O_AO> = P_O_P1> + P_P1_AO>
P_O_P2> = P_O_P1> + P_P1_P2>
P_O_BO> = P_O_P2> + P_P2_BO>
P_O_P3> = P_O_P2> + P_P2_P3>
P_O_P4> = P_O_P3> + P_P3_P4>
P_O_CO> = P_O_P3> + P_P3_CO>
P_O_P5> = P_O_P3> + P_P3_P5>
P_O_DO> = P_O_P5> + P_P5_DO>
P_O_P6> = P_O_P5> + P_P5_P6>
P_O_EO> = P_O_P6> + P_P6_EO>
P_O_P7> = P_O_P6> + P_P6_P7>
P_O_P8> = P_O_P6> + P_P6_P8>
P_O_FO> = P_O_P8> + P_P8_FO>
P_O_P9> = P_O_P8> + P_P8_P9>
P_O_GO> = P_O_P9> + P_P9_GO>
P_O_P10> = P_O_P9> + P_P9_P10>

P_O_CM> = CM(O)

POP1X = DOT(P_O_P1>,N1>)
POP1Z = DOT(P_O_P1>,N2>)
POP2X = DOT(P_O_P2>,N1>)
POP2Z = DOT(P_O_P2>,N2>)
POP3X = DOT(P_O_P3>,N1>)
POP3Z = DOT(P_O_P3>,N2>)
POP4X = DOT(P_O_P4>,N1>)
POP4Z = DOT(P_O_P4>,N2>)
POP5X = DOT(P_O_P5>,N1>)
POP5Z = DOT(P_O_P5>,N2>)
POP6X = DOT(P_O_P6>,N1>)
POP6Z = DOT(P_O_P6>,N2>)
POP7X = DOT(P_O_P7>,N1>)
POP7Z = DOT(P_O_P7>,N2>)
POP8X = DOT(P_O_P8>,N1>)
POP8Z = DOT(P_O_P8>,N2>)
POP9X = DOT(P_O_P9>,N1>)
POP9Z = DOT(P_O_P9>,N2>)
POP10X = DOT(P_O_P10>,N1>)
POP10Z = DOT(P_O_P10>,N2>)
POAOX = DOT(P_O_AO>,N1>)
POAOZ = DOT(P_O_AO>,N2>)
POBOX = DOT(P_O_BO>,N1>)
POBOZ = DOT(P_O_BO>,N2>)
POCOX = DOT(P_O_CO>,N1>)
```

```
POCOZ = DOT(P_O_CO>,N2>)
PODOX = DOT(P_O_DO>,N1>)
PODOZ = DOT(P_O_DO>,N2>)
POEOX = DOT(P_O_EO>,N1>)
POEOZ = DOT(P_O_EO>,N2>)
POFOX = DOT(P_O_FO>,N1>)
POFOZ = DOT(P_O_FO>,N2>)
POGOX = DOT(P_O_GO>,N1>)
POGOZ = DOT(P_O_GO>,N2>)
POCMX = DOT(P_O_CM>,N1>)
POCMZ = DOT(P_O_CM>,N2>)


%----------------------------------------------------------------------
% KINEMATICAL DIFFERENTIAL EQUATIONS

Q1' = U1
Q2' = U2
Q3' = U3


%----------------------------------------------------------------------
% ANGULAR VELOCITY & ACCELERATIONS

W_E_N> = U3*E3>
W_E_D> = QHIP'*E3> + U4*E3>
W_C_D> = QKNE'*C3> + U5*C3>
W_C_B> = QANK'*C3> + U6*C3>
W_B_A> = QBAL'*B3> + U7*B3>
W_T_B> = 0>
W_F_E> = QSHO'*F3> + U8*F3>
W_F_G> = QELB'*F3> + U9*F3>

ALF_E_N> = U3'*E3>
ALF_E_D> = QHIP''*E3>
ALF_C_D> = QKNE''*C3>
ALF_C_B> = QANK''*C3>
ALF_B_A> = QBAL''*B3>
ALF_T_B> = 0>
ALF_F_E> = QSHO''*F3>
ALF_F_G> = QELB''*F3>


%----------------------------------------------------------------------
% LINEAR VELOCITY

V_O_N> = 0>
V_P1_N> = DT(P_O_P1>,N)
V2PTS(N,A,P1,AO)
V2PTS(N,A,P1,P2)
V2PTS(N,B,P2,BO)
V2PTS(N,B,P2,P3)
V2PTS(N,T,P3,P4)
V2PTS(N,C,P3,CO)
V2PTS(N,C,P3,P5)
V2PTS(N,D,P5,DO)
V2PTS(N,D,P5,P6)
V2PTS(N,E,P6,EO)
V2PTS(N,E,P6,P7)
V2PTS(N,E,P6,P8)
V2PTS(N,F,P8,FO)
V2PTS(N,F,P8,P9)
V2PTS(N,G,P8,GO)
V2PTS(N,G,P8,P10)
V_CM_N> = DT(P_O_CM>,N)

VOP1X = DOT(V_P1_N>,N1>)
VOP1Z = DOT(V_P1_N>,N2>)
VOP2X = DOT(V_P2_N>,N1>)
VOP2Z = DOT(V_P2_N>,N2>)
VOP3X = DOT(V_P3_N>,N1>)
```

180

```
VOP3Z = DOT(V_P3_N>,N2>)
VOP4X = DOT(V_P4_N>,N1>)
VOP4Z = DOT(V_P4_N>,N2>)
VOP5X = DOT(V_P5_N>,N1>)
VOP5Z = DOT(V_P5_N>,N2>)
VOP6X = DOT(V_P6_N>,N1>)
VOP6Z = DOT(V_P6_N>,N2>)
VOP7X = DOT(V_P7_N>,N1>)
VOP7Z = DOT(V_P7_N>,N2>)
VOP8X = DOT(V_P8_N>,N1>)
VOP8Z = DOT(V_P8_N>,N2>)
VOP9X = DOT(V_P9_N>,N1>)
VOP9Z = DOT(V_P9_N>,N2>)
VOP10X = DOT(V_P10_N>,N1>)
VOP10Z = DOT(V_P10_N>,N2>)
VOAOX = DOT(V_AO_N>,N1>)
VOAOZ = DOT(V_AO_N>,N2>)
VOBOX = DOT(V_BO_N>,N1>)
VOBOZ = DOT(V_BO_N>,N2>)
VOCOX = DOT(V_CO_N>,N1>)
VOCOZ = DOT(V_CO_N>,N2>)
VODOX = DOT(V_DO_N>,N1>)
VODOZ = DOT(V_DO_N>,N2>)
VOEOX = DOT(V_EO_N>,N1>)
VOEOZ = DOT(V_EO_N>,N2>)
VOFOX = DOT(V_FO_N>,N1>)
VOFOZ = DOT(V_FO_N>,N2>)
VOGOX = DOT(V_GO_N>,N1>)
VOGOZ = DOT(V_GO_N>,N2>)
VOCMX = DOT(V_CM_N>,N1>)
VOCMZ = DOT(V_CM_N>,N2>)


%------------------------------------------------------------------
% LINEAR ACCELERATION

A_O_N> = 0>
A_P1_N> = DT(V_P1_N>,N)
A_P2_N> = DT(V_P2_N>,N)
A_P3_N> = DT(V_P3_N>,N)
A_P4_N> = DT(V_P4_N>,N)
A_P5_N> = DT(V_P5_N>,N)
A_P6_N> = DT(V_P6_N>,N)
A_P7_N> = DT(V_P7_N>,N)
A_P8_N> = DT(V_P8_N>,N)
A_P9_N> = DT(V_P9_N>,N)
A_P10_N> = DT(V_P10_N>,N)
A_AO_N> = DT(V_AO_N>,N)
A_BO_N> = DT(V_BO_N>,N)
A_CO_N> = DT(V_CO_N>,N)
A_DO_N> = DT(V_DO_N>,N)
A_EO_N> = DT(V_EO_N>,N)
A_FO_N> = DT(V_FO_N>,N)
A_GO_N> = DT(V_GO_N>,N)
A_CM_N> = DT(V_CM_N>,N)

AOP1X = DOT(A_P1_N>,N1>)
AOP1Z = DOT(A_P1_N>,N2>)
AOP2X = DOT(A_P2_N>,N1>)
AOP2Z = DOT(A_P2_N>,N2>)
AOP4X = DOT(A_P4_N>,N1>)
AOP4Z = DOT(A_P4_N>,N2>)
AOCMX = DOT(A_CM_N>,N1>)
AOCMZ = DOT(A_CM_N>,N2>)


%------------------------------------------------------------------
% AUXILIARY CONSTRAIN

AUXILIARY[1] = U4
```

```
AUXILIARY[2] = U5
AUXILIARY[3] = U6
AUXILIARY[4] = U7
AUXILIARY[5] = U8
AUXILIARY[6] = U9
CONSTRAIN (AUXILIARY[U4,U5,U6,U7,U8,U9])

%----------------------------------------------------------------------
% ENERGY

KEA = KE(A)
KEB = KE(B)
KEC = KE(C)
KED = KE(D)
KEE = KE(E)
KEF = KE(F)
KEG = KE(G)
KECM = KE(A,B,C,D,E,F,G)

PEA = -MA*G*POAOZ
PEB = -MB*G*POBOZ
PEC = -MC*G*POCOZ
PED = -MD*G*PODOZ
PEE = -ME*G*POEOZ
PEF = -MF*G*POFOZ
PEG = -MG*G*POGOZ
PECM = -M*G*POCMZ

%----------------------------------------------------------------------
% ANGULAR & LINEAR MOMENTUM

AMOM> = MOMENTUM(ANGULAR,CM)
ANGMOM = DOT(AMOM>,N3>)

LMOM> = MOMENTUM(LINEAR)
HORMOM = DOT(LMOM>,N1>)
VERMOM = DOT(LMOM>,N2>)

%----------------------------------------------------------------------
% FORCES

GRAVITY(G*N2>)

FORCE(P1,RX1*N1> + RZ1*N2>)
FORCE(P2,RX2*N1> + RZ2*N2>)
FORCE(P4,RX3*N1> + RZ3*N2>)

TORQUE(B/A,TBAL*N3>)
TORQUE(C/B,TANK*N3>)
TORQUE(C/D,TKNE*N3>)
TORQUE(E/D,THIP*N3>)
TORQUE(F/E,TSHO*N3>)
TORQUE(F/G,TELB*N3>)

%----------------------------------------------------------------------
% EQUATIONS OF MOTION

ZERO = FR() + FRSTAR()

KANE(TBAL,TANK,TKNE,THIP,TSHO,TELB)

%----------------------------------------------------------------------
% INPUTS

INPUT TINITIAL=0.0,TFINAL=1.0,INTEGSTP=0.001,PRINTINT=100
INPUT ABSERR=1.0E-08,RELERR=1.0E-07
INPUT G=-9.806,THETA=32.543
INPUT MA=0.2762,MB=1.5878,MC=7.7935,MD=14.9787,ME=29.2589,&
```

```
      MF=3.2917,MG=3.1395
INPUT Q1=0,Q2=0,Q3=90,U1=0,U2=5,U3=0
INPUT L1=0.0650,L2=0.0283,L3=0.1450,L4=0.0608,L5=0.0171,L6=0.048,&
      L7=0.078,L8=0.4065,L9=0.1711,L10=0.371,L11=0.1648,L12=0.8650,&
      L13=0.3827,L14=0.5650,L15=0.2450,L16=0.1118,&
      L17=0.4255,L18=0.1618
INPUT IA=0.0002,IB=0.0033,IC=0.0996,ID=0.1786,IE=1.5544,&
      IF=0.0184,IG=0.0408


%----------------------------------------------------------------------
% OUTPUTS

OUTPUT T,POP1X,POP1Z,POP2X,POP2Z,POP3X,POP3Z,POP4X,POP4Z,&
         POP5X,POP5Z,POP6X,POP6Z,POP7X,POP7Z,POP8X,POP8Z,&
         POP9X,POP9Z,POP10X,POP10Z,POCMX,POCMZ
OUTPUT T,VOP1X,VOP1Z,VOP2X,VOP2Z,VOP3X,VOP3Z,VOP4X,VOP4Z,&
         VOP5X,VOP5Z,VOP6X,VOP6Z,VOP7X,VOP7Z,VOP8X,VOP8Z,&
         VOP9X,VOP9Z,VOP10X,VOP10Z
OUTPUT T,POCMX,POCMZ,VOCMX,VOCMZ,AOCMX,AOCMZ
OUTPUT T,Q3,QBAL,QANK,QKNE,QHIP,QSHO,QELB
OUTPUT T,U3,QBAL',QANK',QKNE',QHIP',QSHO',QELB'
OUTPUT T,U3',QBAL'',QANK'',QKNE'',QHIP'',QSHO'',QELB''
OUTPUT T,TBAL,TANK,TKNE,THIP,TSHO,TELB
OUTPUT T,RX1,RZ1,RX2,RZ2,RX3,RZ3
OUTPUT T,HORMOM,VERMOM,ANGMOM
OUTPUT T,KECM,KEA,KEB,KEC,KED,KEE,KEF,KEG
OUTPUT T,PECM,PEA,PEB,PEC,PED,PEE,PEF,PEG


%----------------------------------------------------------------------
% UNITS

UNITS T=S,[M,MA,MB,MC,MD,ME,MF,MG]=KG
UNITS [IA,IB,IC,ID,IE,IF,IG]=KGM^2
UNITS [Q3,QBAL,QANK,QKNE,QHIP,QSHO,QELB,THETA]=RAD
UNITS [U3,QBAL',QANK',QKNE',QHIP',QSHO',QELB']=RAD/S
UNITS [U3',QBAL'',QANK'',QKNE'',QHIP'',QSHO'',QELB'']=RAD/S^2
UNITS [Q1,Q2,L1,L2,L3,L4,L5,L6,L7,L8,L9,L10,L11]=M
UNITS [L12,L13,L14,L15,L16,L17,L18]=M
UNITS [POP1X,POP1Z,POP2X,POP2Z,POP3X,POP3Z,POP4X,POP4Z]=M
UNITS [POP5X,POP5Z,POP6X,POP6Z,POP7X,POP7Z,POP8X,POP8Z]=M
UNITS [POP9X,POP9Z,POP10X,POP10Z,POCMX,POCMZ]=M
UNITS [VOP1X,VOP1Z,VOP2X,VOP2Z,VOP3X,VOP3Z,VOP4X,VOP4Z]=M/S
UNITS [VOP5X,VOP5Z,VOP6X,VOP6Z,VOP7X,VOP7Z,VOP8X,VOP8Z]=M/S
UNITS [VOP9X,VOP9Z,VOP10X,VOP10Z,VOCMX,VOCMZ,U1,U2]=M/S
UNITS [U1',U2',AOCMX,AOCMZ,G]=M/S^2
UNITS [RX1,RX2,RX3,RZ1,RZ2,RZ3]=N
UNITS [TBAL,TANK,TKNE,THIP,TSHO,TELB]=NM
UNITS ANGMOM=KGM^2/S,[HORMOM,VERMOM]=KGM/S
UNITS [KECM,KEA,KEB,KEC,KED,KEE,KEF,KEG]=J
UNITS [PECM,PEA,PEB,PEC,PED,PEE,PEF,PEG]=J


%----------------------------------------------------------------------

SAVE TRAMP_ANG.ALL

CODE DYNAMICS() TRAMP_ANG.F, SUBS

%----------------------------------------------------------------------
% END END END END END END END END END END END END END
%----------------------------------------------------------------------
```

```
% TRAMPTQ.AL

% TORQUE-DRIVEN 7-SEGMENT MODEL OF A TRAMPOLINE TAKEOFF
% -TRIANGULAR 2-SEGMENT FOOT
% -FORCE RELATIONSHIP TO BE REPLACED IN FORTRAN CODE
% -JOINT TORQUES TO BE CALCULATED IN FORTRAN CODE

%-------------------------------------------------------------------
% PHYSICAL DECLARATION

NEWTONIAN N
FRAMES T                                        % TRIANGULAR FOOT
BODIES A,B,C,D,E,F,G
POINTS CM,O,P1,P2,P3,P4,P5,P6,P7,P8,P9,P10

AUTOZ ON

%-------------------------------------------------------------------
% MATHEMATICAL DECLARATION

MASS      A=MA,B=MB,C=MC,D=MD,E=ME,F=MF,G=MG
INERTIA   A,0,0,IA
INERTIA   B,0,0,IB
INERTIA   C,0,0,IC
INERTIA   D,0,0,ID
INERTIA   E,0,0,IE
INERTIA   F,0,0,IF
INERTIA   G,0,0,IG
SPECIFIED TBAL,TANK,TKNE,THIP,TSHO,TELB,&       % TORQUE
          RX{3},RZ{3}                           % REACTION FORCES
CONSTANTS THETA,G,&                   % TRIANGULAR FOOT ANGLE,GRAVITY
          L{18}                               % LENGTHS
VARIABLES Q{9}'                               % DEGREES OF FREEDOM
VARIABLES U{9}'
VARIABLES POAOX,POAOZ,POBOX,POBOZ,POCOX,POCOZ,PODOX,PODOZ,&
          POEOX,POEOZ,POFOX,POFOZ,POGOX,POGOZ,POP1X,POP1Z,&
          POP2X,POP2Z,POP3X,POP3Z,POP4X,POP4Z,POP5X,POP5Z,&
          POP6X,POP6Z,POP7X,POP7Z,POP8X,POP8Z,POP9X,POP9Z,&
          POP10X,POP10Z
VARIABLES VOAOX,VOAOZ,VOBOX,VOBOZ,VOCOX,VOCOZ,VODOX,VODOZ,&
          VOEOX,VOEOZ,VOFOX,VOFOZ,VOGOX,VOGOZ,VOP1X,VOP1Z,&
          VOP2X,VOP2Z,VOP3X,VOP3Z,VOP4X,VOP4Z,VOP5X,VOP5Z,&
          VOP6X,VOP6Z,VOP7X,VOP7Z,VOP8X,VOP8Z,VOP9X,VOP9Z,&
          VOP10X,VOP10Z
VARIABLES POCMX,POCMZ,VOCMX,VOCMZ,AOCMX,AOCMZ,&
          KET,KECM,KEA,KEB,KEC,KED,KEE,KEF,KEG,&
          PET,PECM,PEA,PEB,PEC,PED,PEE,PEF,PEG,&
          M,ANGMOM,HORMOM,VERMOM

ZEE_NOT = [RX1,RX2,RX3,RZ1,RZ2,RZ3]

M = MA + MB + MC + MD + ME + MF + MG

%-------------------------------------------------------------------
% GEOMETRICAL RELATION

SIMPROT(N,E,3,Q3)                               % TRUNK/HORIZONTAL
SIMPROT(D,E,3,Q7)                               % TRUNK/THIGH
SIMPROT(D,C,3,Q6)                               % THIGH/SHANK
SIMPROT(B,C,3,Q5)                               % SHANK/FOOT
SIMPROT(A,B,3,Q4)                               % FOOT/TOES
SIMPROT(B,T,3,THETA)                            % FIXED TRIANGULAR FOOT
SIMPROT(E,F,3,Q8)                               % TRUNK/UPPER ARM
SIMPROT(G,F,3,Q9)                               % UPPER ARM/FOREARM
```

```
%-------------------------------------------------------------------
% POSITION

P_O_P1> = Q1*N1> + Q2*N2>
P_P1_AO> = (L1-L2)*A1>
P_P1_P2> = L1*A1>
P_P2_P3> = -L3*B1>
P_P3_BO> = L4*B1> - L5*B2>
P_P3_P4> = -L6*T1> - L7*T2>
P_P3_CO> = (L8-L9)*C1>
P_P3_P5> = L8*C1>
P_P5_DO> = -(L10-L11)*D1>
P_P5_P6> = -L10*D1>
P_P6_EO> = L13*E1>
P_P6_P7> = L12*E1>
P_P6_P8> = L14*E1>
P_P8_FO> = -L16*F1>
P_P8_P9> = -L15*F1>
P_P9_GO> = L18*G1>
P_P9_P10> = L17*G1>
P_O_AO> = P_O_P1> + P_P1_AO>
P_O_P2> = P_O_P1> + P_P1_P2>
P_O_BO> = P_O_P2> + P_P2_BO>
P_O_P3> = P_O_P2> + P_P2_P3>
P_O_P4> = P_O_P3> + P_P3_P4>
P_O_CO> = P_O_P3> + P_P3_CO>
P_O_P5> = P_O_P3> + P_P3_P5>
P_O_DO> = P_O_P5> + P_P5_DO>
P_O_P6> = P_O_P5> + P_P5_P6>
P_O_EO> = P_O_P6> + P_P6_EO>
P_O_P7> = P_O_P6> + P_P6_P7>
P_O_P8> = P_O_P6> + P_P6_P8>
P_O_FO> = P_O_P8> + P_P8_EO>
P_O_P9> = P_O_P8> + P_P8_P9>
P_O_GO> = P_O_P9> + P_P9_GO>
P_O_P10> = P_O_P9> + P_P9_P10>

P_O_CM> = CM(O)

POP1X = DOT(P_O_P1>,N1>)
POP1Z = DOT(P_O_P1>,N2>)
POP2X = DOT(P_O_P2>,N1>)
POP2Z = DOT(P_O_P2>,N2>)
POP3X = DOT(P_O_P3>,N1>)
POP3Z = DOT(P_O_P3>,N2>)
POP4X = DOT(P_O_P4>,N1>)
POP4Z = DOT(P_O_P4>,N2>)
POP5X = DOT(P_O_P5>,N1>)
POP5Z = DOT(P_O_P5>,N2>)
POP6X = DOT(P_O_P6>,N1>)
POP6Z = DOT(P_O_P6>,N2>)
POP7X = DOT(P_O_P7>,N1>)
POP7Z = DOT(P_O_P7>,N2>)
POP8X = DOT(P_O_P8>,N1>)
POP8Z = DOT(P_O_P8>,N2>)
POP9X = DOT(P_O_P9>,N1>)
POP9Z = DOT(P_O_P9>,N2>)
POP10X = DOT(P_O_P10>,N1>)
POP10Z = DOT(P_O_P10>,N2>)
POAOX = DOT(P_O_AO>,N1>)
POAOZ = DOT(P_O_AO>,N2>)
POBOX = DOT(P_O_BO>,N1>)
POBOZ = DOT(P_O_BO>,N2>)
POCOX = DOT(P_O_CO>,N1>)
POCOZ = DOT(P_O_CO>,N2>)
```

```
PODOX = DOT(P_O_DO>,N1>)
PODOZ = DOT(P_O_DO>,N2>)
POEOX = DOT(P_O_EO>,N1>)
POEOZ = DOT(P_O_EO>,N2>)
POFOX = DOT(P_O_FO>,N1>)
POFOZ = DOT(P_O_FO>,N2>)
POGOX = DOT(P_O_GO>,N1>)
POGOZ = DOT(P_O_GO>,N2>)
POCMX = DOT(P_O_CM>,N1>)
POCMZ = DOT(P_O_CM>,N2>)

%----------------------------------------------------------------------
% KINEMATICAL DIFFERENTIAL EQUATIONS

Q1' = U1
Q2' = U2
Q3' = U3
Q4' = U4
Q5' = U5
Q6' = U6
Q7' = U7
Q8' = U8
Q9' = U9


%----------------------------------------------------------------------
% ANGULAR VELOCITY & ACCELERATIONS

W_E_N> = U3*E3>
W_E_D> = U7*E3>
W_C_D> = U6*C3>
W_C_B> = U5*C3>
W_B_A> = U4*B3>
W_F_E> = U8*F3>
W_F_G> = U9*F3>
W_T_B> = 0>

ALF_E_N> = U3'*E3>
ALF_E_D> = U7'*E3>
ALF_C_D> = U6'*C3>
ALF_C_B> = U5'*C3>
ALF_B_A> = U4'*B3>
ALF_F_E> = U8'*F3>
ALF_F_G> = U9'*F3>
ALF_T_B> = 0>

%----------------------------------------------------------------------
% LINEAR VELOCITY

V_O_N> = 0>
V_P1_N> = DT(P_O_P1>,N)
V2PTS(N,A,P1,AO)
V2PTS(N,A,P1,P2)
V2PTS(N,B,P2,BO)
V2PTS(N,B,P2,P3)
V2PTS(N,T,P3,P4)
V2PTS(N,C,P3,CO)
V2PTS(N,C,P3,P5)
V2PTS(N,D,P5,DO)
V2PTS(N,D,P5,P6)
V2PTS(N,E,P6,EO)
V2PTS(N,E,P6,P7)
V2PTS(N,E,P6,P8)
V2PTS(N,F,P8,FO)
V2PTS(N,F,P8,P9)
V2PTS(N,G,P9,GO)
```

186

```
V2PTS(N,G,P9,P10)
V_CM_N> = DT(P_O_CM>,N)

VOP1X = DOT(V_P1_N>,N1>)
VOP1Z = DOT(V_P1_N>,N2>)
VOP2X = DOT(V_P2_N>,N1>)
VOP2Z = DOT(V_P2_N>,N2>)
VOP3X = DOT(V_P3_N>,N1>)
VOP3Z = DOT(V_P3_N>,N2>)
VOP4X = DOT(V_P4_N>,N1>)
VOP4Z = DOT(V_P4_N>,N2>)
VOP5X = DOT(V_P5_N>,N1>)
VOP5Z = DOT(V_P5_N>,N2>)
VOP6X = DOT(V_P6_N>,N1>)
VOP6Z = DOT(V_P6_N>,N2>)
VOP7X = DOT(V_P7_N>,N1>)
VOP7Z = DOT(V_P7_N>,N2>)
VOP8X = DOT(V_P8_N>,N1>)
VOP8Z = DOT(V_P8_N>,N2>)
VOP9X = DOT(V_P9_N>,N1>)
VOP9Z = DOT(V_P9_N>,N2>)
VOP10X = DOT(V_P10_N>,N1>)
VOP10Z = DOT(V_P10_N>,N2>)
VOAOX = DOT(V_AO_N>,N1>)
VOAOZ = DOT(V_AO_N>,N2>)
VOBOX = DOT(V_BO_N>,N1>)
VOBOZ = DOT(V_BO_N>,N2>)
VOCOX = DOT(V_CO_N>,N1>)
VOCOZ = DOT(V_CO_N>,N2>)
VODOX = DOT(V_DO_N>,N1>)
VODOZ = DOT(V_DO_N>,N2>)
VOEOX = DOT(V_EO_N>,N1>)
VOEOZ = DOT(V_EO_N>,N2>)
VOFOX = DOT(V_FO_N>,N1>)
VOFOZ = DOT(V_FO_N>,N2>)
VOGOX = DOT(V_GO_N>,N1>)
VOGOZ = DOT(V_GO_N>,N2>)
VOCMX = DOT(V_CM_N>,N1>)
VOCMZ = DOT(V_CM_N>,N2>)

%-----------------------------------------------------------------
% LINEAR ACCELERATION

A_O_N> = 0>
A_P1_N> = DT(V_P1_N>,N)
A_P2_N> = DT(V_P2_N>,N)
A_P3_N> = DT(V_P3_N>,N)
A_P4_N> = DT(V_P4_N>,N)
A_P5_N> = DT(V_P5_N>,N)
A_P6_N> = DT(V_P6_N>,N)
A_P7_N> = DT(V_P7_N>,N)
A_P8_N> = DT(V_P8_N>,N)
A_P9_N> = DT(V_P9_N>,N)
A_P10_N> = DT(V_P10_N>,N)
A_AO_N> = DT(V_AO_N>,N)
A_BO_N> = DT(V_BO_N>,N)
A_CO_N> = DT(V_CO_N>,N)
A_DO_N> = DT(V_DO_N>,N)
A_EO_N> = DT(V_EO_N>,N)
A_FO_N> = DT(V_FO_N>,N)
A_GO_N> = DT(V_GO_N>,N)
A_CM_N> = DT(V_CM_N>,N)

AOP1X = DOT(A_P1_N>,N1>)
AOP1Z = DOT(A_P1_N>,N2>)
```

```
AOP2X = DOT(A_P2_N>,N1>)
AOP2Z = DOT(A_P2_N>,N2>)
AOP4X = DOT(A_P4_N>,N1>)
AOP4Z = DOT(A_P4_N>,N2>)
AOCMX = DOT(A_CM_N>,N1>)
AOCMZ = DOT(A_CM_N>,N2>)

%---------------------------------------------------------------------
% ENERGY

KEA = KE(A)
KEB = KE(B)
KEC = KE(C)
KED = KE(D)
KEE = KE(E)
KEF = KE(F)
KEG = KE(G)
KECM = KE(A,B,C,D,E,F,G)

PEA = -MA*G*POAOZ
PEB = -MB*G*POBOZ
PEC = -MC*G*POCOZ
PED = -MD*G*PODOZ
PEE = -ME*G*POEOZ
PEF = -MF*G*POFOZ
PEG = -MG*G*POGOZ
PECM = -M*G*POCMZ

%---------------------------------------------------------------------
% ANGULAR & LINEAR MOMENTUM

AMOM> = MOMENTUM(ANGULAR,CM)
ANGMOM = DOT(AMOM>,N3>)

LMOM> = MOMENTUM(LINEAR)
HORMOM = DOT(LMOM>,N1>)
VERMOM = DOT(LMOM>,N2>)

%---------------------------------------------------------------------
% FORCES

GRAVITY(G*N2>)

FORCE(P1,RX1*N1> + RZ1*N2>)
FORCE(P2,RX2*N1> + RZ2*N2>)
FORCE(P4,RX3*N1> + RZ3*N2>)

TBAL = T^3                    % CALL TORQUE SUBROUTINE TO OVERWRITE
TANK = T^3
TKNE = T^3
THIP = T^3
TSHO = T^3
TELB = T^3

TORQUE(B/A,TBAL*N3>)
TORQUE(C/B,TANK*N3>)
TORQUE(C/D,TKNE*N3>)
TORQUE(E/D,THIP*N3>)
TORQUE(F/E,TSHO*N3>)
TORQUE(F/G,TELB*N3>)

%---------------------------------------------------------------------
% EQUATIONS OF MOTION

ZERO = FR() + FRSTAR()
```

```
KANE ()

%---------------------------------------------------------------------
% INPUTS

INPUT TINITIAL=0.0,TFINAL=1.0,INTEGSTP=0.001,PRINTINT=100
INPUT ABSERR=1.0E-08,RELERR=1.0E-07
INPUT G=-9.806,THETA=32.543
INPUT MA=0.2762,MB=1.5878,MC=7.7935,MD=14.9787,ME=29.2589,&
      MF=3.2917,MG=3.1395
INPUT Q1=0,Q2=0,Q3=90,Q4=0,Q5=0,Q6=0,Q7=0,Q8=0,&
      U1=0,U2=5,U3=0,U4=0,U5=0,U6=0,U7=0,U8=0
INPUT L1=0.650,L2=0.0283,L3=0.1450,L4=0.0608,L5=0.0171,L6=0.048,&
      L7=0.078,L8=0.4065,L9=0.1711,L10=0.371,L11=0.1648,L12=0.8650,&
      L13=0.3827,L14=0.5650,L15=0.2450,L16=0.1118,&
      L17=0.4255,L18=0.1618
INPUT IA=0.0002,IB=0.0033,IC=0.0996,ID=0.1786,IE=1.5544,&
      IF=0.0184,IG=0.0408

%---------------------------------------------------------------------
% OUTPUTS

OUTPUT T,POP1X,POP1Z,POP2X,POP2Z,POP3X,POP3Z,POP4X,POP4Z,&
       POP5X,POP5Z,POP6X,POP6Z,POP7X,POP7Z,POP8X,POP8Z,&
       POP9X,POP9Z,POP10X,POP10Z,POCMX,POCMZ
OUTPUT T,VOP1X,VOP1Z,VOP2X,VOP2Z,VOP3X,VOP3Z,VOP4X,VOP4Z,&
       VOP5X,VOP5Z,VOP6X,VOP6Z,VOP7X,VOP7Z,VOP8X,VOP8Z,&
       VOP9X,VOP9Z,VOP10X,VOP10Z
OUTPUT T,POCMX,POCMZ,VOCMX,VOCMZ,AOCMX,AOCMZ
OUTPUT T,Q3,Q4,Q5,Q6,Q7,Q8,Q9
OUTPUT T,U3,U4,U5,U6,U7,U8,U9
OUTPUT T,U3',U4',U5',U6',U7',U8',Q9'
OUTPUT T,TBAL,TANK,TKNE,THIP,TSHO,TELB
OUTPUT T,RX1,RZ1,RX2,RZ2,RX3,RZ3
OUTPUT T,HORMOM,VERMOM,ANGMOM
OUTPUT T,KECM,KEA,KEB,KEC,KED,KEE,KEF,KEG
OUTPUT T,PECM,PEA,PEB,PEC,PED,PEE,PEF,PEG

%---------------------------------------------------------------------
% UNITS

UNITS T=S,[M,MA,MB,MC,MD,ME,MF,MG]=KG
UNITS [IA,IB,IC,ID,IE,IF,IG]=KGM^2
UNITS [Q3,Q4,Q5,Q6,Q7,Q8,Q9,THETA]=DEG
UNITS [U3,U4,U5,U6,U7,U8,U9']=RAD/S
UNITS [U3',U4',U5',U6',U7',U8',U9']=RAD/S^2
UNITS [Q1,Q2,L1,L2,L3,L4,L5,L6,L7,L8,L9,L10,L11]=M
UNITS [L12,L13,L14,L15,L16,L17,L18]=M
UNITS [POP1X,POP1Z,POP2X,POP2Z,POP3X,POP3Z,POP4X,POP4Z]=M
UNITS [POP5X,POP5Z,POP6X,POP6Z,POP7X,POP7Z,POP8X,POP8Z]=M
UNITS [POP9X,POP9Z,POP10X,POP10Z,POCMX,POCMZ]=M
UNITS [VOP1X,VOP1Z,VOP2X,VOP2Z,VOP3X,VOP3Z,VOP4X,VOP4Z]=M/S
UNITS [VOP5X,VOP5Z,VOP6X,VOP6Z,VOP7X,VOP7Z,VOP8X,VOP8Z]=M/S
UNITS [VOP9X,VOP9Z,VOP10X,VOP10Z,VOCMX,VOCMZ,U1,U2]=M/S
UNITS [U1',U2',AOCMX,AOCMZ,G]=M/S^2
UNITS [RX1,RX2,RX3,RZ1,RZ2,RZ3]=N
UNITS [TBAL,TANK,TKNE,THIP,TSHO,TELB]=NM
UNITS ANGMOM=KGM^2/S,[HORMOM,VERMOM]=KGM/S
UNITS [KECM,KEA,KEB,KEC,KED,KEE,KEF,KEG]=J
UNITS [PECM,PEA,PEB,PEC,PED,PEE,PEF,PEG]=J

%---------------------------------------------------------------------

SAVE TRAMPTQ.ALL
```

189

```
CODE DYNAMICS() TRAMPTQ.F, SUBS

%--------------------------------------------------------------------
% END END END END END END END END END END END END END
%--------------------------------------------------------------------
```

APPENDIX 4

Joint Torque Profiles from Angle-Driven Matching Simulations

4a. Metatarsal-phalangeal joint
4b. Ankle joint
4c. Knee joint
4d. Hip joint
4e. Shoulder joint
4f. Elbow joint

Legend

— S   Straight Jumping

— F1   Straight single forward somersault

— F2   Piked 1¾ forward somersault

— F3   Piked triffus

— B1   Piked single backward somersault

— B2   Straight single backward somersault

— B3   Piked double backward somersault

4a.
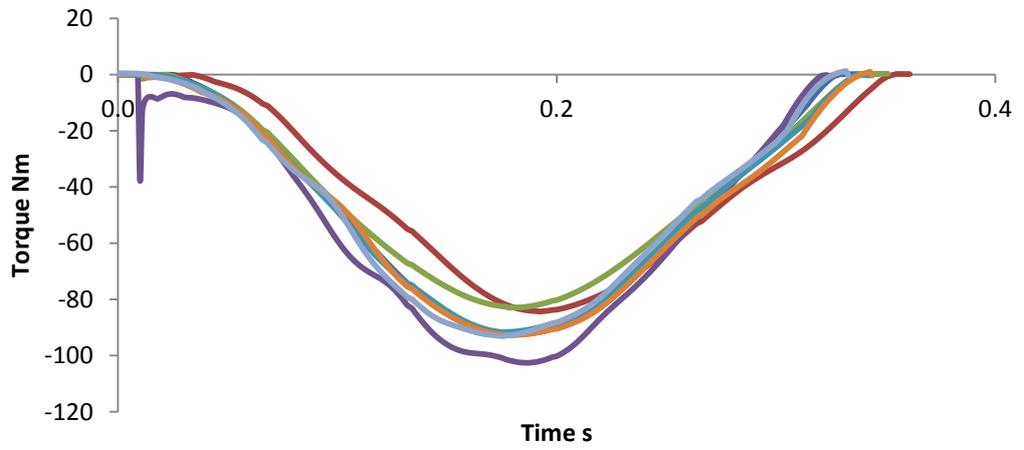
4b.
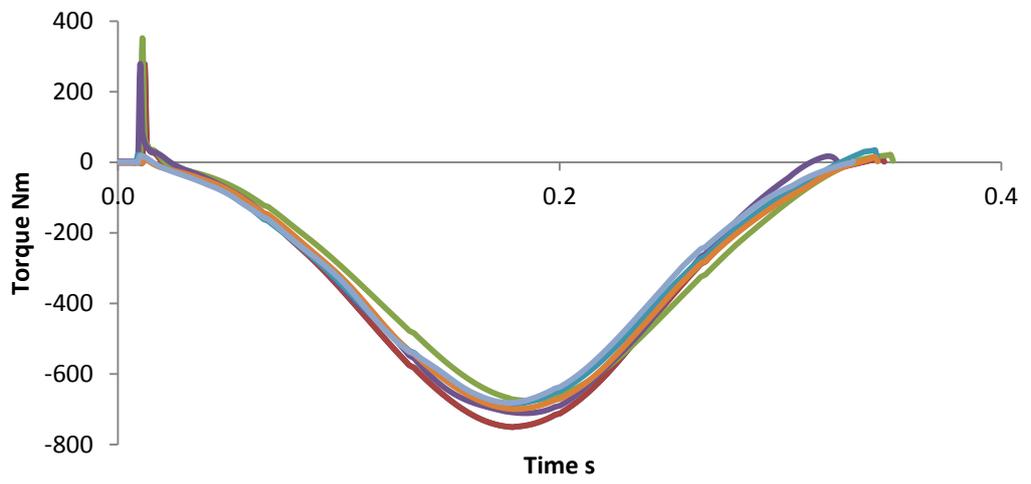
4c.
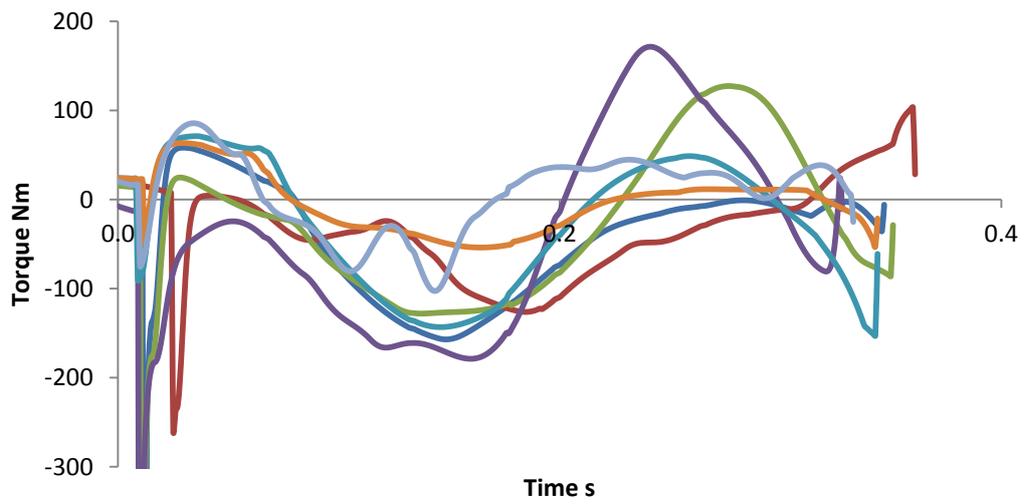
4d.
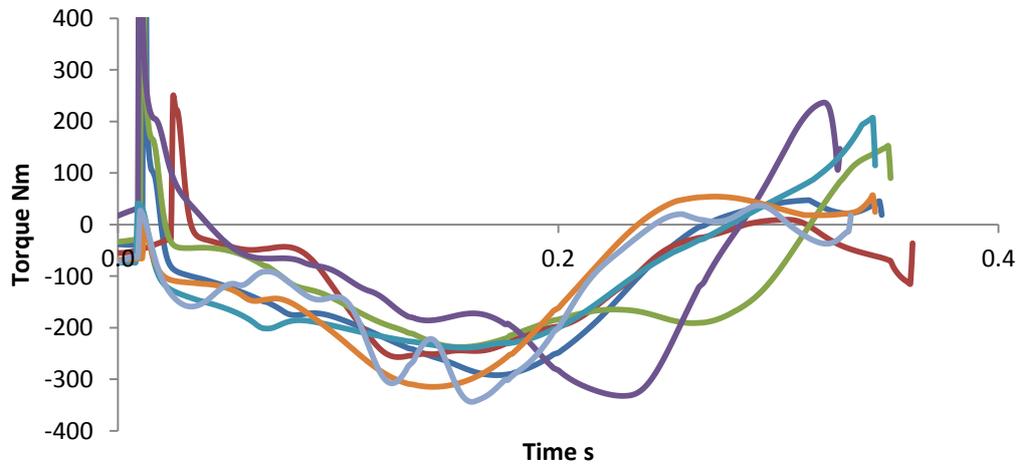
4e.
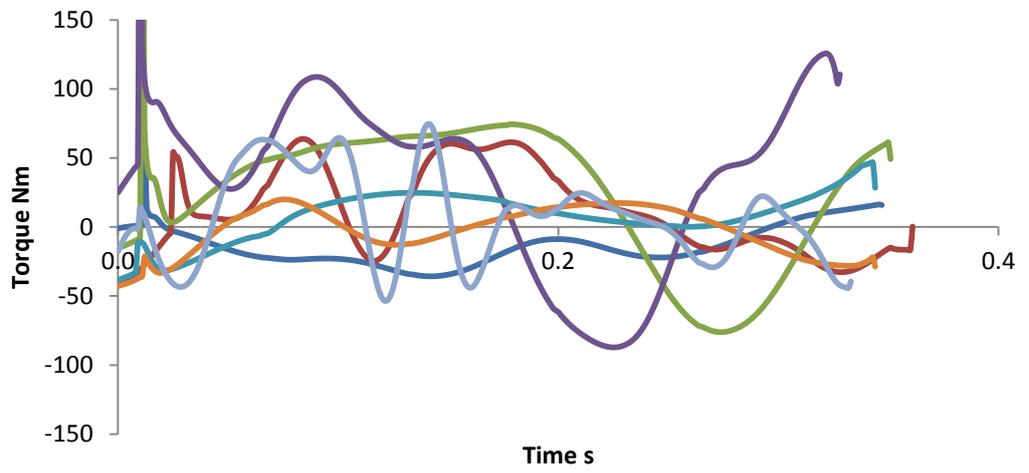
4f.
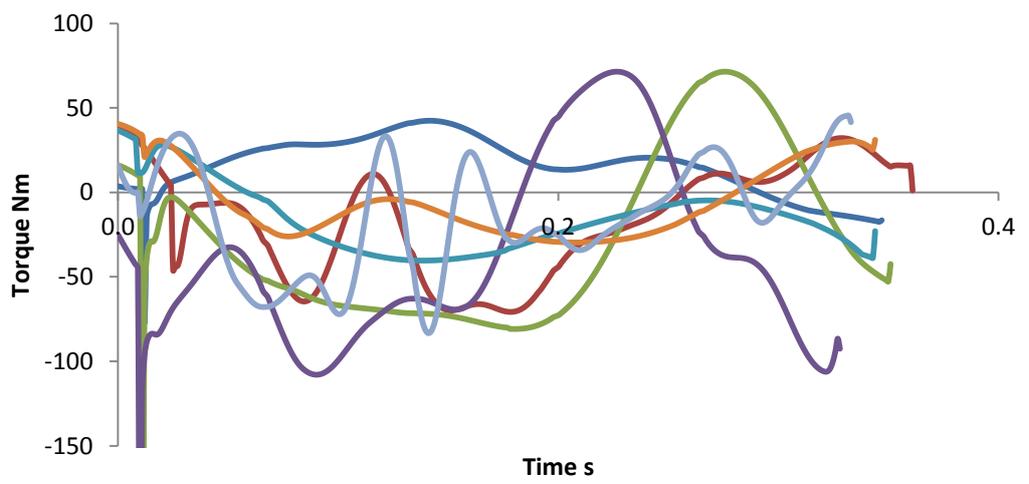
APPENDIX 5

Torque Generator Activation Parameters from Strength Scaling Torque-Driven Matching Simulations

5a. Straight front somersault, F_1
5b. Piked 1 ¾ front somersault, F_2
5c. Piked triffus, F_3

5a.

	A0	A1	A2	TS1	TR1	I	TR2
Ankle Plantar Flexion	0.049	1.000	0.330	-0.018	0.186	0.017	0.161
Ankle Dorsi Flexion	0.157	0.000	0.168	0.019	0.129	0.019	0.180
Knee Extension	0.102	1.000	0.192	0.017	0.109	0.097	0.145
Knee Flexion	0.307	0.047	0.475	-0.018	0.229	0.041	0.192
Hip Extension	0.043	1.000	0.250	-0.015	0.117	0.010	0.140
Hip Flexion	0.057	0.000	0.453	-0.020	0.130	0.009	0.176
Shoulder Flexion	0.297	0.792	0.115	-0.008	0.109	0.011	0.156
Shoulder Extension	0.341	0.170	0.916	-0.030	0.100	0.093	0.134

5b.

	A0	A1	A2	TS1	TR1	I	TR2
Ankle Plantar Flexion	0.142	1.000	0.544	0.004	0.194	0.000	0.125
Ankle Dorsi Flexion	0.458	0.000	0.419	-0.019	0.145	0.004	0.103
Knee Extension	0.142	1.000	0.292	0.020	0.139	0.063	0.189
Knee Flexion	0.427	0.224	0.183	-0.003	0.207	0.057	0.292
Hip Extension	0.059	1.000	0.266	-0.029	0.154	0.014	0.180
Hip Flexion	0.078	0.000	0.831	-0.009	0.128	0.007	0.155
Shoulder Flexion	0.201	0.902	0.075	-0.002	0.102	0.014	0.127
Shoulder Extension	0.232	0.079	0.741	-0.040	0.145	0.012	0.154

5c.

|	A0	A1	A2	TS1	TR1	I	TR2
Ankle Plantar Flexion	0.158	1.000	0.557	0.007	0.184	0.020	0.179
Ankle Dorsi Flexion	0.508	0.000	0.413	0.006	0.121	0.002	0.127
Knee Extension	0.158	1.000	0.202	-0.014	0.106	0.071	0.130
Knee Flexion	0.473	0.047	0.776	0.015	0.257	0.136	0.202
Hip Extension	0.066	1.000	0.001	0.010	0.116	0.015	0.102
Hip Flexion	0.089	0.000	0.958	0.000	0.150	0.100	0.103
Shoulder Flexion	0.191	0.503	0.144	-0.036	0.140	0.024	0.100
Shoulder Extension	0.220	0.156	0.615	-0.040	0.104	0.201	0.176

APPENDIX 6

Torque Generator Activation Parameters from Fixed Strength Torque-Driven Matching Simulations

6a. Straight front somersault, F_1
6b. Piked 1 ¾ front somersault, F_2
6c. Piked triffus, F_3

6a.

	A0	A1	A2	TS1	TR1	I	TR2
Ankle Plantar Flexion	0.024	0.591	0.577	-0.016	0.181	0.009	0.129
Ankle Dorsi Flexion	0.090	0.011	0.577	0.016	0.127	0.003	0.205
Knee Extension	0.081	0.810	0.062	0.018	0.109	0.074	0.130
Knee Flexion	0.234	0.002	0.976	-0.012	0.235	0.116	0.208
Hip Extension	0.038	0.926	0.186	-0.015	0.117	0.003	0.169
Hip Flexion	0.051	0.004	0.267	-0.017	0.113	0.023	0.134
Shoulder Flexion	0.204	0.549	0.012	-0.009	0.112	0.007	0.154
Shoulder Extension	0.226	0.119	0.905	-0.030	0.101	0.102	0.214

6b.

	A0	A1	A2	TS1	TR1	I	TR2
Ankle Plantar Flexion	0.123	0.862	0.846	0.004	0.189	0.010	0.132
Ankle Dorsi Flexion	0.379	0.048	0.682	-0.018	0.141	0.005	0.127
Knee Extension	0.069	0.456	0.724	0.019	0.139	0.092	0.189
Knee Flexion	0.205	0.080	0.200	-0.006	0.220	0.129	0.249
Hip Extension	0.061	0.996	0.263	-0.030	0.158	0.011	0.186
Hip Flexion	0.069	0.004	0.799	-0.008	0.125	0.016	0.117
Shoulder Flexion	0.170	0.746	0.027	-0.002	0.102	0.030	0.145
Shoulder Extension	0.192	0.067	0.621	-0.040	0.146	0.001	0.143

6c.

	A0	A1	A2	TS1	TR1	I	TR2
Ankle Plantar Flexion	0.042	0.993	0.024	0.004	0.184	0.011	0.175
Ankle Dorsi Flexion	0.069	0.263	0.874	-0.012	0.397	0.005	0.106
Knee Extension	0.220	0.857	0.537	-0.013	0.110	0.028	0.184
Knee Flexion	0.435	0.089	0.377	0.010	0.254	0.379	0.130
Hip Extension	0.043	0.932	0.004	0.011	0.121	0.018	0.116
Hip Flexion	0.069	0.228	0.339	0.016	0.449	0.150	0.182
Shoulder Flexion	0.202	0.515	0.037	-0.036	0.137	0.002	0.138
Shoulder Extension	0.224	0.146	0.316	-0.034	0.110	0.313	0.215

APPENDIX 7

Torque Generator Activation Parameters
from Optimisations

7a. Height in a single straight somersault
7b. Height in a 1¾ piked somersault
7c. Height in a piked triffus
7d. Rotation using half the length of the jump zone
7e. Rotation using the full length of the jump zone

7a.

	A0	A1	A2	TS1	TR1	I	TR2
Ankle Plantar Flexion	0.035	0.687	0.652	0.164	0.292	0.016	0.149
Ankle Dorsi Flexion	0.090	0.002	0.468	0.022	0.117	0.014	0.210
Knee Extension	0.105	0.904	0.292	0.021	0.117	0.085	0.164
Knee Flexion	0.237	0.015	0.930	-0.007	0.235	0.035	0.227
Hip Extension	0.070	0.899	0.129	-0.013	0.112	0.020	0.162
Hip Flexion	0.053	0.004	0.222	-0.011	0.119	0.032	0.124
Shoulder Flexion	0.242	0.466	0.090	-0.016	0.114	0.003	0.146
Shoulder Extension	0.191	0.119	0.877	-0.023	0.102	0.108	0.245

7b.

	A0	A1	A2	TS1	TR1	I	TR2
Ankle Plantar Flexion	0.105	0.909	0.935	0.194	0.796	0.001	0.136
Ankle Dorsi Flexion	0.300	0.040	0.582	-0.010	0.151	0.015	0.137
Knee Extension	0.066	0.448	0.796	0.019	0.129	0.086	0.194
Knee Flexion	0.206	0.079	0.142	-0.009	0.227	0.125	0.253
Hip Extension	0.061	0.994	0.363	-0.030	0.154	0.021	0.196
Hip Flexion	0.068	0.004	0.700	-0.006	0.134	0.026	0.127
Shoulder Flexion	0.173	0.771	0.127	-0.002	0.103	0.021	0.135
Shoulder Extension	0.192	0.071	0.585	-0.039	0.144	0.004	0.135

7c.

	A0	A1	A2	TS1	TR1	I	TR2
Ankle Plantar Flexion	0.035	0.999	0.010	0.188	0.637	0.018	0.168
Ankle Dorsi Flexion	0.128	0.165	0.870	-0.010	0.392	0.005	0.102
Knee Extension	0.280	0.869	0.637	-0.007	0.112	0.024	0.188
Knee Flexion	0.468	0.018	0.310	0.012	0.246	0.384	0.135
Hip Extension	0.045	0.997	0.069	0.011	0.111	0.008	0.122
Hip Flexion	0.070	0.149	0.376	0.013	0.450	0.145	0.175
Shoulder Flexion	0.177	0.500	0.130	-0.038	0.132	0.011	0.138
Shoulder Extension	0.218	0.146	0.406	-0.036	0.119	0.319	0.223

7d.

	A0	A1	A2	TS1	TR1	I	TR2
Ankle Plantar Flexion	0.031	0.999	0.000	0.193	0.637	0.002	0.165
Ankle Dorsi Flexion	0.082	0.288	0.874	-0.009	0.395	0.012	0.107
Knee Extension	0.286	0.820	0.637	-0.014	0.113	0.037	0.193
Knee Flexion	0.430	0.013	0.354	0.006	0.249	0.378	0.123
Hip Extension	0.049	0.931	0.001	0.014	0.112	0.008	0.107
Hip Flexion	0.067	0.316	0.379	0.013	0.445	0.152	0.185
Shoulder Flexion	0.222	0.508	0.117	-0.036	0.140	0.009	0.130
Shoulder Extension	0.203	0.169	0.382	-0.025	0.113	0.305	0.210

7e.

	A0	A1	A2	TS1	TR1	I	TR2
Ankle Plantar Flexion	0.119	0.990	0.002	0.181	0.602	0.020	0.165
Ankle Dorsi Flexion	0.169	0.321	0.864	-0.002	0.397	0.003	0.108
Knee Extension	0.235	0.924	0.602	-0.016	0.111	0.034	0.181
Knee Flexion	0.354	0.112	0.436	0.013	0.252	0.370	0.128
Hip Extension	0.027	0.840	0.001	0.005	0.114	0.008	0.106
Hip Flexion	0.064	0.320	0.376	0.019	0.440	0.145	0.177
Shoulder Flexion	0.186	0.493	0.083	-0.040	0.134	0.004	0.134
Shoulder Extension	0.225	0.145	0.232	-0.029	0.102	0.310	0.215